50

HYDRODYNAMIC PROPERTIES OF SOME AMYLOSE ESTERS

by

Ann Maconnachie

Department of Chemistry

An abstract of a thesis submitted to the

University of Stirling

DECEMBER 1972

ProQuest LLC.
789 East Eisenhower Parkway
P.O. Box 1346
Ann Arbor, MI 48106 – 1346

CORRECTIONS

PAGE	LINE	COMMENTS
2	20	(29) to (2a)
5	18	is to in
9	5	vary to very
15	5	$\eta\ \eta_o$ to η/η_o
19	12	h to Δh
22	13	osmometic to osmotic
"	"	guage to gauge
27	6	erase the
28	7	vapourisation to vaporisation
32	11	value to volume
34		equation (53) erase (before $\sin^2\theta/2$
"	24	thermostated to thermostatted
52	11	vivial to virial.
53	12	(1) to (17)
57		Table III.4 α values incorrect,should read 1.47,1.36,1.35.
58		Table III.5 Δs missing.
62		second column should read $\bar{M}_w$
64	24	(1) to (17)
71		Comments on α incorrect,in fact they do show reasonable expansion.
71	13	born to borne
76	6	Arogadro's to Avogadro's
80		Table III.15 (a),(b) and(c) missing, these refer to the Ist,2nd and 3rd pairs of columns ,respectively.
81	3	cellubsic -> cellulosic.
83	4	on to of
88	19	n to Δn
94	14	spurio s to spurious
106		Table IVI33 missing,see attached sheet.
110	3	it's to its
113	20	defined to definite
119		Table IV.5 A_m for ATB in THF should read 182.0

CORRECTIONS, continued.

PAGE	LINE	COMMENTS
120	4	σ missing
122	12	hinderance → hindrance .
124	1	α missing
125		equation(9) multiply by 4.14
128	5&6	should read ~1240cm^{-1} and ~1170cm^{-1}
131	15	valume to volume
140		Reference (48) should read 21, 10 (1953).

ABSTRACT

This thesis is concerned with the properties of amylose esters in solution. Three esters have been studied in various solvents, the tributyrate, tripropionate and to a lesser extent the triacetate.

Chapter I gives details of the various experimental methods used and their theoretical background. Measurements of the limiting viscosity number, the weight average molecular weight and the number average molecular weight have been made. No change in the viscosity was found with decreasing shear rate.

Chapter II details the methods of preparation of linear amylose and the three esters. The amylose was analysed for linearity and purity by β-amylolysis. The esters were prepared by reaction of amylose with the appropriate anhydride in pyridine. Two batches of the tripropionate and the tributyrate were prepared. Low molecular weight fractions of the triacetate and tripropionate were obtained. Difficulty was found on trying to fractionate the high molecular weight sample of the tripropionate. This sample was found to exhibit anomalous solution behaviour in subsequent measurements. The degree of substitution was checked by Infra-red spectroscopy.

In Chapter III the results are recorded for each ester. Measurements of A_2 by osmometry are discussed in the light of theories concerning its dependence on molecular weight. Theories relating the expansion coefficient to the molecular weight are also discussed.

Various theories have been used to estimate the unperturbed dimensions from viscosity measurements in good solvents. The

methods due to Stockmayer and Fixman, Kurata and Stockmayer, Flory and Fox, Ptitsyn, Berry, Bohdanecky and Inagaki, Suzuki and Kurata were used.

The unperturbed dimensions of amylose tributyrate were found to vary with solvent and values of $(\bar{r}_0^2/\bar{M}_w)^{\frac{1}{2}}$ varied from 523 x 10^{-11}cm to 576 x 10^{-11}cm (Φ_0 equals 2.87 x 10^{23}). The temperature dependence of the unperturbed dimensions of amylose tributyrate shows a minimum at about 308K and a tentative explanation of change in ring conformation has been put forward.

The unperturbed dimensions of the tripropionate and triacetate were not found to be solvent dependent and had values for $(\bar{r}_0^2/\bar{M}_w)^{\frac{1}{2}}$ of 575 x 10^{-11}cm and 559 x 10^{-11}cm, respectively. Both esters exhibit a negative temperature dependence of viscosity and unperturbed dimensions. The flexibility of the esters, in terms of parameters such as the Kuhn statistical segment and the Kirkwood-Riseman effective bond length, was found to decrease as the side chain lengthened. The esters were compared with the cellulosic polymers and found to be much less extended and more flexible in solution. The esters were also compared with synthetic polymers and found to be less flexible.

ACKNOWLEDGEMENTS

I wish to thank everyone in the University of Stirling who has helped and advised me during the last three years. A special thank you goes to Dr. J. M. G. Cowie for all his patience, help and support which were much appreciated.

Thanks are also due to Mr. J. Maizey for allowing GPC measurements to be made at RAPRA and Dr. J. Evans for carrying them out. I also wish to thank Dr. W. Banks for carrying out the analysis of the amylose and SRC for their financial support.

Finally I wish to thank Mary Ross and Rajinder Bhagrath for all their help in preparing and typing this thesis.

CONTENTS

			Page
Abstract			i
Acknowledgements			iii
Introduction			1
CHAPTER I	Physical Experimental Methods and Theory		
	Section I	Viscosity	9
	Section II	Measurements of Average Molecular Weights	
		1. Osmometry	20
		2. Vapour Pressure Osmometry	25
		3. Light-Scattering	30
CHAPTER II	Preparation of Amylose Esters		
	Section I	Preparation of Linear Amylose	40
	Section II	Preparation of Amylose Esters	43
	Section III	Fractionation of the Esters	48
CHAPTER III	Hydrodynamic Properties of Amylose Esters		
	Section I	Hydrodynamic Properties of Amylose Tributyrate	52
	Section II	Hydrodynamic Properties of Amylose Tripropionate	83
	Section III	Hydrodynamic Properties of Amylose Triacetate	99
CHAPTER IV	Comparison of the Properties of Amylose Esters		109
APPENDIX	Gel Permeation Chromatography		130
BIBLIOGRAPHY			138

INTRODUCTION

Starch is a high molecular weight polysaccharide which acts as a plant food reserve. It is composed of two components amylose and amylopectin. Both amylose and amylopectin are polyglucans. Amylose is essentially a linear molecule composed of anhydroglucose units linked α-D-(1 → 4), whereas amylopectin has a highly ramified structure with amylose - like chains which are linked α-D- (1 → 6) to produce branching. In Figure 1 schematic diagrams of amylose and amylopectin show the different linkages and structures.

Starch can be extracted from any plant, where it is stored in the form of granules which vary in size from 3 to 100μ in diameter. The percentage of amylose in the starch granules can vary from <1% to 66% depending on the botanical source (1), for example, potato starch has an amylose content of about 23%. The fractionation of starch into its components has been a subject of study for many years. The starch granule has to be treated so that the water soluble amylose fraction can be extracted. Two basic methods are used to extract amylose,

(a) complete granular dispersion in water at 373K and

(b) aqueous leaching at a lower temperature.

In both methods amylose can be separated by complexing it with a specific reagent. These complexes, which have been shown to be helical in the solid state by X-ray analysis, can be formed between amylose and various alcohols. The complexing agent occupies the centre of the amylose helix. When an alcohol is added to an aqueous solution of impure amylose an insoluble complex with the alcohol is formed which precipitates leaving

FIGURE 1

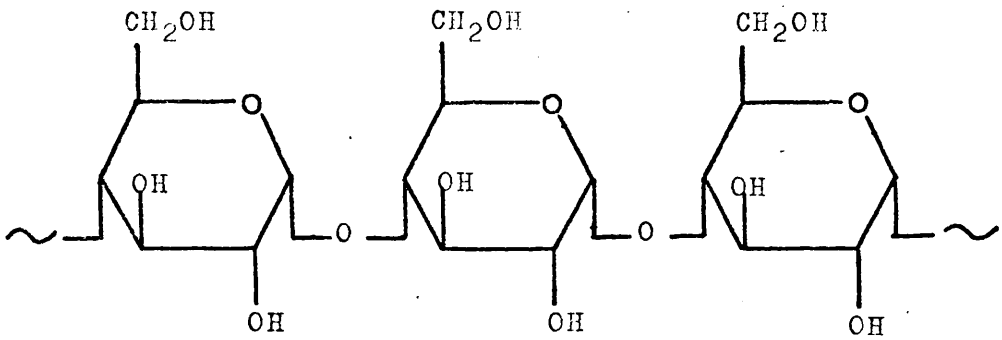

AMYLOSE

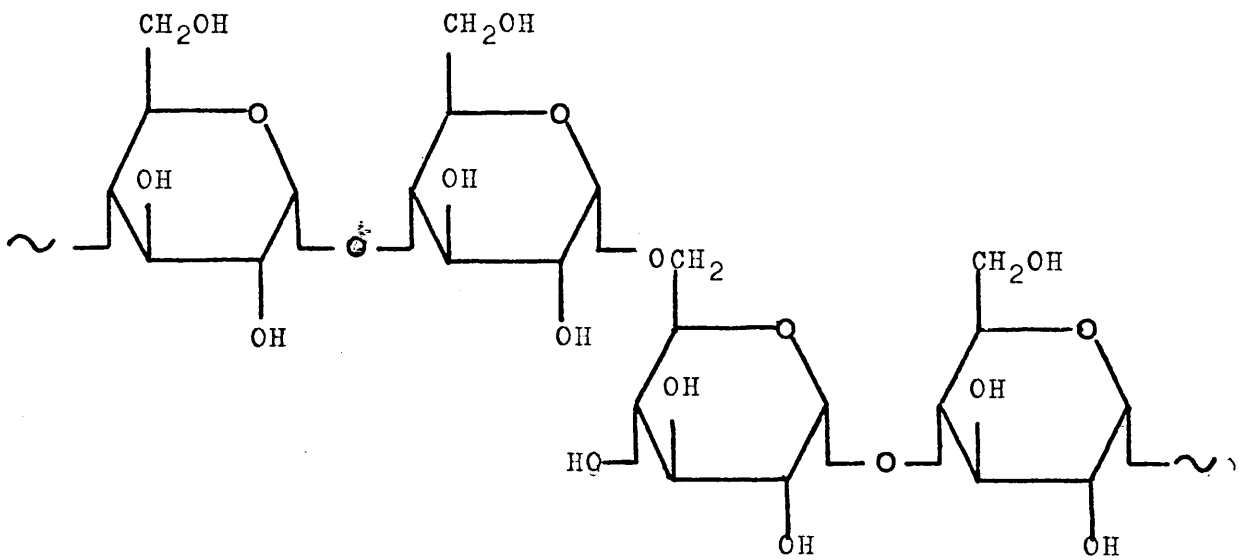

AMYLOPECTIN

FIGURE 2

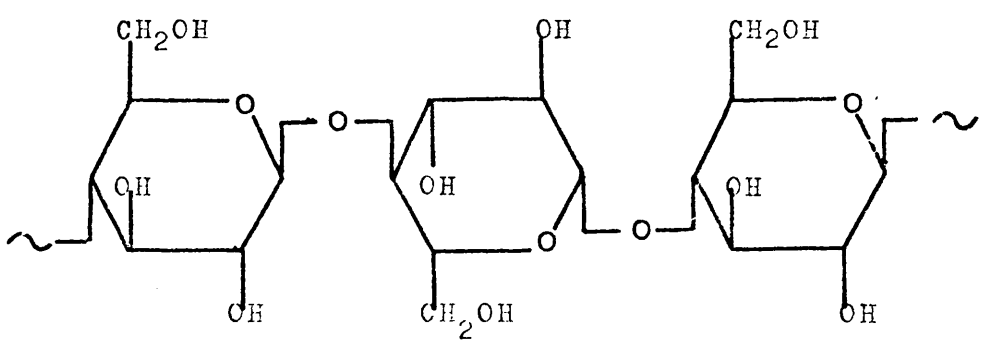

CELLULOSE

any contaminating amylopectin behind. This method is used in further recrystallisations.

Greenwood and various co-workers (2) have made an exhaustive study of the fractionation of starch and the characterisation of the two fractions, particularly the amylose fraction. The characterisation of amylose involves two factors, the purity and the linearity of the fraction. The purity of an amylose sample can be measured in two ways. The first method requires the determination of the iodine affinity of the sample by a potentiometric method (3) and the second method is an enzymic analysis. Iodine reacts with amylose to give a characteristic deep blue-coloured complex containing one iodine molecule for each seven or eight anhydroglucose units. The amylose iodine complex is believed to be a helically coiled amylose molecule, with a period of six anhydroglucose units, with iodine atoms situated in the core of the helix (30). A pure sample of amylose has an iodine affinity of 20% of iodine by weight. By measuring iodine affinity the amount of contaminating amylopectin can be calculated provided it is greater than about 3% (2a). In a more sensitive method the percentage conversion of amylose into maltose, using a commercial sample of the enzyme β - amylase, is measured. Commercial samples of β-amylase contain another carbohydrase, Z-enzyme, an α-amylase which does not hydrolyse amylopectin completely because the branch points impose barriers to further hydrolysis. This inability to convert amylopectin entirely into maltose is the basis of the method for determining the purity of amylose. If the (β+Z) limit is considerably less than 100% then the amylose is considered

to be contaminated with amylopectin.

The linearity of amylose can be measured by the action of pure β-amylase. The enzyme only attacks non-reducing end-groups and degrades the molecule in a step-wise manner into maltose. It is only capable of hydrolysing α- (1 → 4) links so that any other linkage such as α- (1 → 6) (found in amylopectin) stops the hydrolysis process. Whilst linear amylose will be completely hydrolysed by β-amylase (2a), amylopectin, the highly branched structure, will only have its external chains hydrolysed. The hydrolysis stops at a branch point and leaves a β-limit dextrin.

Amylose prepared by complete granular dispersion in water followed by addition of a complexing agent, such as thymol or butanol, was found to have a β-amylolysis limit of $< 100\%$ and as low as 72% (1). According to the iodine affinity values and the (β+ ~~E~~) limit these samples were pure amylose so that some barrier to β - amylolysis must exist in the chain. The β- amylolysis limit can be increased by decreasing the temperature and using a leaching technique (1). Accompanying this increase in the β- amylolysis limit is a decrease in the viscosity $[\eta]$, therefore the molecular weight must decrease as well. The barrier to β - amylolysis would seem then to be concentrated in the higher molecular weight material. The nature of this barrier is thought by Banks and Greenwood (4), on the basis of enzymic studies, to be an anomalous point in the chain causing long chain branching.

The optimum temperature for obtaining linear amylose by a leaching process depends on the origin of the starch and

can vary from 353K for amylomaize to about 333K for potato starch. It has also been shown (5) that oxidative modification of amylose is unlikely to occur if the extraction is carried out under nitrogen. Modifications can occur if the extraction is carried out in the presence of oxygen. The amylose in the present work was extracted from potatoes at 335K under nitrogen and to ensure complete linearity the top molecular weight fraction was discarded.

The amylose used in hydrodynamic studies carried out before Greenwood et al established its structure and showed the existence of an anomalous link in the chain is likely to have contained some non-linear material (6 - 9). Establishing the linearity of amylose is important when considering hydrodynamic properties. Any sample which is non-linear will exhibit different behaviour in solution compared with a completely linear sample (2a). Since the linearity of the amylose used in previous studies is unknown and the degree of branching could vary among samples it is difficult to compare results. However, bearing this in mind, previous studies will be considered.

Closely related to amylose is cellulose, another polysaccharide. Cellulose is a linear polyglucan made up of anhydroglucose units linked β - D - (1 $\rightarrow$ 4) (Fig. 2). Amylose can be regarded as an isotactic glucan in contrast to the syndiotactic cellulose polymer. Due to the β linkages cellulose has a much more extended, rigid structure than amylose. This rigidity is utilized in nature as cellulose is a structural material in plants and animals. Fibrous cellulose, isolated from natural sources, is shown by X-ray

diffraction to be partially crystalline. It is probable that the linear molecules are associated for parts of their length in an ordered, parallel arrangement interspersed with amorphous regions. In contrast amylose is amorphous in the natural state although the starch granules do exhibit a Maltese cross optical extinction pattern in polarised light which is characteristic of spherulitic structure.

Cellulose is extremely insoluble in most solvents except strong mineral acids and some complex solvents such as cupriethylenediamine. Difficulties are also encountered when working with aqueous solutions of amylose because it has a tendency to retrograde or spontaneously precipitate. Since amylose is soluble in few organic solvents retrogradation is hard to avoid.

Because amylose is known to be helical in the solid state there is a possibility that it might exhibit this type of behaviour in solution. Macromolecules such as DNA are known to keep their helical conformation is solution as well as the solid state. It has not been firmly established whether or not the helical form of amylose exists in solution. Considerable differences exist between results in the literature. Foster and Hixon (10) considered amylose to exist as a stiff rod in solution and in support of this view found a value for the Mark-Houwink exponent of 1.5 for amylose in ethylenediamine. Potter and Hassid (11) working with the same system found a value of a = 1, whereas Cowie (31) found a = 0.7. Szejtli and Augustat (12) put forward the idea of an interrupted helix, that is short sections of helical amylose connected by sections of non-helical amylose (Fig. 3).

FIGURE 3 PROPOSED MODELS FOR AMYLOSE.

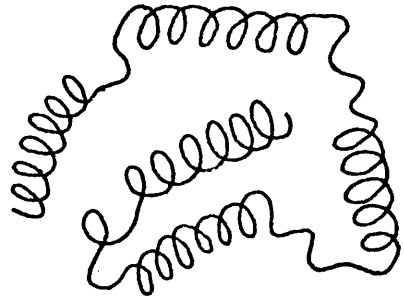

INTERRUPTED HELIX

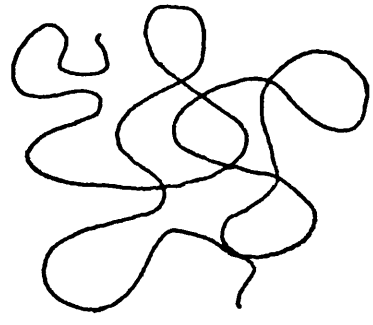

RANDOM COIL

Burchard (13) and, Banks and Greenwood (14) could find no evidence of helical formation in solution. This view is supported by the work of Everett and Foster (15) who looked at the temperature dependence of the optical rotation of amylose in aqueous solution and could find no evidence of a helix-coil transition. They also considered that the light scattering data fitted the theories of random coils. Another idea which has been put forward by Cowie (16) is that there are two different configurations depending on the solvent environment.

Because of solubility problems amylose and cellulose are difficult to work with, but this can be overcome by considering their derivatives. These are soluble in a large number of organic solvents and the amylose derivatives do not retrograde.

The conformations of cellulose and some of its derivatives in solution have been the subject of argument for some time. The commonly held view, until Kurata and Stockmayer (17) reviewed the results, was that certain cellulose derivatives (notably the trinitrate) are supposed to have abnormally extended unperturbed chains and a very small expansion coefficient in good solvents. If the theory of Kurata and Stockmayer is applied to these polymers the large Mark-Houwink exponents i.e. > 0.8 can be explained by saying that they have a large expansion coefficient and therefore a relatively small unperturbed dimension. Recent work tends to support the view (18 - 22) that cellulose and its derivatives behave as normal flexible polymers. The cellulose derivatives which have been studied include the triacetate (23), tributyrate (19,24)

and tricarbanilate (18, 20).

Amylose derivatives such as the triacetate (25, 26) and tricarbanilate (20, 27) have been studied in various solvents including theta and mixed solvents and no indication of helical behaviour has been found. Hence both amylose and cellulose derivatives are thought to behave as random coils in solution but the crystal structure of amylose triacetate is believed by Sarko and Marchessault (28) to be a non-integral helix. According to Bryant and Kwon Min (29) sodium carboxymethyl amylose behaves as a random coil in solution but this coil consists of interrupted helices.

Although the conformation of amylose triacetate is almost certainly a random coil it would be interesting to investigate the effect of an increasing side-chain on the amylose backbone. With this in mind the esters form an interesting group since the side-chain increases in a regular manner. The tripropionate and tributyrate have been studied (and to a less extent the triacetate) to see what effect this has on the conformation of the molecule in solution. Viscosity, light scattering and osmotic pressure measurements have been made on these esters in several solvents. The temperature dependence of the unperturbed dimensions has also been investigated.

Chapter I deals with the basic theory and experimental techniques used, Chapter II concerns the preparative side of the investigation and the remaining chapters contain the results and a comparison of the hydrodynamic behaviour of the esters.

C H A P T E R I

PHYSICAL EXPERIMENTAL METHODS AND THEORY

SECTION I VISCOSITY

(a) VISCOSITY THEORY

INTRODUCTION

It was Staudinger (32) in 1930 who first drew attention to the relationship between the viscosity of a polymer solution and the molecular weight of the polymer. The viscosity of a simple liquid is greatly enhanced by the addition of an amount of polymer. This is true down to very low concentrations and dilute solution viscosity measurements are made on solutions of concentrations of less than about $0.03 g/cm^3$.

Viscosity measurements are a major way of characterising a polymer due to the simplicity, accuracy and short time-scale of such measurements. Unfortunately, it is not an absolute method for determining molecular weights and the viscosities have first to be calibrated using polymer fractions of known molecular weight.

The empirical relationship which Staudinger first proposed was:

$$[\eta] = KM \qquad (1)$$

where $[\eta]$ is the limiting viscosity number, M, the molecular weight and K is a proportionality constant. This expression was found to hold for polymers of relatively low molecular weight. Mark (33) and Houwink (34) have since put forward a more general expression:

$$[\eta] = KM^a \qquad (2)$$

where the exponent a may vary between 0.5 and 2. These limiting values correspond to a tightly coiled molecule and

a rigid, rod-like molecule respectively while, for a randomly coiled molecule a may vary between 0.5 and 1. The values of K and a can be determined at a particular temperature, for a given polymer/solvent system, from a double logarithimic plot of $\log[\eta]$ against log M.

The Concentration Dependence of Viscosity

The ratio of the viscosity of a polymer solution, η, divided by the viscosity of the solvent, η_o, is called the relative viscosity, η_r. The variation of the relative viscosity with concentration of dissolved polymer can be expressed as a power series in concentration as follows:

$$\eta/\eta_o = \eta_r = 1+[\eta]c + kc^2 + \ldots\ldots \qquad (3)$$

where, in a given polymer/solvent system at a fixed temperature, $[\eta]$ and k are constants for a particular molecular weight.

For dilute solutions, only the first three terms of equation (3) need be considered and these can be rearranged to give the following form:

$$(\eta_r - 1)/c = \eta_{sp}/c = [\eta] + kc \qquad (4)$$

η_{SP} is the specific viscosity, $[\eta]$, the limiting viscosity number, is the limiting value of the specific capacity of the polymer to increase the relative viscosity, and

$$k = k' [\eta]^2 \qquad (5)$$

where k' is the Huggins constant. It follows from equation (4) that a plot of η_{SP}/C against C will therefore give $[\eta]$ and k'.

Flory Relationship and Theta Conditions

According to the treatment given by Flory (35), the limiting viscosity number is considered to be proportional to the effective volume of the molecule divided by its molecular weight. This is expressed, in the case of randomly coiled polymer chains, as the root-mean-square end-to-end distance $(\bar{r}^2)^{\frac{1}{2}}$. The expression relating these two quantities is:

$$[\eta] = \Phi(\bar{r}^2/M)^{3/2}M^{1/2} \qquad (6)$$

which can be further expanded to give:

$$[\eta] = \Phi(\bar{r}_0^2/M)^{3/2}M^{1/2}\ \alpha^3 \qquad (7)$$

where $(\bar{r}_0^2)$ is the mean-square unperturbed end-to-end distance of the polymer chain and α is the linear expansion factor. Φ is a "universal" constant which has a theoretical value of 2.87×10^{23}. Unfortunately, Φ has been found to be solvent and sample dependent, but a good experimental value is 2.5×10^{23}. The ratio, $(\bar{r}_0^2)/M$, should be a constant independent of molecular weight and solvent, but it may change with temperature due to variations in hindrance to rotation about polymer chain bonds with temperature which alter the unperturbed dimensions.

Ordinarily, the limiting viscosity number should depend on the molecular weight not only because of the factor $M^{\frac{1}{2}}$ in equation (7) but also because of the molecular weight dependence of α^3. When by a suitable choice of solvent and temperature $\alpha = 1$, equation (7) reduces to:

$$[\eta] = \Phi(\bar{r}_0^2/M)^{3/2}M^{1/2} = KM^{1/2} \qquad (8)$$

The solvent is then a pseudo-ideal or θ-solvent and the polymer chain is in an unperturbed conformation. The temperature at which this occurs is called the θ-temperature.

Effect of the Molecular Weight Distribution on the Viscosity - Molecular Weight Relationship

In order to establish the relationship between limiting viscosity number and molecular weight it is necessary to calibrate the former with an average molecular weight obtained by an absolute method. The molecular weight average which is obtained from viscosity measurements is the viscosity average which is defined as (35):

$$\bar{M}_v = \left[\sum_i w_i M_i\right]^{1/a} \qquad (9)$$

where w_i is the weight fraction of the species i in the whole polymer and M_i is the molecular weight of species i. It follows then that:

$$[\eta] = K \bar{M}_v^{\,a} \qquad (10)$$

and this expression should be used instead of equation (2).

For polymers having the "most probable" distribution, it can be shown that:

$$\bar{M}_n : \bar{M}_v : \bar{M}_w :: 1 : \left[(1 + a)\,\Gamma(1 + a)\right]^{1/a} : 2 \qquad (11)$$

when a = 1, $\bar{M}_v$ equals $\bar{M}_w$ and for a high polymer, with any distribution it is possible to show that $\bar{M}_v$ is always closer to $\bar{M}_w$ than $\bar{M}_n$. If the number average molecular weight is used to calibrate the viscosity - molecular weight relationship, the relationship will be in error to the extent that

the two averages differ. If the ratio of $\bar{M}_v$ to $\bar{M}_n$ is about the same for all of the samples, then the only error will be in the value of K; but, if the value of the ratio is irregular, no consistent relationship will be found.

Careful fractionation will help to eliminate the difference found between molecular weight averages, but it is always better to calibrate using a weight average than a number average because the former is always closer to the viscosity average.

Once a relationship is established, then a viscosity average molecular weight can be calculated using equation (10).

(b) EXPERIMENTAL

Apparatus and Method

Measurements were carried out in a Cannon-Ubbelohde viscometer. This is shown in Figure 4. The viscometer was clamped to a stand, with a three-point suspension which ensured that it could be reproducibly positioned vertically when placed in a water-bath thermostatted to $\pm$ 0.02K.

The solution and solvent were both filtered through G3 sintered glass filters, to remove any extraneous material and placed in the thermostatted bath. A known volume of solution was introduced into the viscometer down tube A, using a pipette. C was closed and pressure applied to A forcing the liquid up B. When the solution was above D, the applied pressure was released and C opened. The time of the fall was measured between the two fiducial marks, D and E, using a stop-watch reading to 0.01 sec. The measurement was repeated until consecutive readings were within

FIGURE 4 CANNON-UBBELOHDE VISCOMETER.

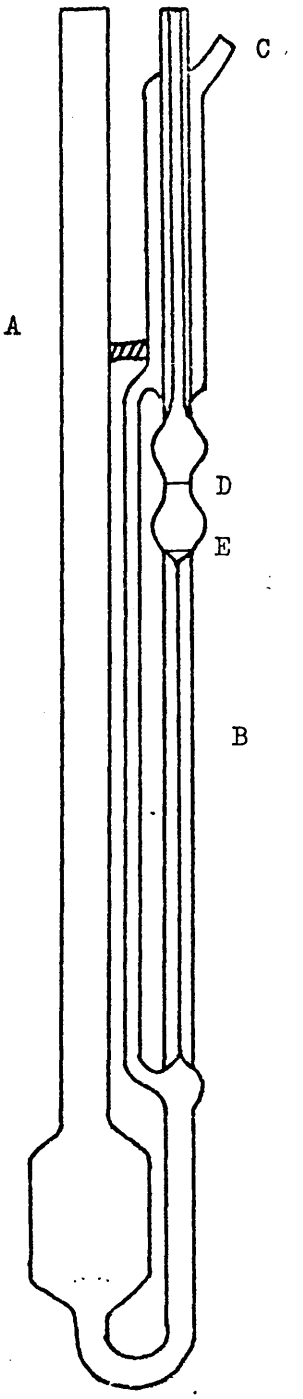

0.1 sec. and an average value was taken as the flow-time. To obtain another concentration, dilution was carried out 'in situ' by adding a known volume of solvent down A and mixing was effected by bubbling air through the viscometer. The procedure detailed above was repeated. Dilution in this way was repeated twice more. The flow-time of the solvent alone was also measured.

Theory

The flow-time of the solution is related to the viscosity by Poiseuille's equation as follows:

$$v = \pi P r^4 / 8\eta l \qquad (12)$$

where v is the volume rate of flow, P is the pressure difference maintaining the flow, r is the radius of the capillary, η is the viscosity of the solution and l is the length of the capillary.

Suppose the volume of liquid contained between the two fixed marks is V and that the flow-times for solvent and solution are t_o and t respectively then equation (12) can be written as:

$$V/t = \pi P r^4 / 8\eta l$$

and

$$V/t_0 = \pi P_0 r^4 / 8\eta_0 l$$

so that

$$\eta/\eta_0 = tP/t_0 P_0 = t\bar{h}\rho g / t_0 \bar{h}_0 \rho_0 g \qquad (13)$$

where ρ and ρ_o are the densities of solution and solvent, respectively, and g is the gravitational constant. Since the height of liquid, $\bar{h}$, in the Cannon-Ubbelohde viscometer

is always the same equation (13) reduces to:

$$\eta/\eta_0 = t\rho/t_0\rho_0 \qquad (14)$$

For very dilute solutions where it can be assumed that $\rho = \rho_0$ equation (14) reduces to:

$$\eta/\eta_0 = t/t_0$$

Therefore

$$\eta_{sp} = \eta_r - 1 = \frac{t - t_o}{t_o}$$

(c) KINETIC ENERGY CORRECTIONS

The viscosity, η, of a liquid measured in a capillary viscometer is calculated from an equation of the form:

$$\eta = A\rho t - B\rho/t \qquad (15)$$

where

$$A = \pi r^4 \bar{h} g/8Vl \qquad (16)$$

and

$$B = mV/8\pi l \qquad (17)$$

m is called the kinetic energy coefficient (36) the value of which varies with Reynolds number causing B to vary as well. The quantity B/t is called the kinetic energy correction. In a well designed viscometer, B/t is usually a small fraction of the At term. Two factors contribute to the kinetic energy correction, these are (i) the effect of contracting the stream of liquid prior to entering the capillary of the viscometer

and (ii) the effect of expanding the stream when it leaves the capillary. The correction term cannot be calculated from the dimensions of the viscometer, it has to be determined experimentally.

When B/t is negligible equation (15) reduces to:

$$\nu = \eta/\rho \qquad (18)$$

where ν is called the kinematic viscosity. Since a suspended level viscometer has the same liquid driving head at all temperatures the viscosity factor, A, is a constant at all temperatures for a particular viscometer, see equation (16).

Four viscometers have been used in the present study at various temperatures. Measurements of the flow-times of four liquids, ethyl acetate, toluene, carbon tetrachloride and water were made in each viscometer at the various temperatures.

Values of A were calculated assuming that equation (18) held. No definite trend was found in the variation of A with temperature for a given solvent. Also, for a particular viscometer, the variation in value of A with solvent was completely random. If the kinetic energy corrections for these viscometers were significant variations in A would be expected with solvent and temperature. Table I.1 gives values of A for the four viscometers together with the mean values and the percentage errors. These indicate that any kinetic energy correction is negligible.

(d) SHEAR DEPENDENCE OF VISCOSITY

In order to study the shear dependence, if any, of the viscosity of the polymer solutions under examination a P.C.L.

Table I.1: Values of A for the Four Viscometers

Viscometer	Solvent	Temperature (K)	A x 10^7	$A_{av.}$ x 10^7
1	A	298	494	490.2 ± 0.8%
	B		490	
	C		491	
	D		486	
2	A	298	187	185.5 ± 0.8%
	B		185	
	C		185	
	D		184	
3	A	298	180	179.3 ± 0.7%
	D		178	
	C		180	
4	A	298	297	295.2 ± 1.0%
	B		296	
	C		296	
	D		292	
1	A	289.8	496	496 ± 0.2%
	D		497	
	C		495	
1	A	307.9	492	494.5 ± 0.3%
	D		497	
	C		495	
1	A	313	490	493 ± 0.4%
	D		495	
	C		494	

Table I.1: Continued

Viscometer	Solvent	Temperature (K)	A x 10^7	$A_{av.}$ x 10^7
1	A	317.5	496	494.3 ± 0.3%
	D		494	
	C		493	
3	A	317.5	182	181.3 ± 0.4%
	D		181	
	C		181	
4	A	317.5	298	296.6 ± 0.5%
	D		296	
	C		296	

A - Ethyl Acetate

B - Water

C - Toluene

D - Carbon Tetrachloride

zero-shear viscometer was used (Figure 5).

Limb A is a precision-bore tube with a diameter of 7.0 mm ± 0.14%. The rate of fall of the meniscus in this tube is faithfully reflected in the attached 0.75mm precision bore reference tube and is closely proportional to the rate of volume efflux through the capillary tubes C,C'. When determining viscosity ratios the actual volume flowing through the tubes need not be calculated and it is only necessary to measure the rate of approach of the solution menisci in the two reference tubes D,D' and to compare this with the same measurement for the solvent. The only driving force is the hydrostatic pressure of the column of liquid and as the two menisci approach, the applied stress, and therefore the shear gradient becomes vanishingly small.

Method

The viscometer was clamped vertically in a water-bath thermostatted to ± 0.02K. Measurements were made first on the solvent. $8cm^3$ of filtered solvent were introduced into the viscometer down B. Pressure was applied to B and the liquid forced up A and D until the meniscus rose slightly above the upper line on D. The pressure was released and the rate of fall of the meniscuswas measured between the two lines. These lines on tube D cover the normal shear rate range (500 - 2,000 reciprocal seconds) common to most dilution viscometers. When the meniscus touched the bottom line the stop-watch was stopped and another started, simultaneously. A cathetometer was set-up with its cross-wires focussed 1cm below the bottom line on D. When the meniscus in D touched this level, the watch was stopped and another

FIGURE 5 P.C.L. ZERO-SHEAR VISCOMETER.

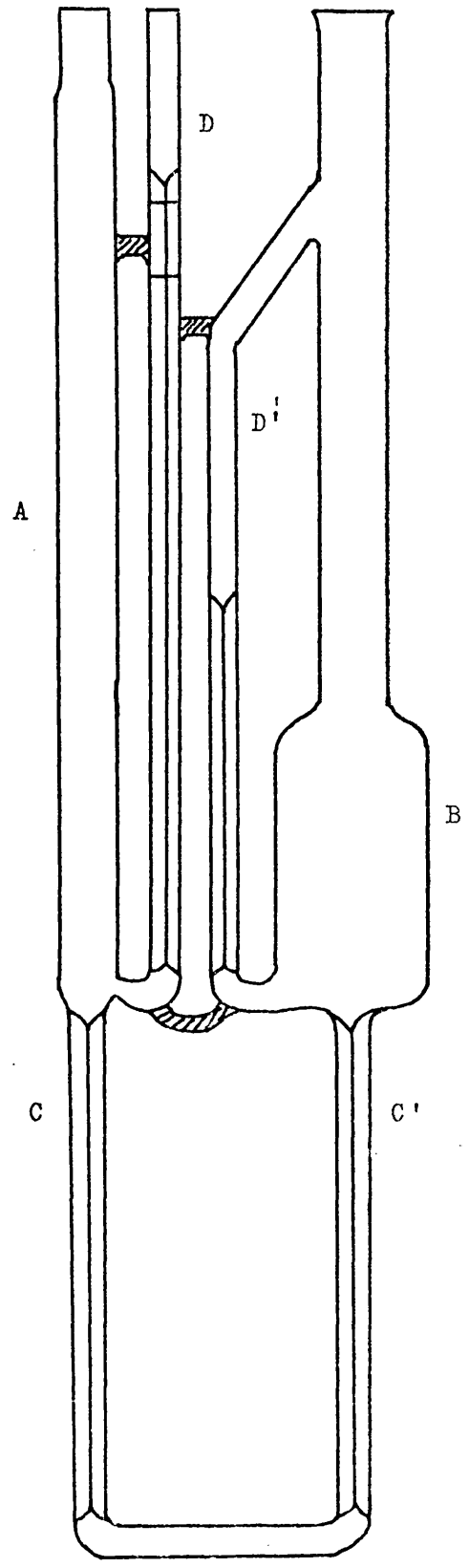

started. Immediately the cathetometer was depressed to read the height of the meniscus in D'. When this was carried out the cathetometer was raised to a level 2cm below the line on D. As long as the measurement of the height in D' was done within about 20 seconds of reading D any error involved is negligible. This is because the level in D' rises at about 4% of the rate of fall of the level in D, due to the differences in cross-sectional area of the two limbs A and B. When the meniscus reached the cross-wires again the watch was stopped and another started and the level in D' read again, as before. The cathetometer was raised to a level 3cm below the line. Measurements were carried out as above until the two menisci were so close or the rate of their approach so slow that the instant at which the cross-wires were reached could not be accurately timed. The height of each meniscus and the time at each reading were recorded. Measurements on a solution were carried out in the same way, using the same volume of liquid.

Interpretation of Results

For a Newtonian liquid, that is a liquid whose viscosity has no shear dependence, it can be shown that a plot of $\log \Delta h$ against cumulative time, t, should be linear. $\Delta h = h - h'$ is the difference in height of the menisci in the limbs D and D' respectively.

If a solution is non-Newtonian a curve will result on plotting $\log \Delta h$ against t. The curve can be transformed into one showing the variation of viscosity with shear gradient. In practice it often suffices to show the variation of the

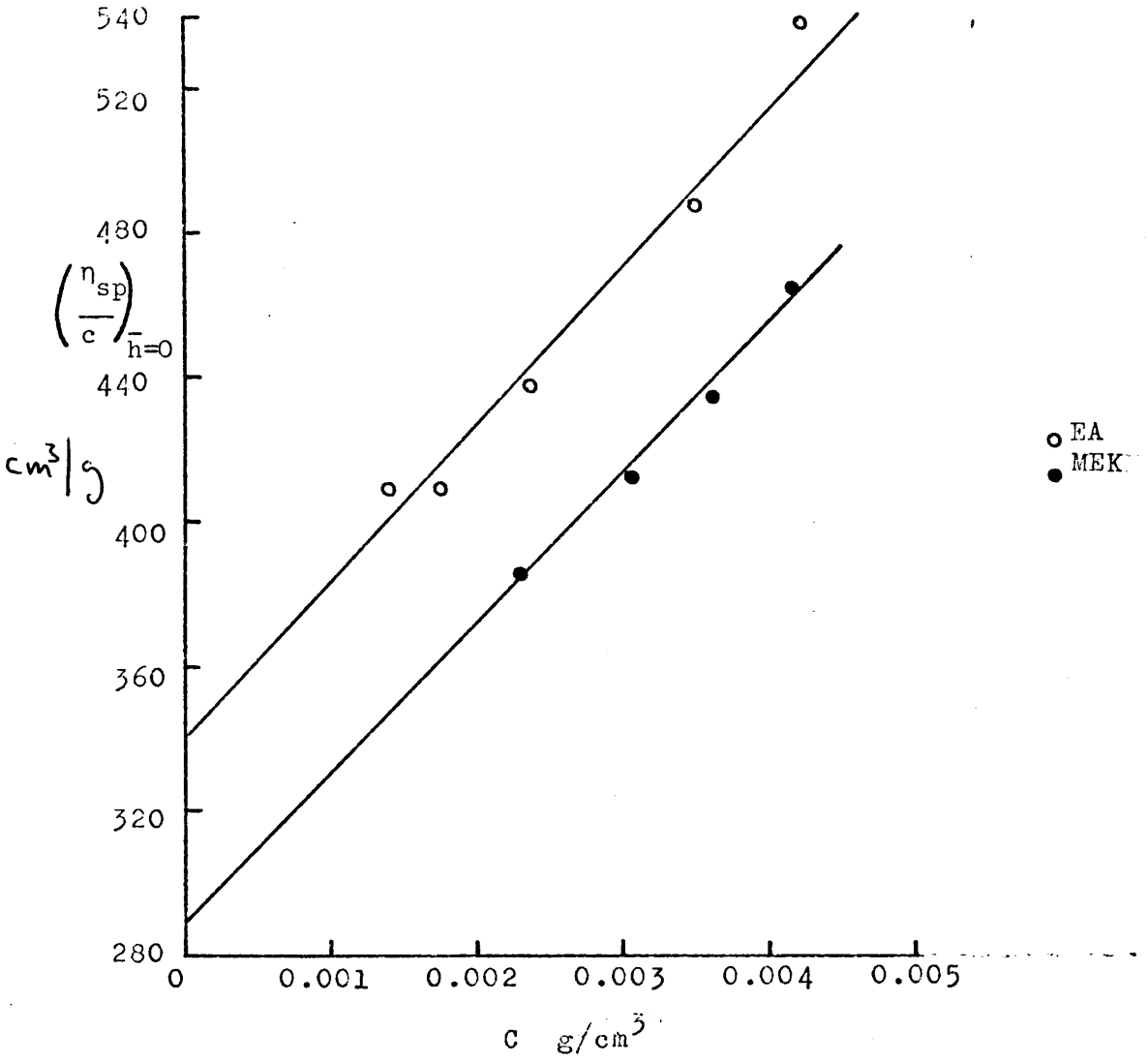

FIGURE 6 η_{sp}/C AGAINST C AT ZERO SHEAR FOR S2a IN MEK AND EA AT 298K, VALUES OF $[\eta]$ AT NORMAL SHEAR RATES ARE 293 AND 340, RESPECTIVELY.

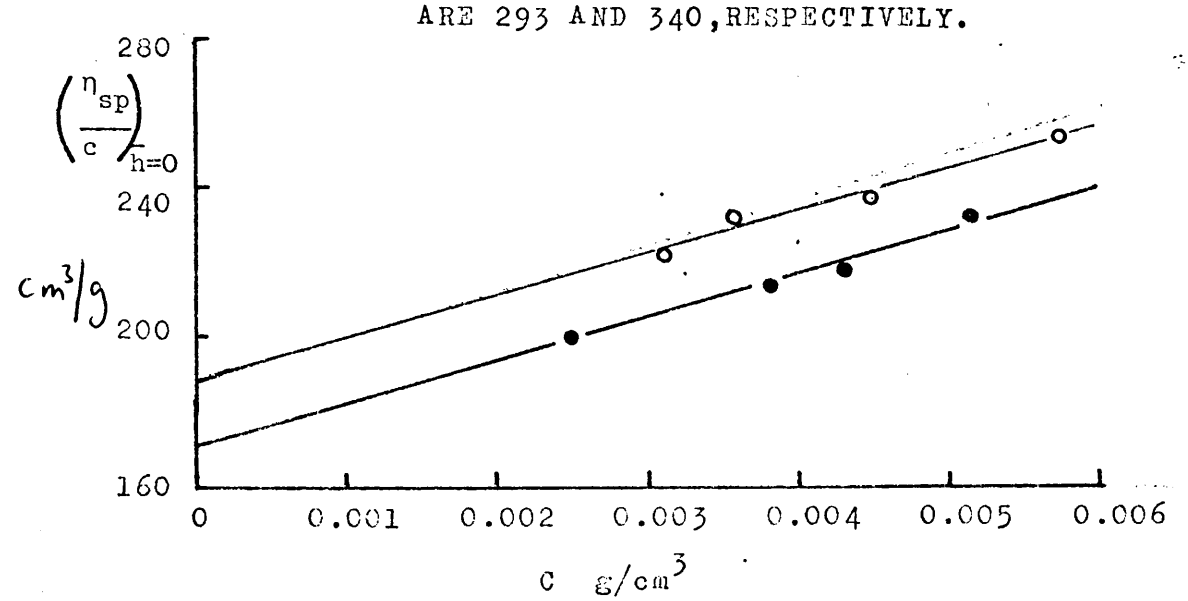

FIGURE 7 η_{sp}/C AGAINST C AT ZERO SHEAR FOR B2' IN MEK AND EA AT 298K, VALUES OF $[\eta]$ AT NORMAL SHEAR RATES ARE 173 AND 189, RESPECTIVELY.

viscosity ratio with the applied stress. This can be done by comparing the $\bar{h}.\Delta t$ product for a fixed interval at the same values of Δh for both solvent and solution. $\bar{h}$ is the mean value of $\Delta(\Delta h)$.

The values of $\bar{h}$ and Δt were obtained from the plots of log Δh against t. The values of t and Δh equal to, 7.5, 6.5, 5.5, 4.5, 3.5, 2.5, 1.5 and 0.5 were found. An interval of $\Delta(\Delta h) = 1$ was used so that $\bar{h}$ values were 1, 2, 3, 4, 5, 6 and 7.

Δt is the difference between adjacent values of t, that is, for $\bar{h} = 1$, $\Delta t = t_{1.5} - t_{0.5}$, where $t_{1.5}$ is the value at $\Delta h = 1.5$ and $t_{0.5}$ is the value corresponding to $\Delta h = 0.5$. Δt is worked out similarly for the other values of $\bar{h}$. This is also done for the solvent so that a list of values of Δt (solvent) and Δt (solution) is collected for fixed values of $\bar{h}$. A plot is then made of

$$\left[(\bar{h}.\ \Delta t\ (\text{solution})/\bar{h}.\ \Delta t\ (\text{solvent})) - 1\right]/C \text{ against } \bar{h}$$

to give η_{sp}/C at zero shear. This value can then be plotted against C to give $[\eta]$ at zero shear.

Figures 6 and 7 show the results of these measurements for the highest molecular weight fractions of amylose propionate and amylose butyrate in various solvents. No shear dependence was found.

SECTION II MEASUREMENTS OF AVERAGE MOLECULAR WEIGHTS

INTRODUCTION

The number average molecular weight, $\bar{M}_n$, of a polymer is defined as

$$\bar{M}_n = \frac{\Sigma_i N_i M_i}{\Sigma_i N_i}$$

where N_i is the number of molecules of species i which have a molecular weight M_i.

It can be measured in various ways all of which are based on the colligative properties of a polymer solution. The addition of a solute to a solvent alters the free energy of the solution and various properties are affected. When solute is added to a solvent the vapour pressure of the solvent is lowered, the boiling point is raised, the freezing point is depressed and an osmotic pressure can be developed. All these changes have in common the fact that they are dependent only on the number of solute particles. If the weight and number of these particles is known the molecular weight can be calculated. Two of these effects have been utilised in the present study to determine $\bar{M}_n$; osmotic pressure and vapour pressure lowering. These two methods cover a range of molecular weight measurements from 50 to 1,000,000.

(1) OSMOMETRY

(a) THEORY

The free energy change per mole of solvent, ΔG, that results from the addition of solute can be expressed in terms of the lowering of the equilibrium vapour pressure from P^o, for

the pure solvent, to P, for the solution.

$$\Delta G = RT \ln \frac{P}{P^o} \tag{19}$$

For equilibrium to be established this free-energy change must be balanced by the effect of applied pressure. When the solution is subjected to an excess pressure, π, the free-energy change per mole of solvent is given by

$$\Delta G = -\pi V \tag{20}$$

where V is the volume of 1 mole of solvent in the solution. Substitution of equation (20) into equation (19) leads to:

$$\pi V = - RT \ln \frac{P}{P^o} \tag{21}$$

and if Raoult's law is obeyed this becomes

$$\pi V = - RT \ln X_1 \tag{22}$$

where X_1 is the mole fraction of solvent. For very dilute solutions

$$\ln X_1 = \ln(1 - X_2) \simeq - X_2$$

so $$\pi V = RTX_2 \tag{23}$$

where X_2 is the mole fraction of solute. From which it follows that:

$$\frac{\pi}{C} = \frac{RT}{M} \tag{24}$$

where C is the concentration in g/dm^3 and M is the molecular weight of the solute. Equation (24) implies that in the ideal case π/C is independent of concentration. This relationship does not hold for polymer solutions where $\pi/C = f(C)$. For solutions of flexible linear molecules it has been shown (35) that:

$$\frac{\pi}{C} = \frac{RT}{M}(1 + \Gamma_2 C + g\Gamma_2^2 C^2) \tag{25}$$

where Γ_2 is one form of the second virial coefficient and depends on the polymer-solvent interaction.

To determine the molecular weight of a polymer π/C is measured at various concentrations and plotted against C. Extrapolation to infinite dilution will produce an intercept such that:

$$\bar{M}_n = RT/\lim_{c \to 0} [\pi/ c] \qquad (26)$$

(b) EXPERIMENTAL

Instrumentation

The osmometer used was a Melabs Recording Osmometer, model CSM-2, which employs the static method to measure osmotic pressure in the temperature range 278K to 403K. The method used to measure the osmometic pressure is a strain-guage detection system. This records pressure changes to the required accuracy, with very little solvent flow through the membrane.

The solvent is contained in a closed chamber, one wall of which is a flexible diaphragm. As solvent diffuses through the membrane, which is held rigidly in place, the diaphragm distends and changes the volume of the chamber. This change of volume is coincident with a corresponding change in pressure caused by the elasticity of the diaphragm. The diaphragm is mechanically connected to a strain-guage detector system which measures the diaphragm motion to 2.5mm. This sensitivity requires that only $3 \times 10^{-3} cm^3$ of solvent need pass through the membrane to generate a pressure equal to a head of 1cm of water. The osmometer comes to equilibrium 100 times faster

than the conventional osmometer since such small volumes are used in the cell. The molecular weight of polymer can be determined inside three hours.

The recorder used in conjunction with the osmometer was a Bryans potentiometric recorder with 1mV full scale sensitivity.

Membranes

Pecel 600 membranes were conditioned to methyl ethyl ketone in a step-wise manner. The membranes were placed in 20% methyl ethyl ketone (MEK)/80% iso-propanol for twenty-four hours. The ratio of MEK/iso-propanol was then changed to 40/60 for a further twenty-four hours. The percentage of MEK was increased in this way every twenty-four hours until the membranes had been in pure MEK for a day. They were then used in the osmometer having first been cut to the correct size.

Method

A series of four concentrations was prepared, the highest being approximately $0.005 g/cm^3$. Solutions and solvent were both filtered through G3 sintered glass filters to remove any extraneous materials which might affect the performance of the osmometer.

The wet membrane was installed in the osmometer and particular care was taken to ensure that no drying occured even in limited areas. Temperature settings of Coarse 1, Fine 5.71 were chosen and the osmometer left for a few hours to allow it to come to temperature equilibrium. The temperature settings chosen correspond to 295.5K. Having achieved

temperature equilibrium the osmometer was calibrated so that 5cm pressure of solvent gave a full scale deflection on the recorder.

When the osmometer had stabilised and had been calibrated the following procedure was followed to measure the osmotic pressure. The solvent inlet valve (Figure 8) was slowly closed and the level of solvent was dropped by opening the solution drain valve until a reading of 60 was indicated nn the level meter. The cell was allowed to stabilise, indicated by a straight line on the recorder. The 'recorder zero control' was adjusted to zero the recorder. Between $0.5cm^3$ and $1cm^3$ of the least concentrated solution was introduced into the osmometer down the solution inlet tube. The solution drain valve was opened and the level of solution dropped until a reading of 60 was indicated on the level meter. The valve was closed and the osmometer allowed to stabilise. If necessary the level was readjusted to 60. The instrument was allowed to restabilise over a period of a few minutes before the osmotic pressure was read off the recorder in centimeters of solvent pressure.

The osmotic pressure, π, was measured three times for each concentration. The first value was disregarded since this was usually affected by the previous concentration. An average of the second and third measurements was taken as the value of π in centimeters.

A plot of π/C against C gave a value for $RT/\bar{M}_n$.

The osmotic pressure is observed in centimeters of solvent h, so that

$$\pi = h\rho_0 g$$

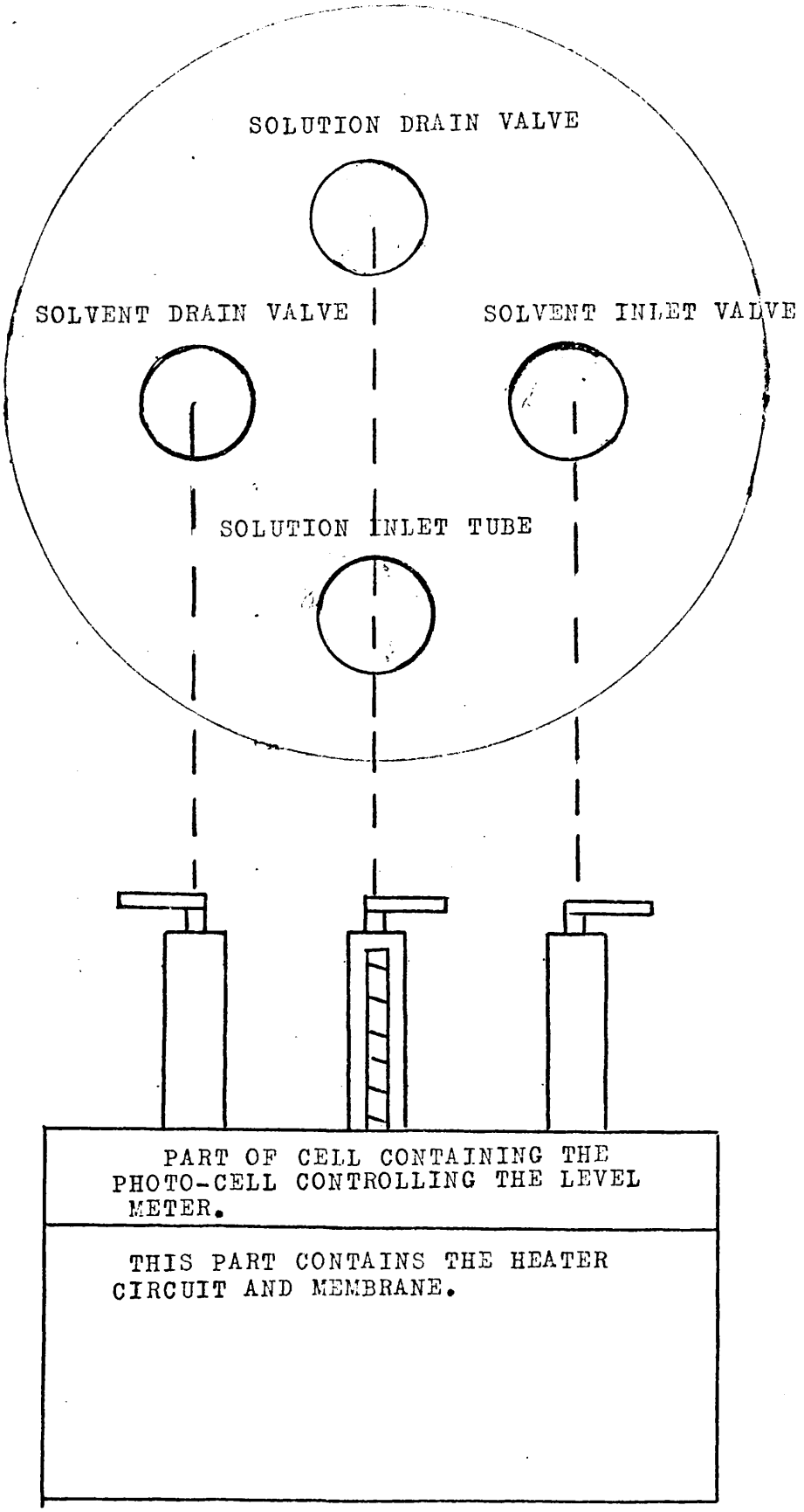

FIGURE 8 SCHEMATIC DIAGRAM OF THE MEMBRANE OSMOMETER.

where ρ_o is the density of solvent in kg/dm^3 at temperature T, in degrees K and g is the gravitational constant and has a value of $9.81 m/s^2$. If the concentration C is measured in g/dm^3 and R is $8.314 J\ mol^{-1}K^{-1}$ then

$$\bar{M}_n = 1/[\pi/c]_{c=0} RT/\rho_0 g$$

$$= 1/[\pi/c]_{c=0} 846.8T/\rho_0 \qquad kg\ mol^{-1}$$

Relative molecular mass $M = 1/[\pi/c]_{c=0} 846.8T/\rho_0 \times 10^3\ g\ mol^{-1}$

(2) VAPOUR PRESSURE OSMOMETRY

(a) EXPERIMENTAL

Instrumentation

A Hewlett-Packard Vapour Pressure Osmometer 302B was used to carry out the measurements. This consists of a thermostatted chamber, controlled to 0.002K saturated with solvent vapour in which two matched thermistors in close proximity to one another form two arms of a Wheatstone bridge. Drops of solvent were placed on the thermistors and the bridge balanced. When one of the solvent drops is replaced with solution, there is a temperature rise caused by solvent distilling onto the solution drop. This alters the resistance of the thermistors so that the bridge has to be rebalanced. The compensating resistance can then be related to the molecular weight of the solute. Number average molecular weights in the range 50 - 25,000 can be measured satisfactorily.

The instrument was used in the recording mode because data found manually was not consistent. The recorder used

was a Bryans potentiometric recorder on 1mV full scale sensitivity. An operating temperature setting of 229 was used corresponding to 303.6K.

General Method

For each molecular weight fraction a series of concentrations were prepared. Approximately $5cm^3$ of solution was made up with a concentration of about 0.05g/g solvent. All polymer solutions were made up as weight/weight solutions to minimise errors in concentrations. A stock solution whose initial concentration depended on the quantity of sample available was prepared. A small amount of this solution was weighed into three bottles. Varying amounts of solvent were then weighed into these bottles to obtain three different concentrations. The concentrations were then calculated knowing the concentration of the first solution. By adding solvent last, errors due to evaporation were minimised.

The instrument was set up and left overnight to equilibrate. The temperature stability was checked using the manufacturer's procedure. A solvent drop was placed on each thermistor and the base line checked on a recorder. One drop was replaced and the base line was rechecked. This procedure was repeated until a reproducable base line was obtained. The thermistor was rinsed with a few drops of the lowest concentration solution and finally one drop was placed on it. The recorder trace was observed and when the steady state was reached another drop was placed on the thermistor and the procedure repeated. Three measurements were made for each concentration, the first one of which was disregarded due to possible alterations to

FIGURE 9a VPO CALIBRATION CURVE FOR MEK AT 303.6K.

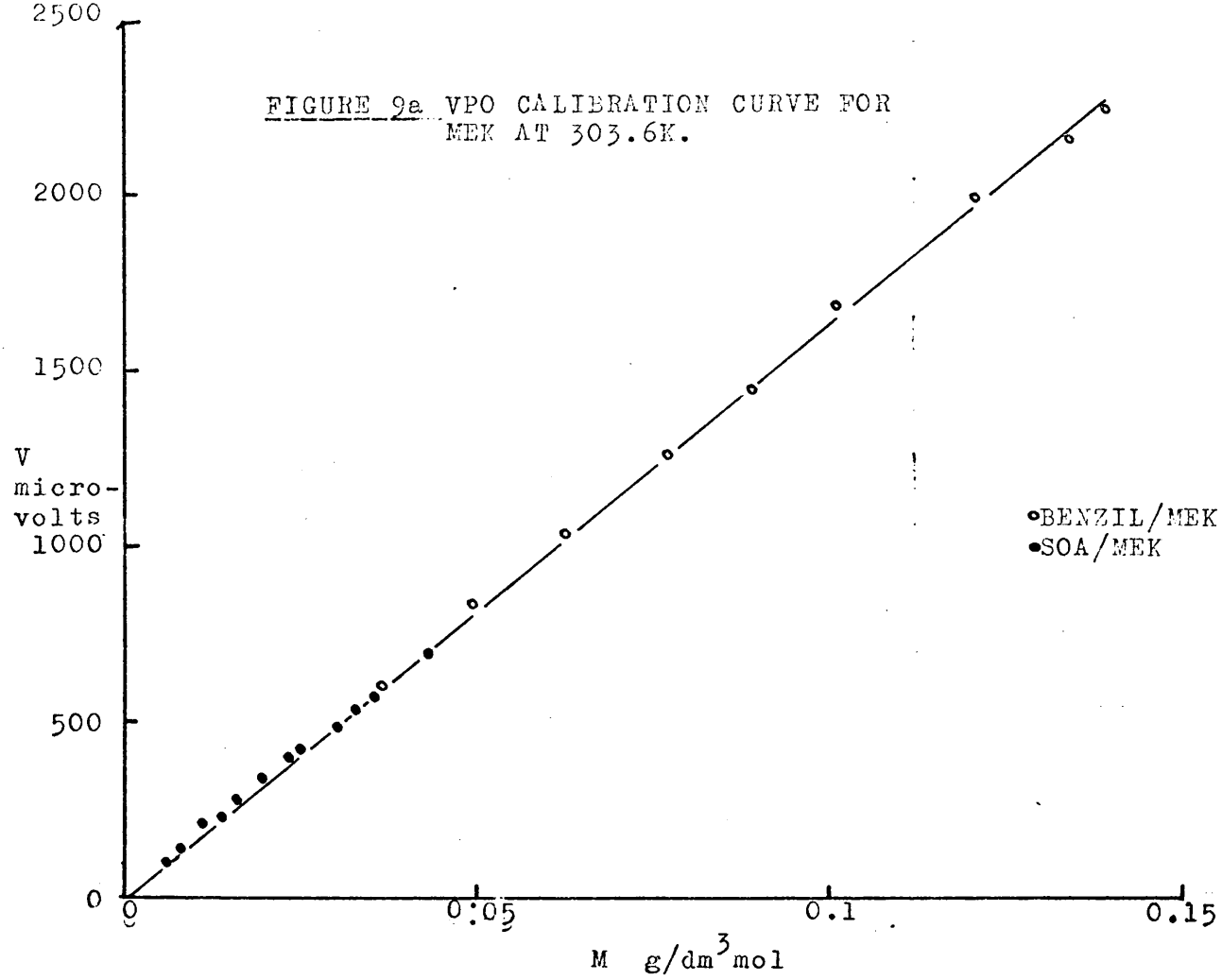

FIGURE 9b VPO CALIBRATION CURVE FOR EA AT 303,6K.

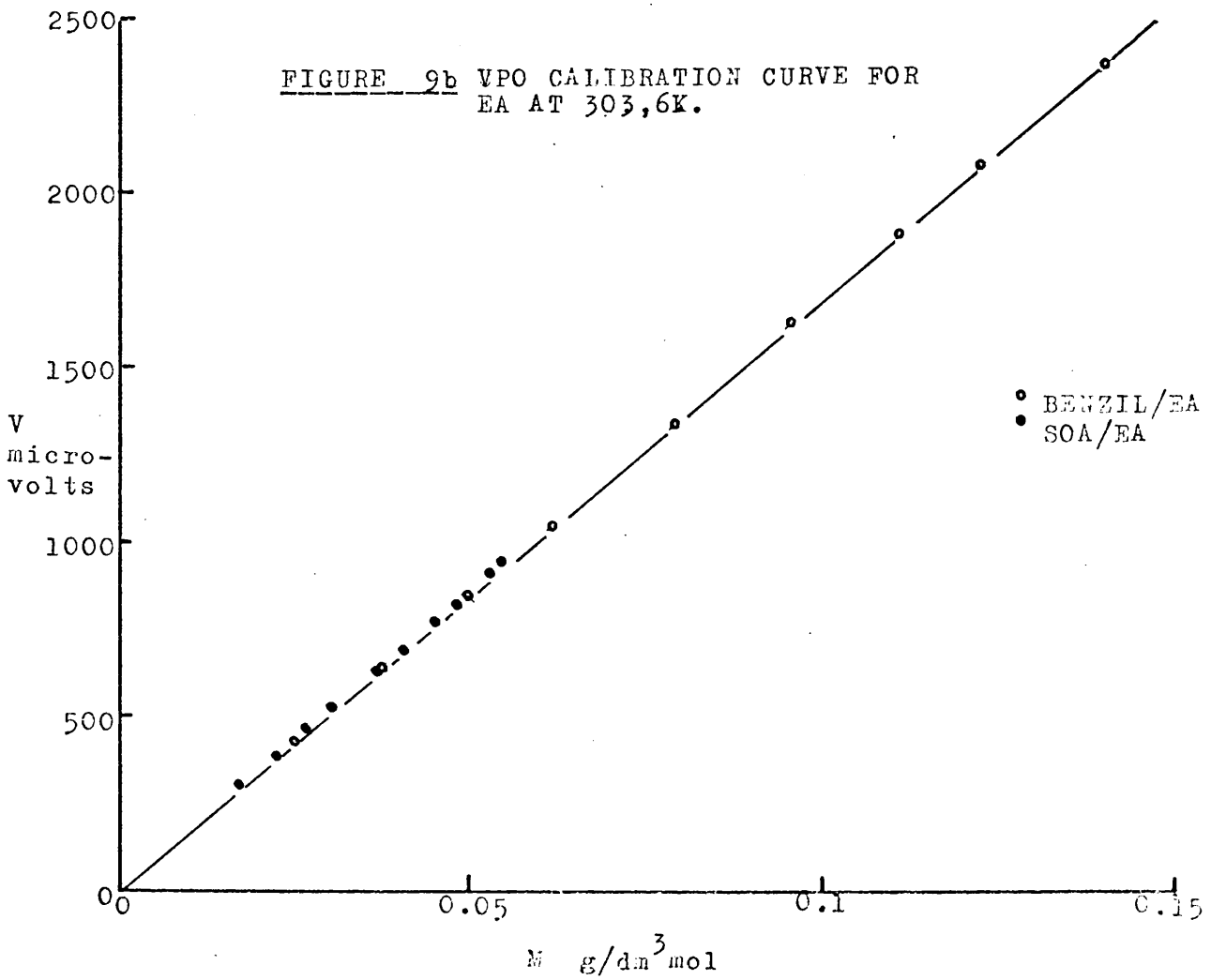

the concentration, the other two were averaged to give V in microvolts. The base line was rechecked after each concentration to eliminate errors due to base line drift.

Calibration

The instrument was calibrated using sucrose octaacetate and benzil in the methyl ethyl ketone (MEK) and ethyl acetate (EA). Solutions with concentrations ranging from $4 g/dm^3$ to $40 g/dm^3$ were prepared. Since the molecular weights of these two compounds are low, 678.6 and 210.2 respectively, V was consequently much larger so that any error due to base line drift was minimal. The zero was only checked before and after a complete concentration series. The calibration curve for MEK and EA at 303.6K are shown in Figure 9. The values of the calibration constants obtained were:

$$k = 1.695 \times 10^4 \ \mu V \ dm^3 \ mol^{-1}$$

and

$$k = 1.655 \times 10^4 \ \mu V \ dm^3 \ mol^{-1}$$

(b) THEORY

When a solution drop in the vapour pressure osmometer (VPO) is exposed to an atmosphere saturated with solvent vapour, condensation takes place until the vapour pressure of the solution equals that of the solvent and the temperature of the solution drop increases.

According to Raoult's law:

$$P_1 = P_1^0 X_1 = P_1^0 (1 - X_2) \qquad (27)$$

therefore

$$\Delta P = P_1^0 - P_1 = P_1^0 X_2$$

where P is the vapour pressure lowering caused by the addition of solute and P_1^0 and P_1 are the vapour pressure of the pure solvent and the partial pressure of solvent above the solution, respectively. The dependence of vapour pressure on temperature is given by the Clapeyron equation:

$$\frac{dP}{dT} = \frac{\Delta H_v}{T\Delta V}$$

where P is the vapour pressure, ΔH_v is the enthalpy of vapourisation and ΔV is the volume change on vaporisation. If it is assumed that the liquid volume is negligible and the vapour behaves like an ideal gas then

$$\frac{dP}{dT} = \frac{P\Delta H_v}{RT^2} \qquad (28)$$

Equation (28) can be rewritten as

$$\int_{T_2}^{T_1} dT = R\int_{P_1}^{P_1^0} T^2 dP/\Delta H_v P \qquad (29)$$

Since temperature changes involved are always small (usually less than 0.1K) the terms T, ΔH_v and P are practically constant and average values can be used so that equation (29) becomes

$$\Delta T = R\bar{T}^2/\Delta\bar{H}_v\bar{P}.\ \Delta P \qquad (30)$$

assuming that Raoult's Law holds in dilute solution

$$\Delta T = R\bar{T}^2/\ \Delta\bar{H}_v\bar{P}.P_1^0X_2 \qquad (31)$$

Because the vapour pressure differences are very small $P_1^0 \simeq P$ and the theoretical temperature rise in the VPO is

$$\Delta T = R\bar{T}^2/\ \Delta\bar{H}_v\bar{X}_2 \qquad (32)$$

This is the theoretical value for a no-loss VPO. In practice

heat losses prevent attainment of the perfect thermodynamic equilibrium. For a particular solvent and temperature it has been found that the losses are always an almost constant percentage of the theoretical maximum temperature difference. Therefore equation (32) can be replaced by an empirical one taking into account these losses.

$$\Delta T = K_1 X_2 \tag{33}$$

where

$$K_1 = 0.5 \text{ to } 0.9\ RT^2/\Delta H_v$$

The VPO output is V microvolts of bridge imbalance and is proportional to T, i.e.

$$\Delta T = K_2 V \tag{34}$$

For very dilute solutions

$$X_2 \simeq \frac{N_2}{N_1} \tag{35}$$

$$= \frac{C_2}{M_2} \times \frac{M_1}{1000} \tag{36}$$

where C_2 is the concentration of solute in g/kg, N_1 and N_2 are the number of moles of solvent and solute, respectively, M_2 is the solute molecular weight and M_1 is the solvent molecular weight. So that

$$K_2 V = \frac{K_1 C_2}{M_2} \times \frac{M_1}{1000} \tag{37}$$

This reduces to

$$\frac{V}{C} = \frac{K}{M} \tag{38}$$

where K is a calibration constant for a particular solvent and operating temperature and is calculated by measuring V/C for samples of known molecular weight.

Strictly equation (38) only holds for ideal solutions. Since polymer solutions approach ideal behaviour at low concentrations the molecular weight is calculated by measuring V/C at various concentrations and extrapolating to zero concentration. For vapour pressure osmometry equations analogous to those used in conventional osmometry can be applied, viz:

$$\frac{V}{C} = \left(\frac{V}{C}\right)_{C=0} (1 + \Gamma_2 C + \Gamma_3 C^2 + \ldots) \qquad (39)$$

where Γ_2 is the second virial coefficient and can be calculated independently of the calibration constant using this form of equation.

(3) LIGHT-SCATTERING

(a) THEORY

The basic concepts of light-scattering were formulated in the late ninteenth century by Rayleigh who concerned himself with scattering from a gas. The gas was considered to be composed of random molecules at large distances from each other such that they made independent contributions to the scattering effect. The phenomenon is caused by the fact that the oscillating electrical field of the incident light wave induces an oscillating dipole in molecules lying in its path, which will then act as secondary scattering centres and radiate light in all directions. It is assumed that only a very small amount of light is scattered so that multiple scattering may be neglected.

Let us assume that the molecules to be considered are electrically isotropic and small compared with the wave length

of the incident light, λ . Consider an unpolarised beam of light travelling along the X direction (see Figure 10) which is scattered by a molecule at O. The intensity of scattered light, I_θ, at P is given by the expression

$$I_\theta = 8\pi^4\alpha^2/\lambda^4 r^2 . I_0(1+\cos^2\theta) \qquad (40)$$

where α is the polarisability of the molecule, I_o is the incident intensity of the light beam and r is the distance from the observer to the scattering centre.

For a very dilute solution the intensity of scattered light due to N particles in volume V is

$$I_\theta = 8\pi^4\alpha^2/\lambda^4 r^2 . I_0(1+\cos^2\theta)N/V \qquad (41)$$

In order to treat the problem of light scattering by non-ideal solutions at finite concentrations, Smoluchowski and Einstein considered fluctuations of refractive index within arbitrarily chosen volume elements δV small compared to λ . These fluctuations originate from two sources: variation in density and in concentration.

The cause of the scattering of light in a solution is the fluctuation of the mass and polarisability of a particular volume element with time. In a pure liquid these fluctuations are density fluctuations but for a solution superimposed on these are also concentration fluctuations. In a solution the latter fluctuations are most important and the intensity of scattered light due to these can be found by subtracting the scattering due to the solvent from that due to the solution.

The particles in the initial treatment are now replaced by small elements of volume, δV, of the solution. The excess

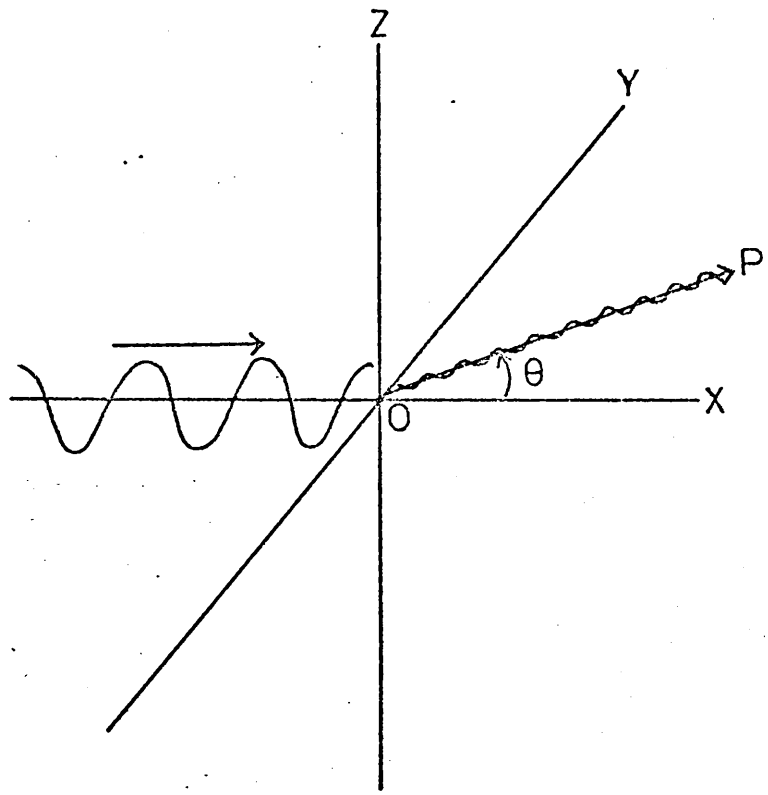

FIGURE 10 See text, page 31.

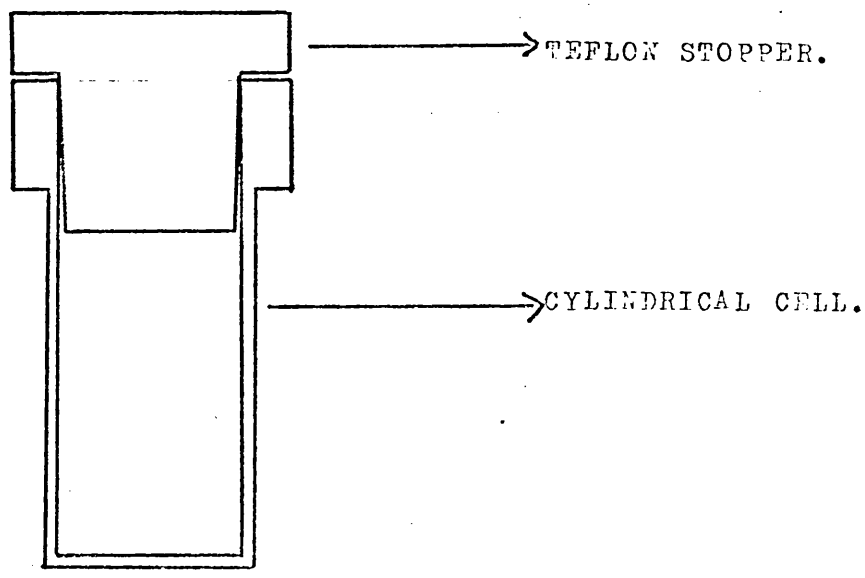

FIGURE 11 LIGHT-SCATTERING CELL.

polarisability of one of these volume elements due to the deviation of its concentration from the average may be written

$$\Delta\alpha = \Delta\varepsilon\ \delta V/4\pi \qquad (42)$$

where $\Delta\varepsilon$ is the difference in optical dielectric constant for the volume element compared with the average for the entire solution. The scattered intensity depends on the average square of $\Delta\alpha$ for all volume elements, $\overline{(\Delta\alpha)^2}$, which replaces α^2 in equation (41). Also the number of particles per unit volume, N/V, is replaced by the number of volume elements per unit value $1/\delta V$. So equation (41) becomes

$$I_\theta = I_0\pi^2/r^2 2\lambda^4 . \overline{(\Delta\varepsilon)^2}\ \delta V(1+\cos^2\theta) \qquad (43)$$

It can be shown that

$$\overline{(\Delta\varepsilon)^2} = (2n_0 dn/dc)^2 kTc/\delta V . 1/(\partial\pi/\partial c) \qquad (44)$$

where k is Boltzmann's constant and n and n_o are the refractive indices of the solution and solvent respectively. Substituting into equation (43) gives

$$R_\theta = I_\theta r^2/I_0 = K.RTc(1+\cos^2\theta)/(\partial\pi/\partial c) \qquad (45)$$

where R_θ is the Rayleigh ratio and

$$K = 2\pi^2 n_0^2/N_A\lambda^4 (dn/dc)^2 \qquad (46)$$

Here N_A is Avogadros' number. The variation of osmotic pressure with concentration can be obtained by differentiating equation (25) to give

$$\partial\pi/\partial c = RT/M(1+ 2\Gamma_2 c+\ldots.) \qquad (47)$$

Substitution of (47) into equation (45) leads to

$$R_\theta = K(1+\cos^2\theta).Mc/(1+2\Gamma_2 c + \ldots.) \qquad (48)$$

where M is actually a weight average molecular weight defined as

$$\bar{M}_w = \Sigma N_i M_i^2 / \Sigma N_i M_i \qquad (49)$$

All the foregoing arguments hold for molecules whose size is very much less than the wavelength of incident light. At dimensions greater than $\lambda/20$ the molecule can no longer be considered as a point source and light scattered from various points on the molecule will no longer be in phase. Consequently, interference effects arise which cause a reduction in the total scattered flux and an unsymmetrical scattering envelope appears. The forward scatter exceeds the backward scatter which means that the dissymmetry coefficient $z = R_\theta / R_{-\theta}$ exceeds 1. The forward scatter at zero angle is unaffected by interference effects. If R_θ and $R_{-\theta}$ differ significantly then interference effects are present and have to be taken into account.

The parameter $P(\theta)$, the particle scattering factor, is defined as

$$P(\theta) = R_\theta / R_\theta^0 = I_\theta / I_\theta^0 \qquad (50)$$

where R_θ^0 and I_θ^0 are the Rayleigh ratio and intensity when interference effects are absent. Equation (48) now becomes

$$K(1+\cos^2\theta)c/R_\theta = 1/MP(\theta)(1+2\Gamma_2 c+\ldots.) \qquad (51)$$

For randomly coiled polymers Debye (37) has shown that

$$P(\theta) = 1-16\pi^2(\bar{s^2})/3\lambda'^2(\sin^2\theta/2 + \ldots\ldots) \quad (52)$$

where λ' is the wavelength of light in the medium and equals λ/n, and $(\bar{s^2})$ is the mean square radius of gyration of the molecule. By substituting this expression for $P(\theta)$ into equation (51) we obtain

$$K(1+\cos^2\theta)c/R_\theta = 1/M(1+2\Gamma_2 c+ \ldots)(1+16\pi^2(\bar{s^2})/3\lambda'^2(\sin^2\theta/2+\ldots) \quad (53)$$

For molecules which show interference effects M, Γ_2 and $(\bar{s^2})$ can be calculated from the scattering data. This is usually accomplished using the method of double extrapolation due to Zimm (38) in which $K(1 + \cos^2\theta)c/R_\theta$ is plotted against $\sin^2\theta/2 + k'c$, where k' is an arbitrary constant. A double extrapolation, to zero angle and zero concentration is then carried out. The intercept of such a plot will give $1/M$ while Γ_2 is derived from the slope of the $\theta = 0$ line and $(\bar{s^2})$ can be calculated from the slope of the $c = 0$ line.

(b) EXPERIMENTAL

Instrumentation and Apparatus

A Photo Gonio Diffusometer Model 42 000 made by S.O.F.I.C.A. was employed for all light-scattering determinations. Measurements were made at fixed angles between 30° and 135° to the incident beam on a minimum of 4 solution concentrations for each molecular weight fraction. The wavelength of light used was 436nm.

The vat, in which the cells are placed, was thermostated to $\pm$ 0.1K. The liquid in the vat was m-xylene whose refractive

index is 1.495 which is sufficiently close to that of the cell glass to ensure that reflections at the cell walls are minimised. Perfectly cylindrical glass cells fitted with Teflon stoppers (see Figure 11), which can be used at high temperatures without solvent evaporation were employed for most measurements. Some measurements were made in the cells provided with the instrument.

Cleaning of the Apparatus

(i) Volumetric Flasks and Pipettes

These were steeped in permanganic acid overnight, rinsed with distilled water then left in hydrogen peroxide solution (approximately 3%) for a further few hours to remove any traces of acid. Finally, they were rinsed with distilled water then acetone and dried on a vacuum line.

(ii) Light-Scattering Cells

The procedure above was followed but after final rinsing with water the cells were dried by inverting them in an oven at 353K for a few hours.

(iii) Sintered-Glass Filters

After the filters had been flushed with solvent, permanganic acid was allowed to drip through the sinters under gravity. When no colour change was observed in the acid before and after travelling through the sinter, cleaning was stopped. Usually 24 hours were needed to make sure the filters were clean. Distilled water was flushed through to remove as much acid as possible followed by the peroxide solution which was allowed to drip through to remove the final traces. Finally the filters were rinsed with more distilled water and put in an oven at 353K to dry overnight.

Method

Two methods of making up solutions were employed. One was a dilution technique starting from stock solution and the other used a series of separately prepared concentrations.

(i) Dilution Method

Between 0.15g and 0.05g of polymer, depending on the probable molecular weight, was dissolved in approximately 25cm^3 of solvent. This solution was filtered under pressure of nitrogen through a G5 sintered-glass filter, which had previously been flushed with solvent, into a 50cm^3 volumetric flask. More solvent was flushed through the filter until the flask contained approximately 50cm^3 of filtered solution.

Solvent was filtered through another G5 filter into a clean dry cell and also into a volumetric flask. The two flasks containing solution and solvent were placed in a water-bath thermostatted at 298K. Varying amounts of solvent and solution were pipetted into the Teflon stoppered cells so that 5 different concentrations in all were made up. The concentrations of the 4 solutions prepared by dilution can be calculated knowing concentration of the first or stock solution. Exactly 2cm^3 of stock solution at 298K were added to a clean, dry, weighed bottle. 5cm^3 of precipitant (which had been previously filtered) were added and the mixture evaporated down to approximately half volume. This was placed in a pistol-oven (small vacuum oven) at 323K for 24 hours. Four separate concentration determinations were carried out for each stock solution. After 24 hours the bottles were allowed to cool down for a few hours under vacuum and then weighed. Weighings were accurate to 1 x 10^{-5}_{g}.

(ii) Concentration Series Method

Five different concentrations were made up in $25cm^3$ volumetric flasks. Each solution was filtered, under nitrogen pressure, through a G5 sintered filter into a cell. The first $5cm^3$ of solution filtered was discarded. Solvent was also filtered directly into a cell. The concentrations were considered to be unchanged by filtration.

Once the solutions and solvent had been filtered into cells, measurements of the angular scatterings were made. The cells were allowed to equilibrate at the temperature of measurement for 15 mins. in the instrument then the scattering was measured at angles between 30^o and 135^o. Galvanometer readings were corrected for variations in scattering volume with angle and then c/I_θ values were computed. Data were plotted according to the Zimm method.

Measurement of the Refractive Index Increment (dn/dc)

Measurements were made using the Brice-Pheenix differential refractometer fitted with a stoppered cell and thermostatted to 298 $\pm$ 0.1K.

The refractive index difference is given by the following equation

$$\Delta n = K\Delta d$$

where Δn is the refractive index difference between a solution and its solvent, K is the calibration constant for the selected wavelength, and Δd is the total slit image displacement (solvent zero corrected) in instrument units.

The instrument was calibrated using potassium chloride/water solutions for which Δn was known, Δd was measured so that K could be calculated. The calibration curve is shown in

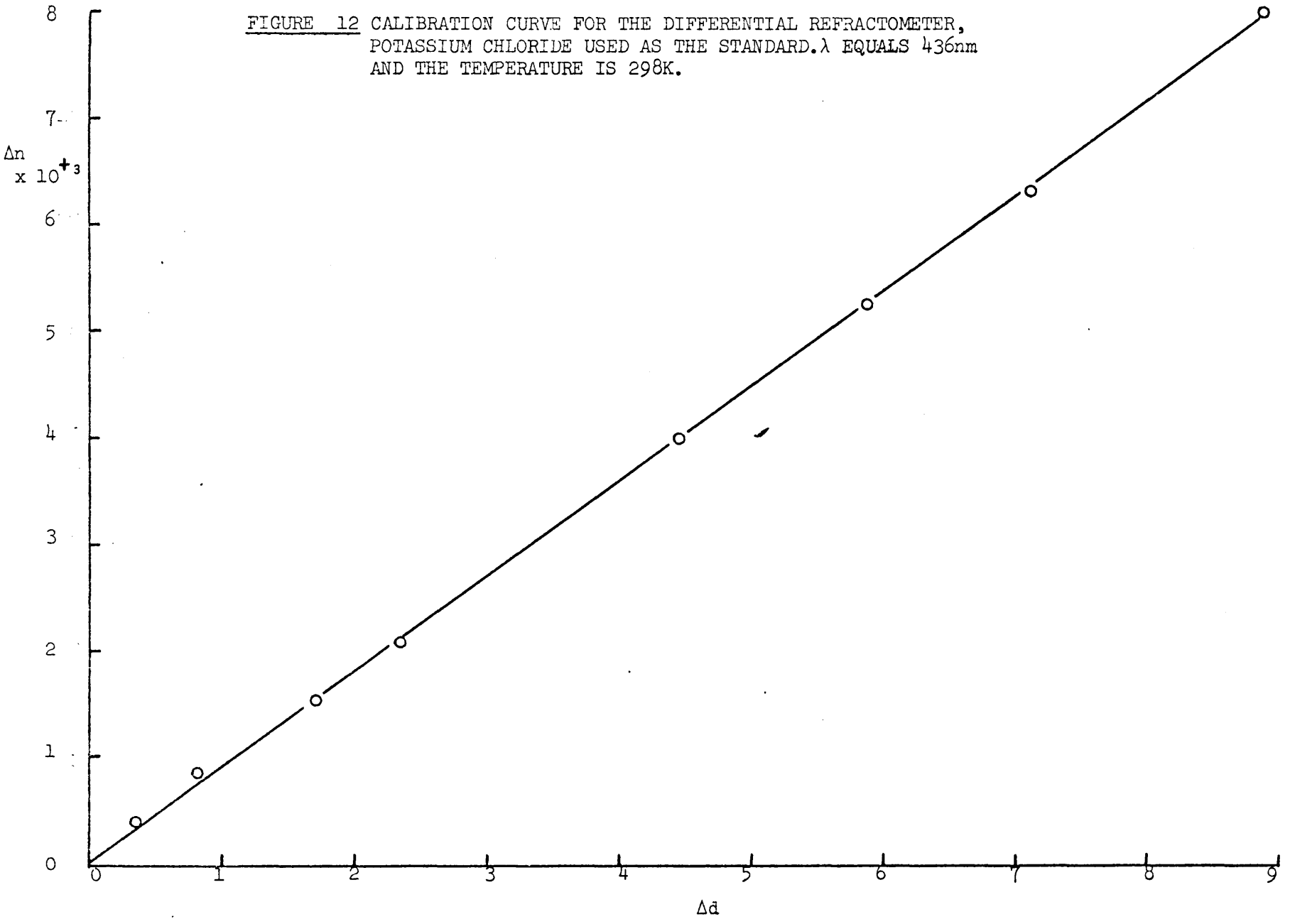

FIGURE 12 CALIBRATION CURVE FOR THE DIFFERENTIAL REFRACTOMETER, POTASSIUM CHLORIDE USED AS THE STANDARD. λ EQUALS 436nm AND THE TEMPERATURE IS 298K.

Figure 12. The value for calibration constant, K, at 436nm is

$K = 0.9 \times 10^3$ instrument units.

Knowing K, Δn could be calculated for any particular polymer/solvent system from measurements of Δd. Six different concentrations in the range $0.02 g/cm^3$ to $0.005 g/cm^3$ were measured to find Δn.

Δn was plotted against C and the slope calculated to give dn/dc.

C H A P T E R II

PREPARATION OF AMYLOSE ESTERS

SECTION I PREPARATION OF LINEAR AMYLOSE

(a) EXTRACTION OF STARCH FROM POTATOES

The potatoes (var. Golden Wonder) were thickly peeled, chopped and put under methanol. The alcohol prevents excessive enzymic activity which might alter the structure of the starch granule. Small batches with a little methanol were masticated in a Sunbeam blender for two minutes. The resultant pulp was filtered through two layers of fine muslin and the filtrate left to stand for a few minutes, by which time the starch had settled out. The supernatant liquid was discarded and the starch washed by repeated sedimentation in 0.1M sodium chloride solution. When the liquid layer was clear most of the cell debris had been removed and the washing process was stopped.

The starch was suspended in 0.1M sodium chloride solution and toluene, 10:1 by volume, respectively, and shaken overnight. By this process, the protein associated with the starch was denatured and separated from the granules. The toluene/brine layer was discarded and this process repeated until no coagulated protein was visible in the toluene layer. The protein appears as froth at the interface between the two liquids. The purified starch was stored under brine/toluene.

Twenty-five kilograms of potatoes will yield approximately one kilogram of wet starch.

(b) EXTRACTION OF LINEAR AMYLOSE FROM POTATO STARCH

In this method of extraction the amylose is leached out of the starch granules leaving mainly amylopectin with some "non-linear" amylose.

Approximately 2.5dm^3 of distilled water were heated to 335K in a three-necked flask fitted with a stirrer and a nitrogen bleed. Enough wet starch was added to the contents of the flask, as a slurry in a small amount of water, so that the concentration of starch in water was approximately 20g/dm^3. The suspension was stirred for one hour at this temperature. The flask was stoppered and allowed to cool to room temperature overnight.

On cooling, the suspension containing swollen granules separated out into a gelatinous layer (mainly amylopectin) leaving an aqueous supernatant layer which contained the soluble amylose. The supernatant was separated from the gelatinous layer by decantation and centrifugation and then heated to about 348K under nitrogen. Butan-1-ol was added in the proportion 1 part butan-1-ol to 10 parts solution, i.e. sufficient to ensure complete saturation of the solution. Stirring was continued for 10 minutes at this temperature. The flask was stoppered and the contents allowed to cool to room temperature overnight. A fine, white precipitate settled out which was the amylose/butan-1-ol complex. This was centrifuged off and dissolved in sufficient dimethyl sulphoxide (DMSO) to make a solution whose approximate concentration was 30g/dm^3. This solution was stirred at room temperature and butan-1-ol added slowly until the first permanent turbidity was observed. The material which precipitated was a fraction containing any non-linear amylose which might be present (2) and was discarded. The remaining amylose was precipitated in butan-1-ol, filtered off and redissolved in DMSO. Further purification of the

amylose was achieved by forming the complex with butan-1-ol twice more from DMSO solutions. The final amylose/butan-1-ol complex was stored under butan-1-ol until it was required.

One kilogram of wet starch will yield approximately 20 grams of linear amylose.

Analysis of Amylose

The amylose was analysed for linearity using the enzyme β-amylase. A β-amylase limit of 98% was found indicating that within experimental error the prepared amylose was linear. The (β + Z) limit was 101%, showing that the amylose contained no contaminating amylopectin.

The author is indebted to Dr. W. Banks for carrying out this analysis.

SECTION II PREPARATION OF AMYLOSE ESTERS

(a) PREPARATION OF AMYLOSE TRIACETATE

The method of Higginbotham and Morrison (39) was followed. AnalaR pyridine dried over molecular sieves and AnalaR acetic anhyride were used as the reagents.

Pyridine ($200cm^3$) and acetic anhydride ($200cm^3$) were added to amylose (7.5g) in a flask and stirred for three days at room temperature. After this time had elapsed the reaction mixture was poured into ice water, to precipitate the triacetate which was filtered off and washed with water to remove any acid. The precipitate was dissolved in chloroform, the solution filtered through a G3 sintered glass filter then injected into 60-80 petroleum ether to reprecipitate the product. This precipitation process was repeated and then the final product was dried in a vacuum oven.

(b) PREPARATION OF AMYLOSE TRIPROPIONATE

The method of preparation was similar to that employed for the acetate. The first batch of amylose to be used had been dried and was found to be difficult to dissolve in pyridine alone so formamide was also added to aid solvation. AnalaR reagents were used.

Method One

Amylose (8.5g) was added to formamide ($100cm^3$). To these were added pyridine ($150cm^3$) and propionic anhydride ($250cm^3$). The mixture was stirred for three days at room temperature. After this time a small amount of amylose still

remained undissolved. The reaction mixture was filtered to remove the unreacted material and then injected into methanol at 243K. The partially esterified product was isolated and dissolved in chloroform. The solution was injected into 60-80 petroleum ether, the precipitate filtered off and dried overnight in a vacuum oven.

The product isolated above was considered to be only partially esterified since some of the amylose remained undissolved. To make certain that complete substitution occurred the esterification was continued. Pyridine ($150cm^3$) and propionic anhydride ($150cm^3$) were added to the partially esterified amylose and the mixture left to stir for a further three days. The product was then isolated as above and labelled P.

Method Two

Amylose/butanol complex (12g) was added to pyridine ($200cm^3$) and propionic anhydride ($200\ cm^3$). The amylose dissolved completely and the reaction mixture was left to stir for five days at room temperature. The product was isolated as for Method One and labelled S.

(c) PREPARATION OF AMYLOSE TRIBUTYRATE

Two samples of the tributyrate were obtained using different methods of preparation. The first method involved refluxing the reaction mixture for a short time. The second method was similar to that used to prepare the acetate and propionate. AnalaR reagents were used.

Method One

Butyric anhydride ($450cm^3$) and pyridine ($450cm^3$) were

added to the amylose (9.3g) in a round-bottomed flask fitted with a reflux condenser. The flask was heated on a water bath at 373K for two hours and then allowed to cool. The reaction mixture was poured into methanol at 243K, to precipitate the ester which was filtered off using a cold filter funnel and washed with cold methanol. The product was quickly dissolved in chloroform, reprecipitated in methanol, filtered off and finally dried in a vacuum oven. This batch was labelled X.

Method Two

Pyridine ($200cm^3$) and butyric anhydride ($250cm^3$) were added to the amylose/butanol complex (9.4g). The mixture was stirred for approximately one hour at 313K to help dissolution and then left to stir at room temperature. After seven days the reaction mixture was filtered through a G3 sintered glass filter, to remove any unreacted amylose, and injected into methanol at 243K. The precipitate was filtered off and washed with cold methanol. Pyridine ($150cm^3$) and butyric anhydride ($150cm^3$) were added to the partially esterified material and the mixture stirred for a further two days at room temperature. The final product was isolated as above and labelled B.

(d) ANALYSIS OF THE ESTERS

The degree of substitution (D.S) of the three esters has to be estimated. The normal method of analysing amylose esters is by a saponification technique in which the ester groups are reacted with potassuim hydroxide.

The sample to be analysed is pulverised, 0.5g accurately weighted out and placed in a 250cm^3 conical flask. 50cm^3 of an ethanol/water mixture (3:1) are added, the flask lightly stoppered and then warmed at 323K for 30 mins. The contents of the flask are allowed to cool to room temperature and 40cm^3 of an aqueous solution of 0.5M potassium hydroxide added using a burette or pipette. The mixture is left for 72 hours. A blank containing the unsubstituted amylose plus the other reagents is run at the same time. The excess potassium hydroxide is back titrated using an aqueous solution of 0.5M hydrochloric acid and phenol phthalein as indicator. The D.S of the sample can be calculated from this information.

$$\% \text{ Alkyl} = \frac{\{\text{cm}^3(\text{blank}) - \text{cm}^3(\text{sample})\} \times \text{molarity of acid} \times 100 \times M_{Alkyl}}{\text{Sample weight g. (dry)} \times 1000}$$

where M_{Alkyl} is the molecular weight of the alkyl group.

$$D.S = \frac{M_A \times \% \text{ Alkyl}}{M_{Alkyl} \times 100 - (M_{Alkyl} \times \% \text{ Alkyl})}$$

where M_A is the molecular weight of amylose.

Analysis by saponification requires a large quantity of material since duplicate measurements are made for each sample. Because of the lack of material another way of analysing for the degree of substitution had to be found. This was done by comparing the Infra-red spectra of samples of known D.S with the samples to be analysed.

The Infra-red spectra of samples of known D.S (analysed using the saponification technique) were examined using a Perkin Elmer 457 spectrophotometer. Dry samples were dissolved

in silica gel dried chloroform, concentrations being approximately 0.1g/cm^3. The spectra were obtained using sodium chloride plates. The solution was spread between the two plates, which were then separated and the chloroform removed in a current of dry air. The samples of unknown D.S were examined in the same way.

Comparison of the spectra indicated that the D.S of the unknown samples was better than 2.9 compared with a theoretical value of 3. The methods of preparation used for the two different samples of both the propionate and the butyrate were shown to produce polymers with the same D.S.

SECTION III FRACTIONATION OF THE ESTERS

(a) AMYLOSE ACETATE

Amylose acetate was dissolved in sufficient nitromethane to make up a solution with a concentration of about 1.5g amylose/100cm^3 nitromethane. The solution was placed in a large round-bottomed flask, fitted with a stirrer, in a water-bath thermostatted at 298K. Methanol was used as the precipitating agent and was added slowly to the flask until the first permanent turbidity occurred. The flask was stirred continuously. The temperature of the water-bath was raised about 10K and stirring continued until the precipitated fraction had redissolved. The solution was allowed to cool down to 298K overnight. The fraction settled out on the sides of the flask. The supernatant liquid was poured into another flask and the fraction left behind was dissolved in chloroform and reprecipitated in 60 - 80 petroleum ether. The precipitate was filtered off, dried and labelled F1. Fractionation was continued in this way until no more polymer was present in solution.

F1 was redissolved in nitromethane and refractionated into 4 fractions. Eight fractions were isolated altogether.

(b) AMYLOSE PROPIONATE

The propionate proved much more difficult to fractionate and various systems were used. Batch P was fractionated using the same method as for the acetate although it was found necessary to change the system half way through. This was because the volume of precipitant needed to bring a fraction down was very large at the low molecular weight end. Fractionation of S was first tried using ethyl acetate/60 - 80 petroleum

ether, as for P, but on addition of petroleum ether nearly all the polymer came down. The next system which was tried was toluene/methanol. In this case on leaving the flask overnight the whole system gelled solid. Nitromethane/methanol was finally used although this too did not behave in a conventional manner.

Batch P

The same procedure used for the acetate was tested with a toluene (solvent)/methanol (precipitant) system. The fractions precipitated as fine powders and had to be separated by centrifugation. After 8 fractions had been isolated the system was very dilute and volumes involved were becoming unwieldy. The remaining solution was evaporated to dryness and the polymer redissolved in ethyl acetate to give a solution of approximate concentration 1.5g propionate/100cm^3 ethyl acetate. Methanol was used again as the precipitating agent. In this system the fractions settled to the sides of the flask and were easily isolated. Thirteen fractions were isolated altogether.

Batch S

The fractionating system used was nitromethane (solvent)/ methanol (precipitant). A solution of 2g propionate/100cm^3 nitromethane was prepared. Methanol was added until the first permanent turbidity occurred and the flask was heated to redissolve the fraction and then allowed to cool overnight as before. Part of the fraction settled to the sides of the flask and part remained as a fine, powdery suspension. The supernatant was poured off and the powdery fraction isolated

by centrifugation and labelled S1. The other fraction was isolated and labelled S2. Methanol was added to the remaining solution. S3 came down very rapidly and was centrifuged off. S4 was isolated in the same way. The final fraction was labelled S5.

S2 was then refractionated, into 4 fractions, using nitromethane/methanol. S2a settled out immediately on addition of methanol. The supernatant was poured off and centrifuged, bringing down fraction S2b. The solution was left standing for one hour and S2c came down. More methanol was added to give the final fraction S2d.

Eight fractions in all were isolated. All the fractions were dissolved in benzene and freeze dried.

(c) AMYLOSE BUTYRATE

The same system toluene/60 - 80 petroleum ether was used for both samples of butyrate.

Batch X

Batch X was fractionated, using the same method as for the acetate, into 12 fractions. The fractions were isolated, dissolved in benzene and freeze dried.

Batch B

Batch B was fractionated in the same way as X, into 4 fractions.

C H A P T E R III

HYDRODYNAMIC PROPERTIES OF AMYLOSE ESTERS

SECTION I HYDRODYNAMIC PROPERTIES OF AMYLOSE TRIBUTYRATE

RESULTS AND DISCUSSION

(1) NUMBER AVERAGE MOLECULAR WEIGHTS, $\bar{M}_n$

Values of $\bar{M}_n$ were measured in methyl ethyl ketone (MEK) at 295.5K for all fractions. The molecular weights were all within the range encompassed by the membrane osmometer. Fraction B2 was too small to allow measurements to be made. The plots of π/C against C are shown in Figure 13 and the values of $(\pi/C)_0$, $\bar{M}_n$ and A_2 obtained from them are recorded in Table III.1, where the parameter Γ_2 in equation (I.25) is related to the second vivial coefficient A_2 by

$$\frac{\Gamma_2}{M} = A_2 \qquad (1)$$

Table III.1: Results from osmotic pressure measurements on ATB samples in MEK at 295.5K

ATB samples	$(\frac{\pi}{C})_o$ $cm^{+1}g^{-1}.dm^3$	$\bar{M}_n \times 10^{-5}$	$A_2 \times 10^4$ $cm^3g^{-2}mol$
B3	0.080	3.91	1.61
B4	0.166	1.88	2.23
B5	0.348	0.898	2.34
X9	0.296	1.06	2.64
X10b	0.466	0.671	3.13
X11	0.480	0.651	8.60
X12	0.640	0.488	6.15
X13	0.830	0.376	7.98

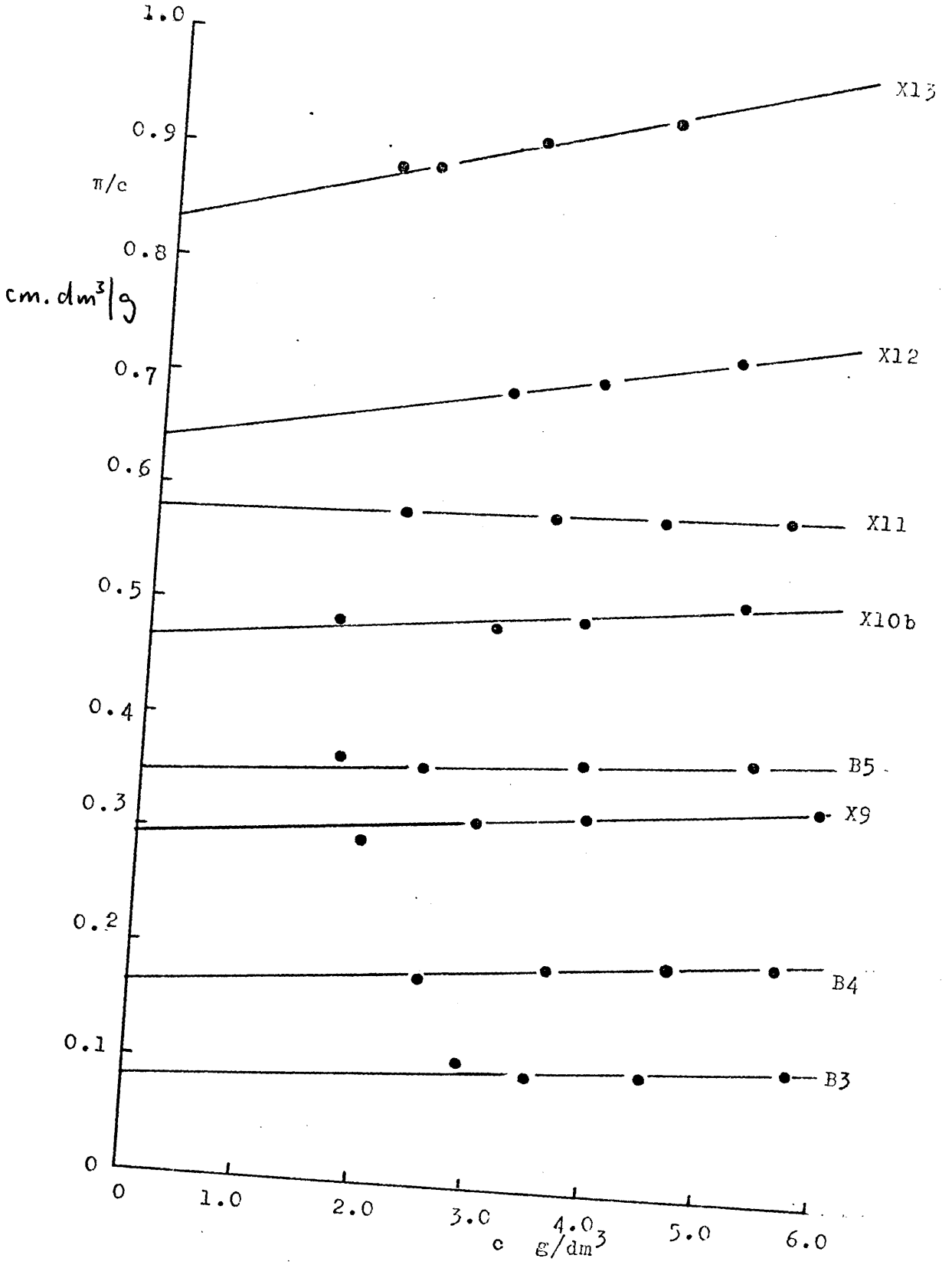

FIGURE 13 PLOTS OF π/c AGAINST c FOR ATB/MEK AT 295.5K

The values of A_2 appear to increase generally with decreasing molecular weight, but the reproducibility of A_2 is rather poor because of the uncertainties involved in its determination. The empirical relation

$$A_2 = K_2 M^{-\gamma} \qquad (2)$$

is followed but the exponent γ has a larger value than that predicted by theory (17). Figure 14 shows a plot of log A_2 against log $\bar{M}_n$. If the three lowest molecular weight points are disregarded a line with a slope of 0.26 can be drawn through the remaining points, but if all the points are used a slope of 0.68 is found. According to Kurata and Stockmayer (17) the largest possible value for γ should be about 0.15 which is considerably lower than the experimental value, but according to Casassa (40) could be 0.25 in very good solvents.

Kurata et al (41) put forward the following expression

$$A_2 = \frac{K_a}{M^{\frac{1}{2}}} + K_b \qquad (3)$$

where $K_a = 1.65 \times 10^{23}\ A^3$

and $K_b = 0.968 \times 10^{23}\ B$

$A = (\bar{r}_o^2/M)^{1/2}$

According to equation (3) it should be possible to derive the unperturbed dimensions of a polymer from a knowledge of A_2 and M. The data for the butyrate (ATB) from osmotic pressure measurements was calculated according to equation (3) and the plot shown in Figure 15. The five highest molecular weight points obey a linear relationship and a line drawn through these gives an intercept of 6.6×10^{-2}. This intercept is equivalent to a value of $(\bar{r}_o^2/M)^{\frac{1}{2}}$ of 737×10^{-11} cm for ATB in MEK. This value of the characteristic ratio correlates well

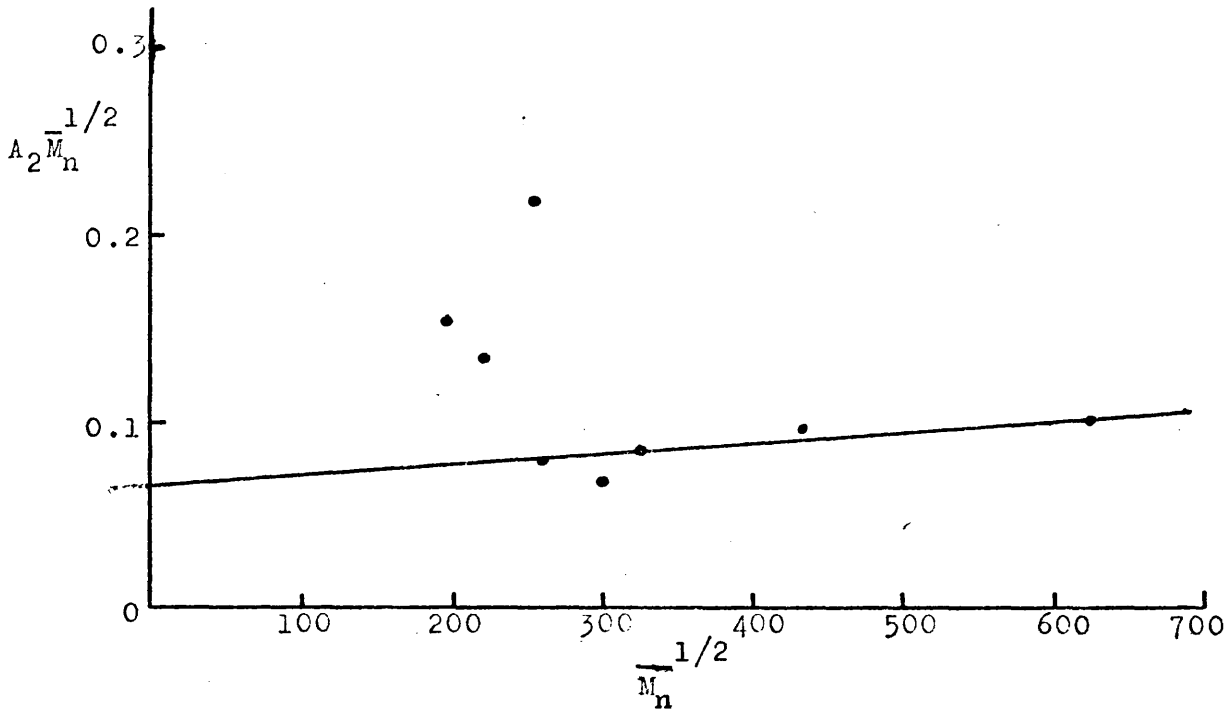

FIGURE 15 DATA FOR ATB IN MEK ACCORDING TO EQUATION (3).

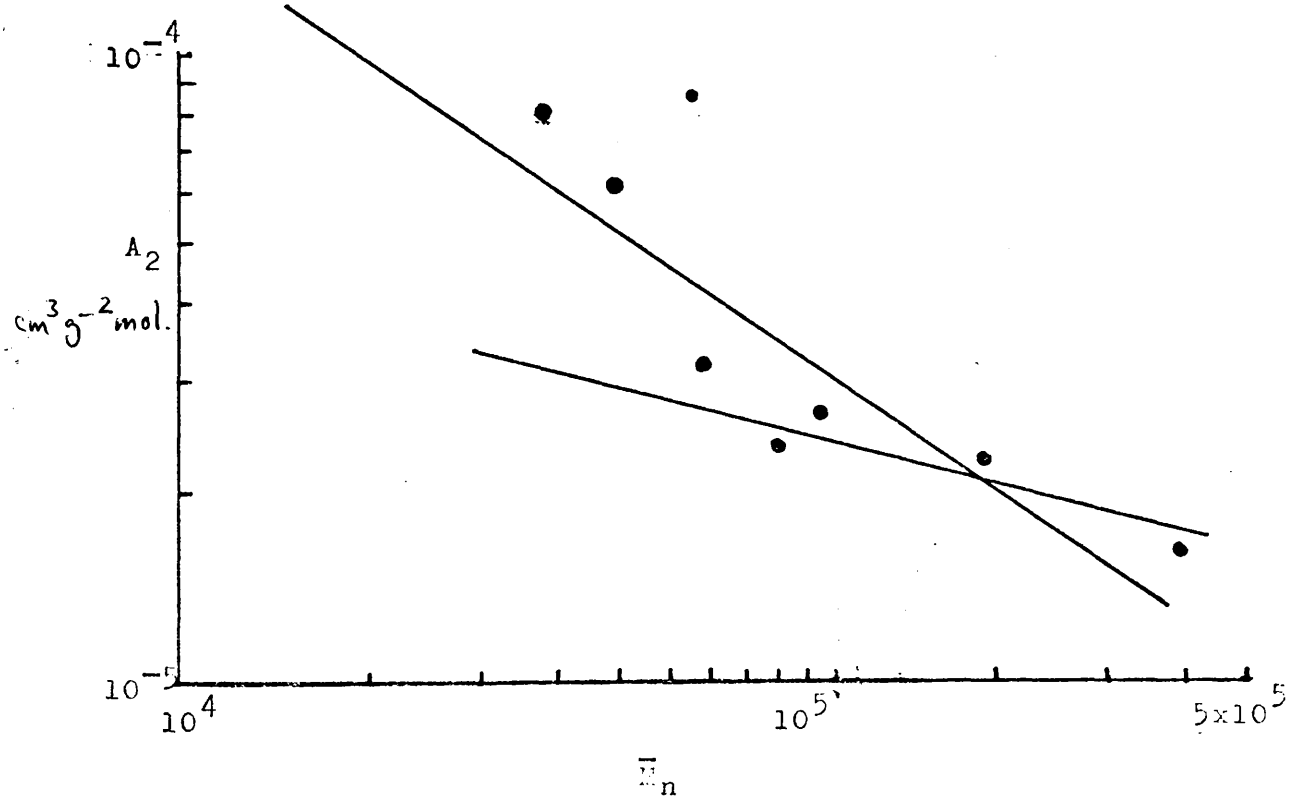

FIGURE 14 DATA FOR ATB IN MEK ACCORDING TO EQUATION (2).

with that calculated from viscosity data using an experimental value of Φ_o, as shown in Table III.9, but is higher than those values calculated using the limiting value of Φ_o and $\Phi(\varepsilon)$. Considering the uncertainties in the values of A_2 the correlation is surprisingly good.

The full data for ATB in MEK does not fit either equation (2) or (3) because of the relatively high values of A_2 for the low molecular weight fractions.

According to the present theories the ratio $A_2M/[\eta]$ should be a function of the expansion coefficient, thus

$$A_2M/[\eta] = f(\alpha) \qquad (4)$$

Orofino and Flory (74) have proposed that $f(\alpha)$ is given by

$$f(\alpha) = \frac{\sqrt{32\ \pi\ N_A}}{27\ \Phi_o}\ 1n[1 + 0.885\ (\alpha^2-1)] \qquad (5)$$

and $\Phi_o = 2.87 \times 10^{23}$ where this is the limiting value according to the theory of Kirkwood, Riseman, Auer and Gardner (42). The values of α calculated using experimentally determined A_2, $\bar{M}_n$ and $[\eta]$ measured in MEK are shown in Table III.2. Values of α_η determined from viscosity data are also included. It can be seen that equations (4) and (5) give α for the high molecular weight fractions which are comparable to α_η values but high values for the other fractions. The expansion coefficient calculated using the Flory-Orofino expression is influenced by A_2 which in this case shows a peculiar dependence on M thus producing the variation in α seen in Table III.2. Use of the limiting value of Φ_o allows a reasonable estimate of α to be made from equation (5).

An experimental value of Φ_o can be calculated using the Flory and Fox relation

$$[\eta] = \Phi_0(\bar{r}^2)^{3/2}/M \qquad (6)$$

where in this case Φ_0 has been corrected for heterogeneity because according to Newman et al (43) number average values must be used in equation (6), thus

$$\Phi_0 = q_\Phi[\eta]\bar{M}_w/(\bar{r}^2)^{3/2} \qquad (7)$$

where

$$q_\Phi = \frac{(h+2)^{3/2}\ \Gamma(h+2)}{(h+1)^2\ \Gamma(h+1.5)}$$

If this is done for ATB in MEK the values of Φ_0 as shown in Table III.3 are derived. Also shown in the same table are the α values calculated using the Flory-Orofino expression and experimental Φ_0 values. The experimental value of Φ_0 is very much lower than the limiting value of 2.87×10^{23}. The expansion coefficients calculated in Table III.3 are very much smaller than the α_η values shown in Table III.2 Equation (5) does not hold using experimental values of Φ_0 but does for the limiting value.

Table III.2: Comparison of values of α obtained using the Flory-Orofino expression with α_η from viscosity data for ATB in MEK

ATB Sample	α from A_2	α_η
B3	1.28	1.46
B4	1.37	1.35
B5	1.28	1.30
X9	1.35	1.29
X10b	1.30	1.24
X11	2.35	1.25
X12	1.76	1.22
X13	2.37	1.17

Table III.3: α values using the Flory-Orofino expression and experimental values of Φ_0

ATB Sample	q_Φ	$\Phi_0 \times 10^{-23}$	α
B3	1.67	1.19	1.11
B4	1.57	0.92	1.11

(2) WEIGHT AVERAGE MOLECULAR WEIGHTS, $\bar{M}_w$

Measurements of $\bar{M}_w$ for B2, B3 and B4 were made by light scattering in both MEK and ethyl acetate (EA) and an average of the two values was used in all calculations involving $\bar{M}_w$. All other values of $\bar{M}_w$ were calculated using experimentally derived $\bar{M}_n$ and the distribution measured by G.P.C. (see Appendix and section on G.P.C.). Measurements of $\bar{M}_w$ were made using vertically polarised blue light.

The refractive index increment, (dn/dc), was measured in MEK and EA according to the method outlined in Chapter I. The values of (dn/dc) for ATB in MEK and EA were 0.0915 $cm^3 g^{-1}$ and 0.0978 $cm^3\ g^{-1}$, respectively. The graphs of Δn against c are shown in Figure 16.

Light scattering data were plotted according to the method of Zimm as described in Chapter I. A typical Zimm plot is shown in Figure 17. Values of A_2, $\bar{M}_w$, $(\bar{s}_z^2)^{\frac{1}{2}}$ and $(\bar{r}_z^2/\bar{M}_w)^{\frac{1}{2}}$ for ATB in MEK are shown in Table III.4. Comparison of the second virial coefficients derived using light-scattering and osmometry shows that the A_2 values from light-scattering are considerably smaller than the osmotic values of A_2.

Unfortunately no θ-solvent has been found for the butyrate so that an estimation of the unperturbed dimensions has had

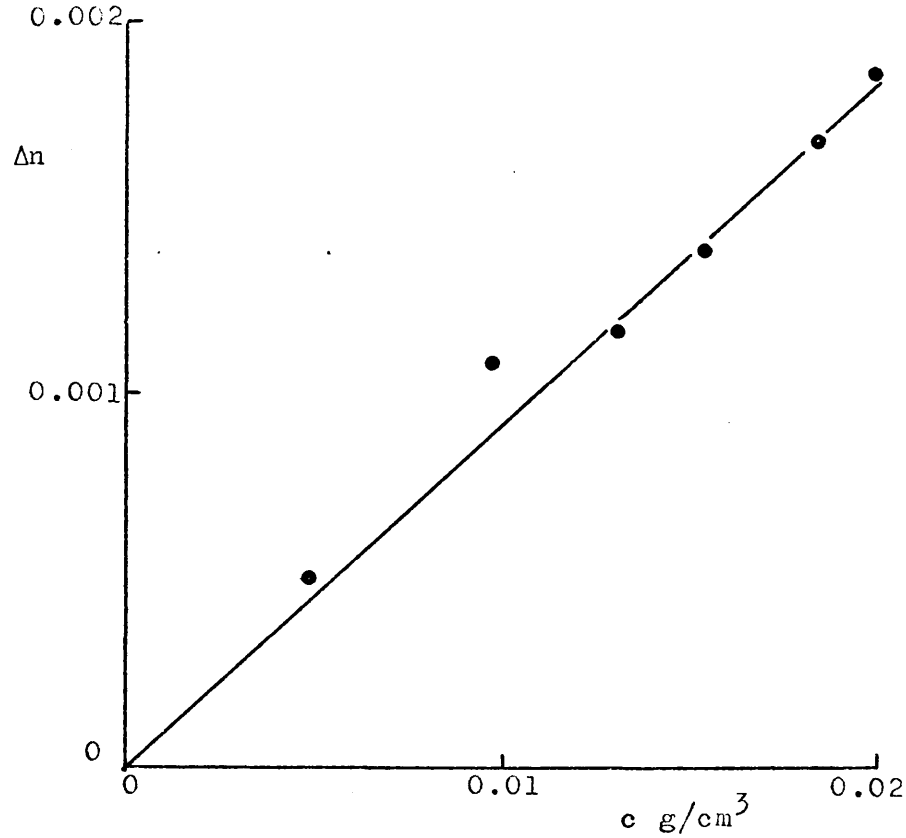

FIGURE 16a PLOT OF Δn AGAINST c FOR ATB/MEK AT 298K, λ EQUALS 436nm.

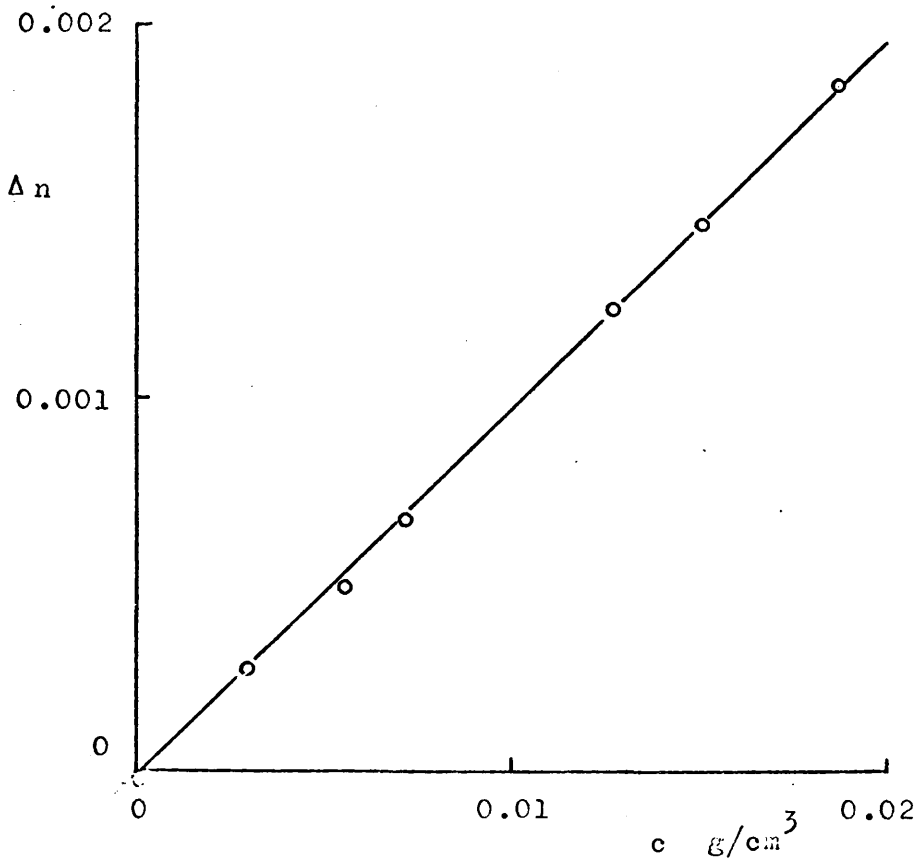

FIGURE 16b PLOT OF Δn AGAINST c FOR ATB/EA 298K. λ EQUALS 436nm.

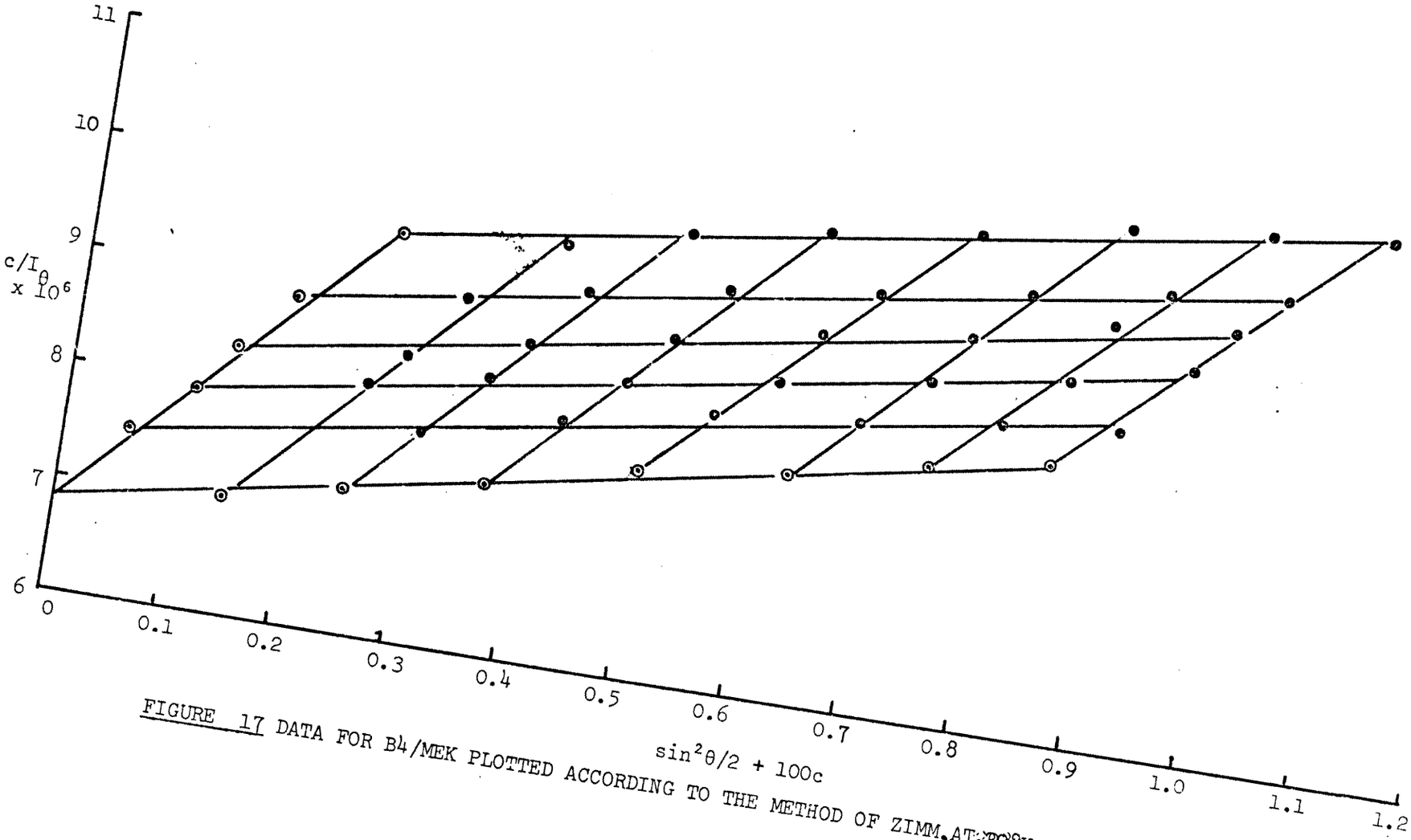

FIGURE 17 DATA FOR B4/MEK PLOTTED ACCORDING TO THE METHOD OF ZIMM, AT 298K.

to be carried out using data from good solvents. Several methods are available based mainly on the use of $[\eta]$ data. These are described in the section on unperturbed dimensions.

Table III.4 Data for ATB in MEK at 298K.

ATB Sample.	$\bar{M}_w \times 10^{-6}$	$(\bar{s}_z^2)^{\frac{1}{2}} \times 10^8$ cm	$(\bar{r}_z^2)^{\frac{1}{2}} \times 10^8$ cm	$[\bar{r}_z^2/M]^{\frac{1}{2}} \times 10^{11}$ cm	α	$A_2 \times 10^6$ $cm^3 g^{-2} mol$
B2	1.557	652	1611	1291	1·47 ~~1.11~~	1.45
B3	0.613	379	937	1196	1·36 ~~1.08~~	2.26
B4	0.275	251	621	1185	1·35 ~~1.07~~	2.99

G.P.C. Results

The results for the molecular weight distributions are shown in the Appendix, and were used in conjunction with the $\bar{M}_n$ measurements from osmometry to calculate $\bar{M}_w$ values for the lower molecular weight fractions. The distributions calculated by the two methods, G.P.C. and, light-scattering and osmometry agree well for B4 but not so well for B3.

(3) VISCOSITY MEASUREMENTS

Measurements of the limiting viscosity number, $[\eta]$, were made in carbon tetrachloride (CT), tetrahydrofuran (THF), MEK and EA at 298K. The temperature dependence of $[\eta]$ was also examined in EA.

Temperature dependence of $[\eta]$

The limiting viscosity number of ATB has a negative temperature dependence in the lower range of temperatures studied. This is in common with cellulose derivatives such as the tributyrate (19) and tricarbanilate (18), but the

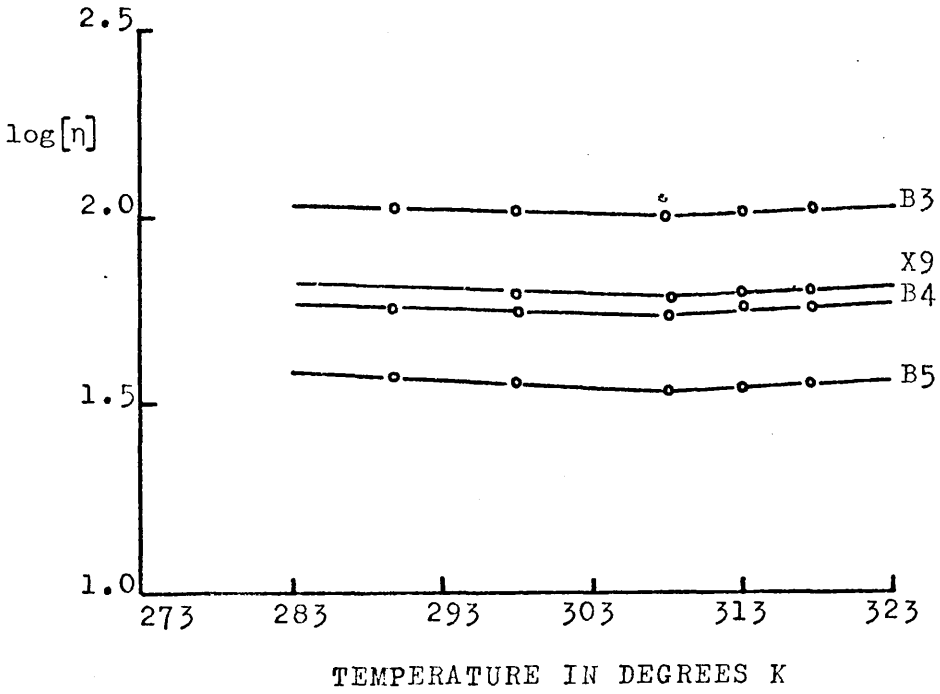

FIGURE 18 TEMPERATURE DEPENDENCE OF VISCOSITY. VARIOUS FRACTIONS OF ATB IN EA.

dependence is much less pronounced than that for the cellulose derivatives.

The variation of $[\eta]$ with temperature is due to the change in the effective dimensions of the molecule. The relation between $[\eta]$ and the dimensions of the molecule can be described by the Flory and Fox (46) relation

$$[\eta] = \Phi_0(\bar{r}^2)^{3/2}/M \qquad (6)$$

or

$$[\eta] = \Phi_0[\bar{r}_0^2/M]^{3/2}M^{1/2}\alpha^3 \qquad (8)$$

Differentiation of the logarithmic form of this equation with respect to temperature gives

$$\frac{d\log[\eta]}{dT} = \frac{d\log\Phi_0}{dT} + \frac{d\log[\bar{r}_0^2/M]^{3/2}}{dT} + \frac{d\log\alpha^3}{dT} \qquad (9)$$

The value for d log $[\eta]$ /dT was calculated from the plot of log $[\eta]$ against T shown in Figure 18.

Table III.5: Temperature dependence of $[\eta]$ for ATB in EA

ATB Samples	$-\Delta\log[\eta]/dT \times 10^3$ cm^3 g^{-1}K^{-1} 289.8K to 307.9K	$\Delta\log[\eta]/dT \times 10^3$ cm^3 g^{-1} K^{-1} 307.9K to 317.5K
B3	1.2	1.7
B4	1.3	2.5
B5	1.2	1.7
X9	1.5	2.0

The values of d log $[\eta]$ /dT calculated from viscosity data at 289.8, 298, 307.9, 313 and 317.5K are recorded in Table III.5. It is seen that the values show no particular trend with

molecular weight and are approximately a factor of 100 smaller than those for the cellulose derivatives (45, 47).

An unusual feature of the temperature dependence of $[\eta]$ is the minimum exhibited by each plot shown in Figure 18. As far as is known this phenomenon has not been observed previously. The minima occur at approximately 308K for each fraction. The positive value of d log $[\eta]$/dT is slightly higher on average than the negative value exhibited below 308K. These values are also recorded in Table III.5.

The temperature coefficient of $[\eta]$ will depend mainly on the factor d log $(\bar{r}_0^2/M)^{3/2}$/dT, and on d log α^3/dT which represents the change in the excluded volume effect with temperature. These two effects are difficult to separate unless the values of the unperturbed dimensions are available. The negative temperature dependence of $[\eta]$ could be accounted for by an increase in flexibility of the chain which should be reflected in a decrease in $(\bar{r}_0^2/M)^{3/2}$ with temperature. If the minima are to be believed a point must come when perhaps due to steric considerations the coil arrives at its limit of flexibility and can no longer decrease in size. Above this temperature the coil expands as indicated by the positive dependence of $[\eta]$ on temperature. A positive dependence is more usual for vinyl polymers and the negative dependence found for cellulose derivatives has been explained by postulating that the molecules are stiff and inflexible.

Table III.6 shows the variation in a, the exponent in the Mark-Houwink expression, with temperature, very little change can be detected.

Table III.6: Mark-Houwink exponents for ATB in EA at various temperatures

Temperature in K	a
289.8	0.76
298	0.74
307.9	0.75
313	0.78
317.5	0.77

Viscosity - Molecular Weight Relationships

The $[\eta]$ - M relations for ATB in EA, MEK, CT and THF at 298K are given below. Relations for both $\bar{M}_n$ and $\bar{M}_w$ have been quoted because the distribution $\bar{M}_w/\bar{M}_n$ is not the same for all fractions. Not only K but also a, will vary according to which molecular weight average is used. From Figure 19 it can be seen that the adoption of the G.P.C. distributions was valid over the molecular weight range under consideration. The correlation between $\bar{M}_w$ derived from light scattering and $\bar{M}_w$ calculated from the G.P.C. distribution using osmotic values of $\bar{M}_n$ is excellent.

EA $[\eta] = 5.59 \times 10^{-3} \bar{M}_w^{0.74}$ at 298K.

$[\eta] = 9.86 \times 10^{-3} \bar{M}_n^{0.72}$

MEK $[\eta] = 3.39 \times 10^{-3} \bar{M}_w^{0.77}$

$[\eta] = 4.88 \times 10^{-3} \bar{M}_n^{0.77}$

CT $[\eta] = 2.65 \times 10^{-3} \bar{M}_w^{0.82}$

$[\eta] = 6.24 \times 10^{-3} \bar{M}_n^{0.77}$

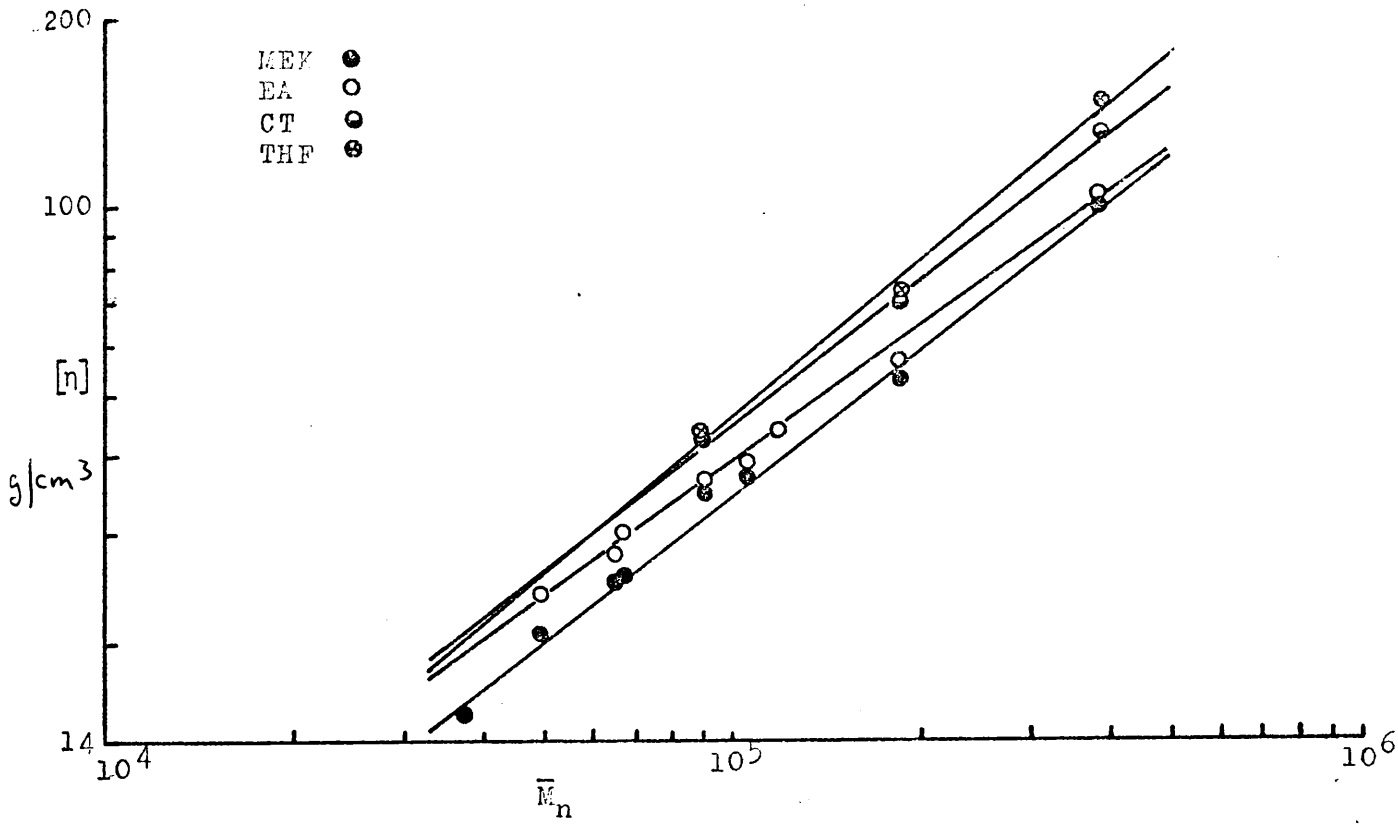

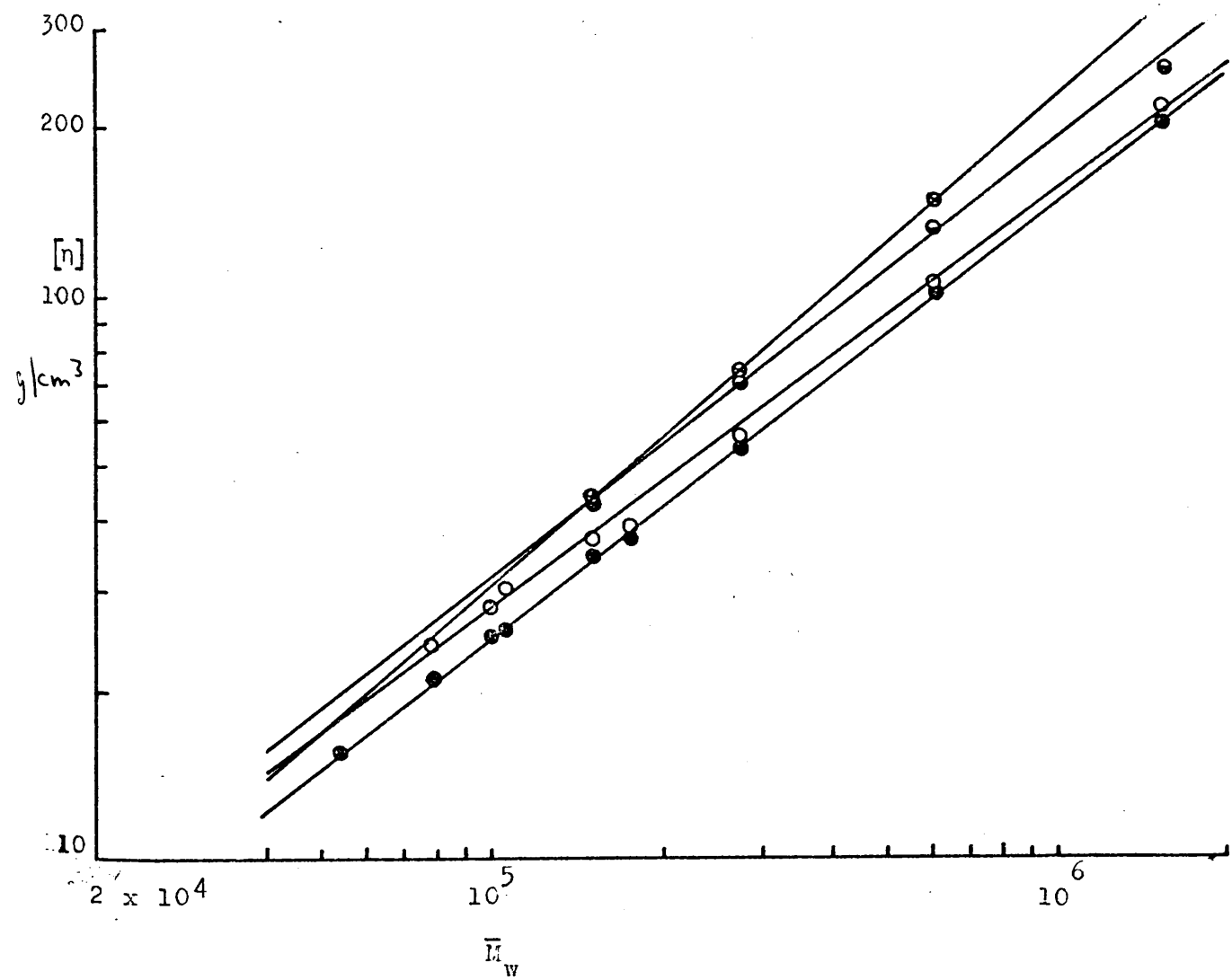

FIGURE 19 VISCOSITY-M RELATIONSHIPS FOR ATB AT 298K.

THF $[\eta] = 1.66 \times 10^{-3} \bar{M}_w^{0.86}$

$[\eta] = 3.24 \times 10^{-3} \bar{M}_n^{0.83}$

Unperturbed dimensions from intrinsic viscosity

Ideally the unperturbed dimensions of a polymer molecule should be determined in a θ-solvent at a given temperature. Unfortunately no θ-solvent has been found for amylose tributyrate, consequently estimation of the unperturbed dimensions is based entirely on data from good solvents. The most reliable procedures are based on the use of viscosity data and a number of extrapolation techniques have been proposed.

The dimensions of a long chain molecule are influenced by interactions between chain segments. These interactions can be divided into two categories, 'short' range and 'long' range. The 'short' range interactions occur between near neighbours or groups of atoms separated by only a short distance. These interactions determine the configuration of the chain i.e. bond angles and the torques hindering internal rotations. 'Long' range interactions take place between elements of the chain which are separated by very many bonds or non-bonded elements i.e. other chains or the solvent. The two categories could also be termed inter and intra molecular interactions. To be able to measure unperturbed dimensions from viscosity data it is necessary to be able to separate the two effects. Under θ-conditions the 'long' range interactions disappear and the dimensions of the chain depend only on the 'short' range interactions.

The expansion of a molecule due to 'long' range interactions gives rise to the excluded volume effect which is expressed in

ATB fraction	$\bar{M}_n \times 10^{-6}$	$\bar{M}_w \times 10^{-6}$	cm^3/g [η] THF 298K	[η] MEK 298K	[η] CT 298K	[η] EA 298.8K	[η] EA 298K	[η] EA 307.9K	[η] EA 313K	[η] EA 317.5K
B2	-	1.557		200.0	253.4		217.3			
B3	0.391	0.613	147.8	100.6	132.6	105.3	103.9	99.8	101.6	104.1
B4	0.188	0.275	73.2	53.2	70.1	57.1	56.3	53.7	57.1	56.6
B5	0.0898	0.150	43.5	34.5	43.2	37.0	36.5	33.8	33.7	34.9
X9	0.106	0.176		37.0			39.2	36.3	37.7	39.8
X10b	0.0671	0.105		25.5			30.4	25.1		
X11	0.0651	0.0997		25.1			27.8	25.4		27
X12	0.0488	0.0781		20.8			23.9	21.2		22.1
X13	0.0376	0.0538		15.4						15.8

Table III.7. $[\eta]$ - M data for ATB.

terms of α, the linear expansion coefficient defined by $\alpha^2 = \bar{r}^2/\bar{r}_0^2$ where $\bar{r}^2$ and $\bar{r}_0^2$ are the perturbed and unperturbed mean square end-to-end distance of the polymer chain, respectively.

The parameter α is thought to be a function of a single variable z which is precisely defined by

$$z = (3/2\pi)^{3/2} B M^{1/2} (\bar{r}_0^2/M)^{3/2} \qquad (10)$$

where B is an interaction parameter. At the θ-point B = 0 and $\alpha = 1$.

For small values of z, exact expressions for the expansion factor can be obtained by means of perturbation calculations using (48 - 50).

$$\alpha^2 = 1 + (4/3)z - 2.08z^2 + \ldots\ldots \qquad (11)$$

This expression converges only very slowly and higher terms are difficult to obtain; these difficulties mean that it is only applicable to very small values of z i.e. near the θ-point.

Obviously a closed expression is required which covers as wide a range of z, and hence α, as possible. The differences between the various theoretical treatments are due to the different forms of the relations suggested between α and z. These will now be considered in turn and applied to the data for ATB.

(a) Flory-Fox

The first theoretical treatment (46, 51) of α yielded the expression

$$\alpha^5 - \alpha^3 = Cz \qquad (12)$$

where C is a numerical constant. Equation (I.7) considers the expansion of the statistical volume of a polymer coil to be the same as the expansion in the equivalent hydrodynamic volume on the basis of uniform expansion of the linear dimensions of the coil. Kurata and Yamakawa (52) have shown that the statistical radius of the coil increases more rapidly than the hydrodynamic radius. The expansion factor in equation (I.7) has to be replaced by α_η, the viscosity expansion factor so equation (I.7) becomes

$$[\eta] = \Phi_0 [\bar{r}_0^2/M]^{3/2} M^{1/2} \alpha_\eta^3 \qquad (13)$$

Substitution of equation (13) and (10) into (12) gives

$$[\eta]^{2/3}/M^{1/3} = K_\theta^{2/3} + K_\theta^{5/3} C_T M/[\eta] \qquad (14)$$

where C_T embodies various constants including B. Equation (14) shows that K_θ and B can be determined from the intercept and slope, respectively, of a plot of $[\eta]^{\frac{2}{3}}/M^{\frac{1}{3}}$ against $M/[\eta]$. Figure 20 shows the data for ATB plotted in this way. Reasonable linearity over the entire molecular weight range can be observed. However the intercept varies with the solvent in a regular manner decreasing as the solvent power increases. In fact the intercepts for THF and CT are negative. This has been found before with other systems to which equation (14) has been applied, especially the cellulose derivatives (19, 17) which have high Mark-Houwink exponents. Kurata and Stockmayer (17) also found the same trend exhibited by various polymers. The values of K_θ are shown in Table III.8.

(b) <u>Kurata-Stockmayer-Roig</u> (44)

The expression put forward in this treatment of the

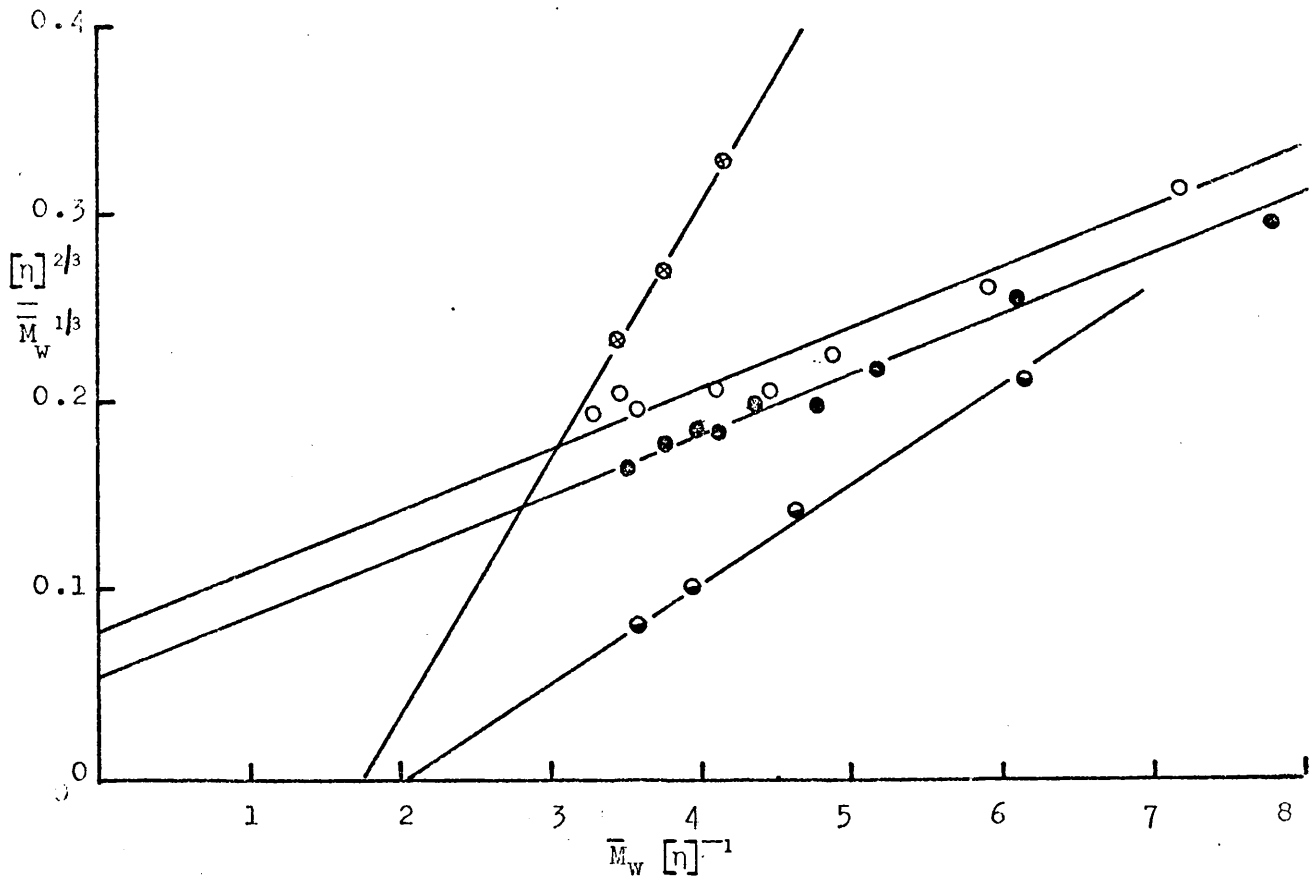

FIGURE 20 DATA FOR ATB ACCORDING TO THE FLORY-FOX EQUATION.

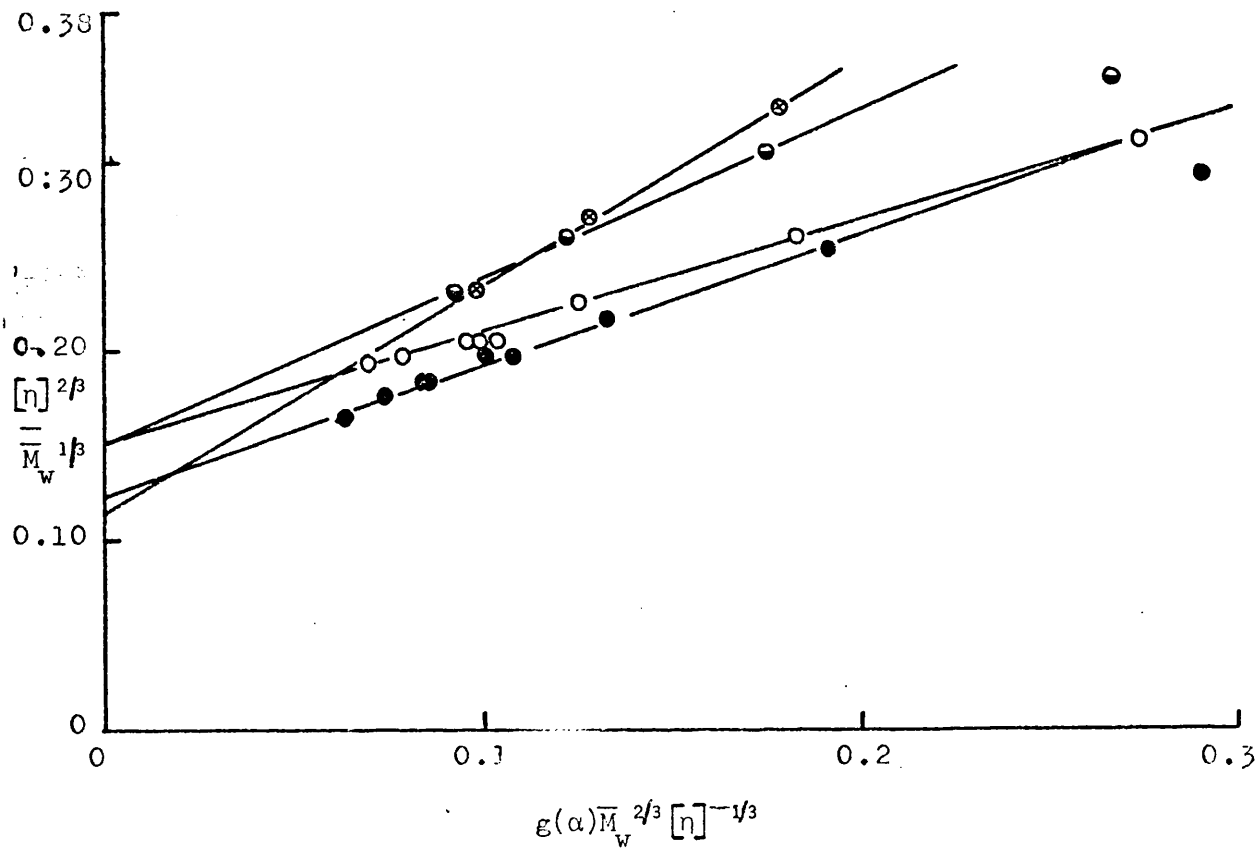

FIGURE 21 DATA FOR ATB ACCORDING TO THE KURATA-STOCKMAYER EQUATION.

excluded volume effect is

$$\alpha_\eta^3 - \alpha_\eta = 1.10\ g(\alpha_\eta)z \qquad (15)$$

which combined with

$$[\eta] = K_\theta M^{1/2}\alpha_\eta^3 \qquad (16)$$

and equation (10) gives

$$[\eta]^{2/3}/M^{1/3} = K_\theta^{2/3} + 0.363\Phi_0 Bg(\alpha_\eta)M^{2/3}/[\eta]^{1/3} \qquad (17)$$

where

$$g(\alpha_\eta) = [4\alpha_\eta^2/(3\alpha_\eta^2 + 1)]^{3/2} \qquad (18)$$

Equation (17) is applied in the following way since $g(\alpha_\eta)$ is unknown. $[\eta]^{\frac{2}{3}}/M^{\frac{1}{3}}$ is plotted against $M^{\frac{2}{3}}/[\eta]^{\frac{1}{3}}$ which gives an intercept, $K_\theta^{\frac{2}{3}}$, this value is then used to calculate $[\eta]_\theta$ using the relation

$$[\eta]_\theta = K_\theta M^{1/2} \qquad (19)$$

Values of $[\eta]_\theta$ obtained in this way allow calculation of α_η from which $g(\alpha_\eta)$ is derived. A plot of $[\eta]^{\frac{2}{3}}/M^{\frac{1}{3}}$ against $g(\alpha_\eta) \times M^{\frac{2}{3}}/[\eta]^{\frac{1}{3}}$ can then be made. This gives another value for K_θ and the process is repeated. On the third trial the difference between K_θ and K_θ from the second trial was less than 3%. The final plot of $[\eta]^{\frac{2}{3}}/M^{\frac{1}{3}}$ against $g(\alpha_\eta)\ M^{\frac{2}{3}}/[\eta]^{\frac{1}{3}}$ is shown in Figure 21. Linearity is observed over virtually the complete range of molecular weights, but the lines do not intersect the axis at the same point. The difference in K_θ values is too large to be classed simply as error. The lines for EA

and CT intersect at the same point and those of MEK and THF intersect fairly close to one another. Changes in K_θ with solvent have also been noted for various cellulose derivatives including the butyrate (19) and the tricarbanilate (45). K_θ values are shown in Table III.8.

(c) Stockmayer-Fixman

This treatment usually ascribed to Stockmayer and Fixman (54) was first put forward by Burchard (53) on the basis of the Kurata-Yamakawa (52) treatment of the viscosity of non-ideal polymer solutions. The excluded volume equation is given by

$$\alpha_\eta^3 = 1 + 1.55z \qquad (20)$$

which when combined with equation (10) and (13) gives

$$[\eta]/M^{1/2} = K_\theta + 0.51\Phi_0 BM^{1/2} \qquad (21)$$

A graph of $[\eta]/M^{\frac{1}{2}}$ against $M^{\frac{1}{2}}$ will give K_θ from the intercept. The data for ATB was plotted in this way and the graph is shown in Figure 22. Again reasonable linearity is observed over the entire range of $\overline{M}_w$. As with the Kurata-Stockmayer plot (Figure 21) K_θ is found to vary with solvent. The values for K_θ are slightly lower than those calculated from the Kurata-Stockmayer plot, the difference being about 5%. Values of K_θ are shown in Table III.8.

(d) Inagaki, Suzuki and Kurata

Inagaki, Suzuki and Kurata (I-S-K) (55) started from the Ptitsyn (56) expression for α

$$\alpha^2 = 0.786 + [(1 + 9.36z)^{2/3}/4.68] \qquad (22)$$

and the relation between α and α_η first put forward by Kurata

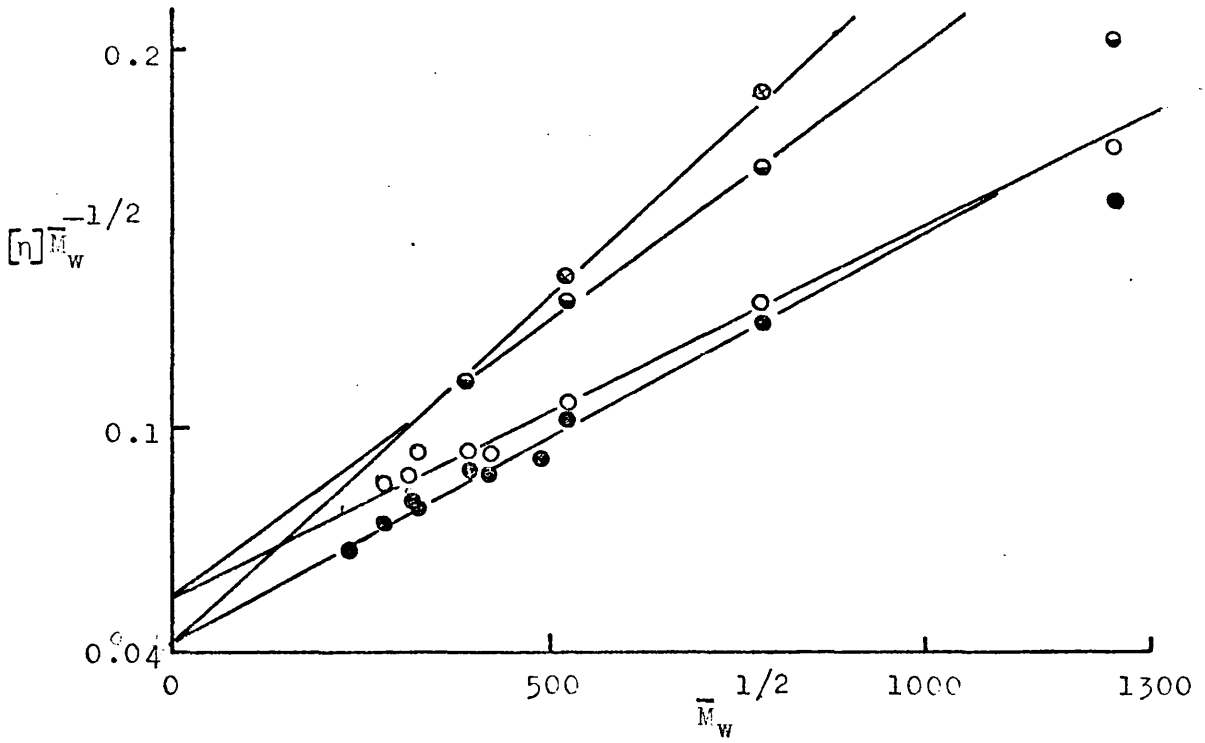

FIGURE 22 DATA FOR ATB ACCORDING TO THE STOCKMAYER-FIXMAN EQUATION.

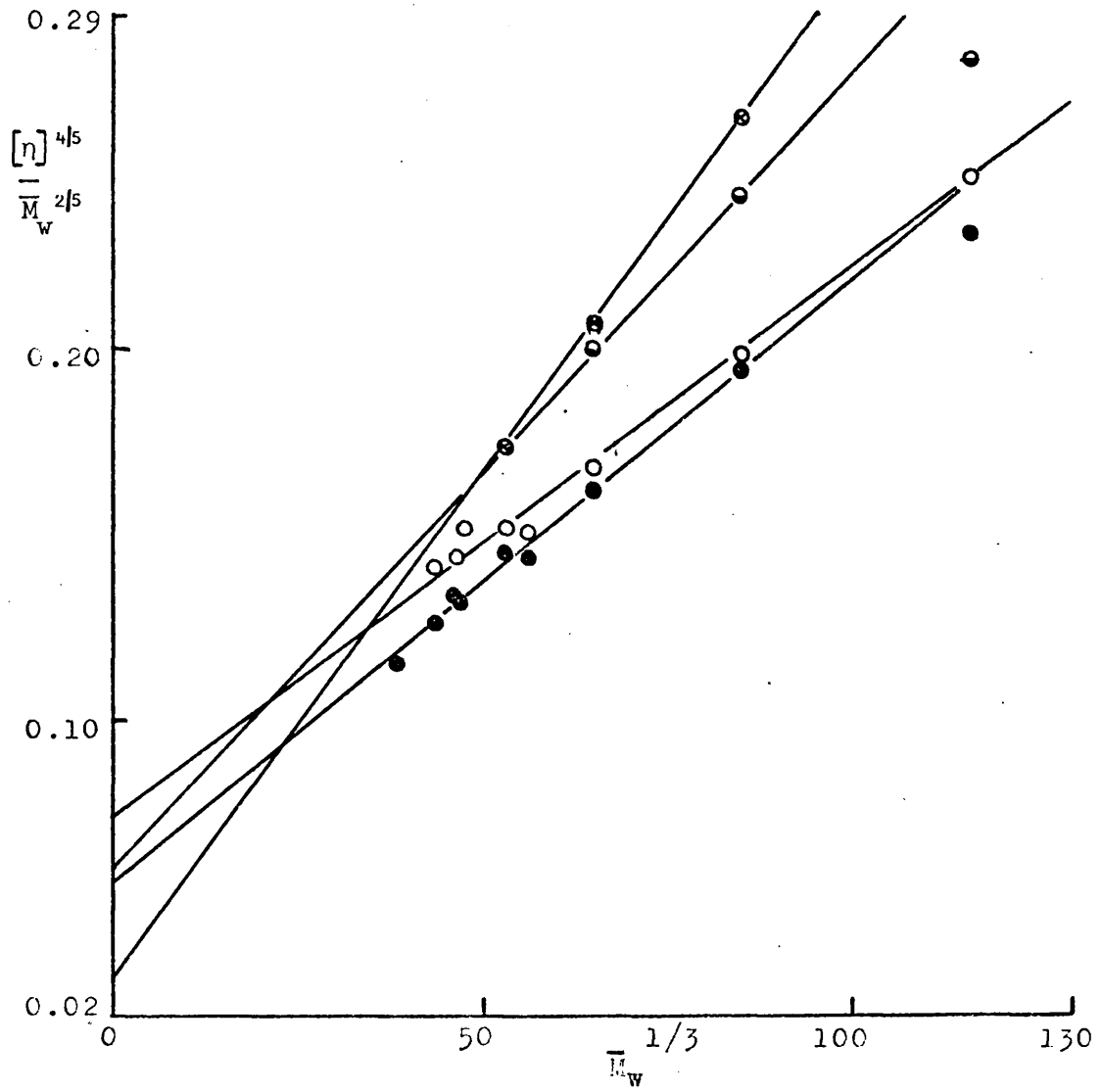

FIGURE 23 DATA FOR ATB ACCORDING TO THE INAGAKI-SUZUKI-KURATA EQUATION.

and Yamakawa (50, 52)

$$\alpha_\eta^3 = \alpha^{5/2} \tag{23}$$

Since by definition

$$\alpha_\eta^3 = [\eta]/K_\theta M^{1/2}$$

$$\alpha^2 = [[\eta]/K_\theta M^{1/2}]^{4/5} \tag{24}$$

Substitution of equation (24) in equation (22) gives the I-S-K expression,

$$([\eta]/M^{1/2})^{4/5} = 0.786K_\theta^{4/5} + 0.950K_\theta^{4/5}\, BA^{-3}0.330M^{1/3} \tag{25}$$

where $A = (\bar{r}_0^2/M)^{\frac{1}{2}}$ and a plot of $([\eta]/M^{\frac{1}{2}})^{4/5}$ against $M^{\frac{2}{3}}$ will lead to K_θ from the intercept. Applying this equation to the ATB data again gives good linearity and solvent dependent values of K_θ (Figure 23). For ATB in EA and MEK the K_θ values are slightly lower than those found using the S-F and K-S treatments. K_θ for THF is ridiculously low and that for CT is also low. Values of K_θ are shown in Table III.8.

(e) Berry

Berry's (57) expression is based on the relation between α and z

$$\alpha^2 = 1 + (134/105)(z/\alpha^3)h(z/\alpha^3) \tag{26}$$

where

$$h(z/\alpha^3) = (3 + z/\alpha^3)/3(1 + z/\alpha^3) \tag{27}$$

The expression which is obtained using these equations is

$$[\eta]^{1/2}/M^{1/4} = K_\theta^{1/2} + 0.42K_\theta^{1/2}\Phi_0 BM/[\eta] \tag{28}$$

According to Berry this relationship will presumably

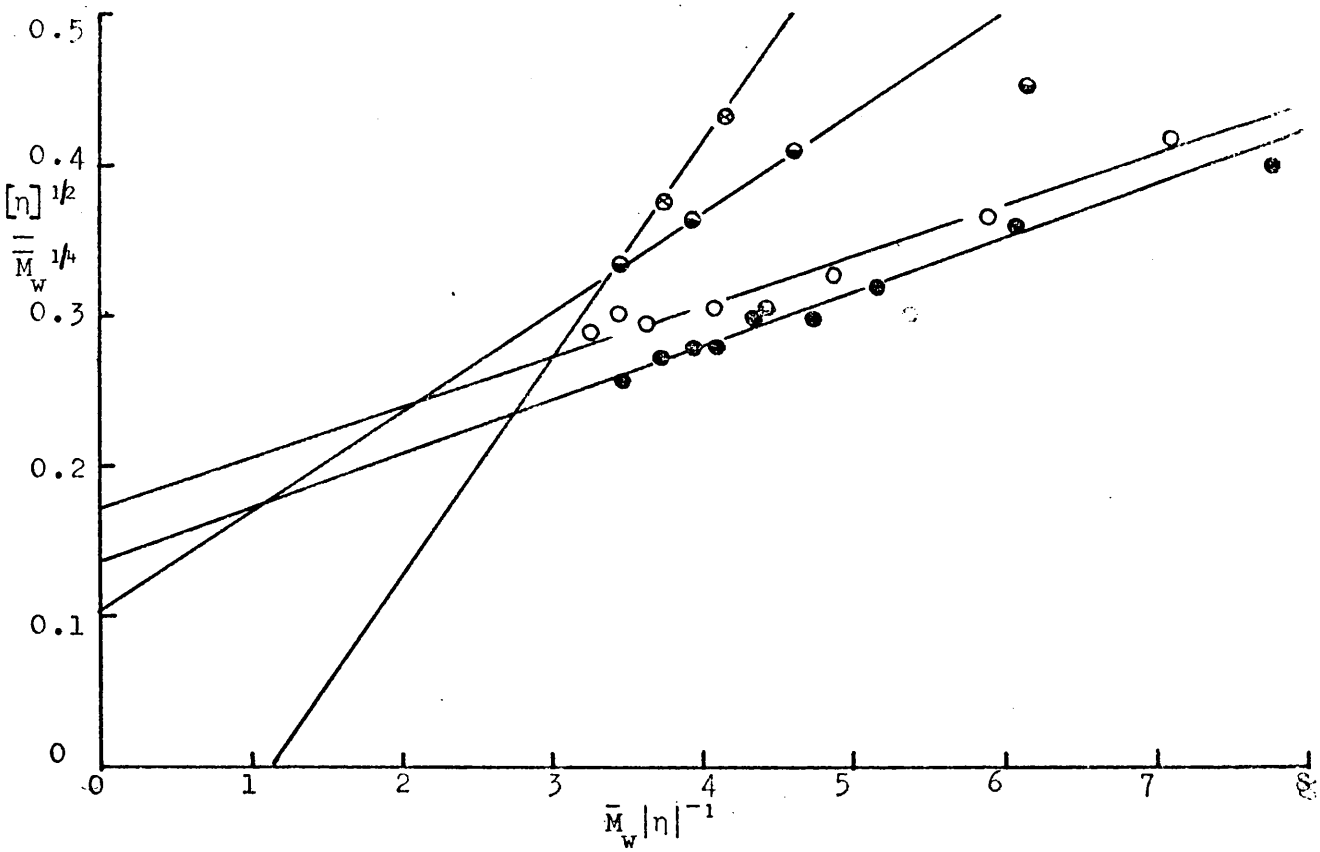

FIGURE 24 DATA FOR ATB ACCORDING TO THE BERRY EQUATION.

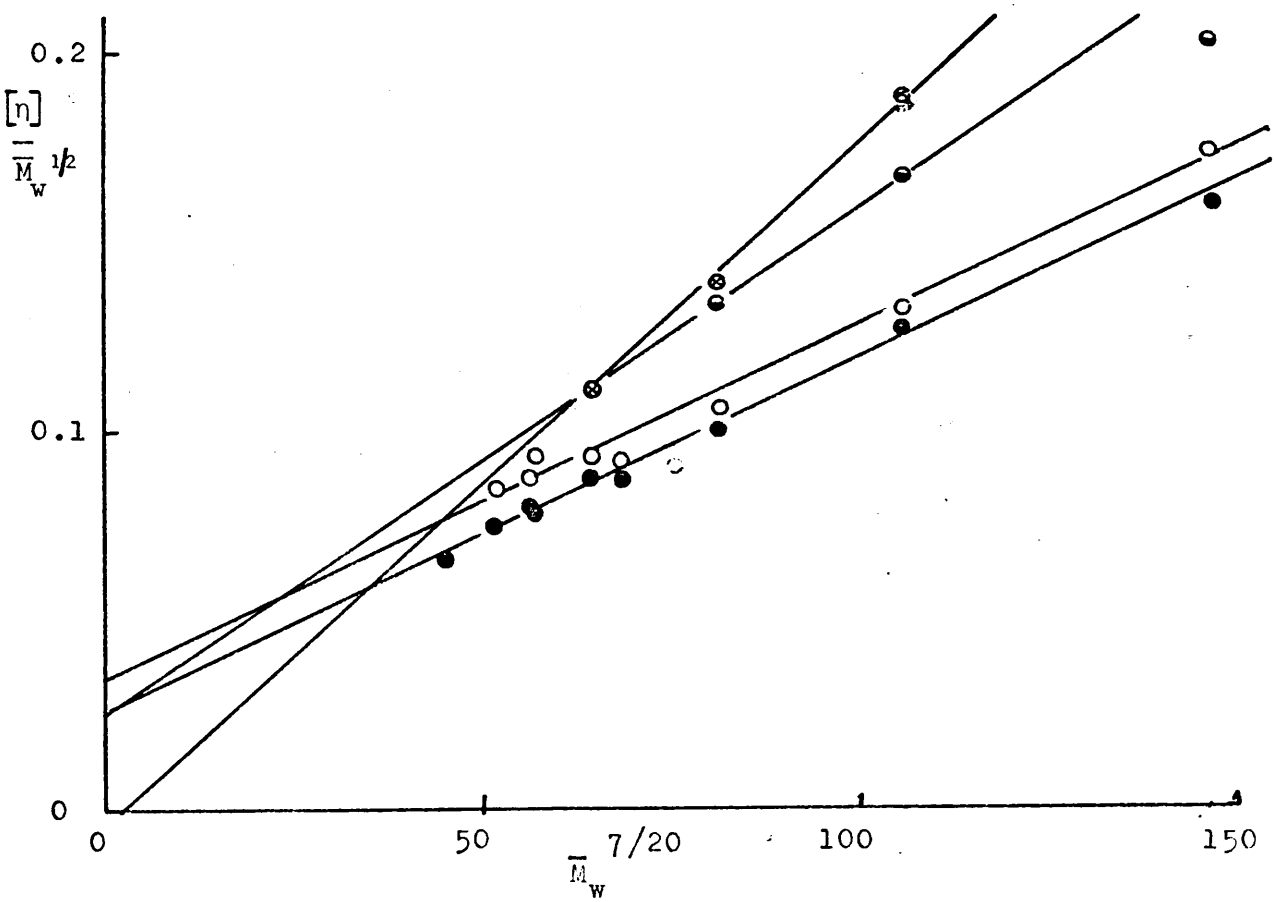

FIGURE 25 DATA FOR ATB ACCORDING TO THE COWIE MODIFIED, BOHDANECKY EQUATION.

apply to solutions of any non-ionic, linear, flexible coil polymer. The range of z/α^3 to which it applies is 0 to 2.4. This relation should hold for higher molecular weights but according to Berry there is a possibility that at low molecular weights the relation may not be valid.

The data was plotted according to equation (28) and is shown in Figure 24. Reasonable linearity can be observed but the values of K_θ are very low and in the case of THF even negative.

Another expression which has been tested using data for ATB was proposed by Bohdanecky (58). Starting from the expression derived by Krigbaum (59, 60)

$$[\eta]/M^{1/2} = K_\theta + 5x10^{-3}A_2M^{1/2} \qquad (29)$$

Bohdanecky arrived at the relation

$$[\eta]/M^{1/2} = K_\theta + 0.762K_\theta k^{7/10}M^{7/20} \qquad (30)$$

where $k = 0.33\ B(M/\bar{r}_0^2)$ and this holds for $z > 0.5$. Equation (30) was found to give K_θ values which were lower than those derived in θ-solvents, so it was empirically modified (58) to give reasonable values of K_θ, thus

$$[\eta]/M^{1/2} = 0.80K_\theta + 0.65K_\theta k^{7/10}M^{7/20} \qquad (31)$$

Cowie (61) further modified equation (31) using Ptitsyn and Eizner's (62) expression for α taking into account the difference between α and α_η. The expression arrived at is

$$[\eta]/M^{1/2} = \frac{\Phi(\varepsilon)K_\theta}{\Phi_0} + \frac{0.9166\Phi(\varepsilon)K_\theta k^{7/10}M^{7/20}}{\Phi_0} \qquad (32)$$

where

$$\Phi(\varepsilon) = \Phi_0(1 - 2.63\varepsilon + 2.86\varepsilon^2) \qquad (33)$$

and ε is given by

$$r^2 = K_r M^{1+\varepsilon} \qquad (34)$$

The exponent a is related to ε by

$$a = (1 + 3\varepsilon)/2 \qquad (35)$$

and thus $\Phi_0 = \Phi(\varepsilon)$ in a theta solvent.

Plots of $[\eta]/M^{\frac{1}{2}}$ against $M^{7/20}$ for ATB are shown in Figure 25. Linearity is observed over the experimental range of molecular weights and the K_θ values, derived using equation (32), are shown in Table III.8. The values for EA and MEK correlate well with those derived using the S-F, K-S and I-S-K expressions. The value for THF is negative and that for CT is slightly lower than the S-F and K-S values.

The unperturbed dimensions $(\bar{r}_0^2/\bar{M}_w)^{\frac{1}{2}}$ were calculated from the average values of K_θ shown is Table III.8, and various values of Φ_0, as indicated in Table III.9.

Table III.8: K_θ values for ATB in EA, MEK, CT and THF calculated using the theories in the text.

ATB Solvent 298K	K_θ S-F	K_θ Cowie	K_θ I-S-K	K_θ K-S	K_θ Berry	K_θ F-F	K_θ * Average values
EA	0.056	0.052	0.052	0.059	0.031	0.021	0.055
MEK	0.042	0.042	0.037	0.044	0.019	0.012	0.041
CT	0.056	0.045	0.040	0.059	0.011	negative	0.050
THF	0.042	negative	0.017	0.040	negative	negative	0.041

*Average values calculated excluding Berry and Flory-Fox values, also in the case of THF excluding Cowie and I-S-K values.

Table III.9: $(\bar{r}_0^2/\bar{M}_w)^{\frac{1}{2}}$ values calculated using K_θ

Solvent	$\left[\frac{\bar{r}_0^2}{\bar{M}_w}\right]^{\frac{1}{2}}$ x 10^{11} cm (a)	$\left[\frac{\bar{r}_0^2}{\bar{M}_w}\right]^{\frac{1}{2}}$ x 10^{11} cm (b)	$\left[\frac{\bar{r}_0^2}{\bar{M}_w}\right]^{\frac{1}{2}}$ x 10^{11} cm (c)
EA	576	794	665
MEK	523	720	613
CT	559	769	674
THF	523	720	645

Calculated using (a) $\Phi_0 = 2.87 \times 10^{23}$

(b) $\Phi_0 = 1.1 \times 10^{23}$

(c) $\Phi(\varepsilon)$ (equation (33))

The unperturbed dimensions of ATB are greater in an ester solvent than in a ketone solvent and this trend is also exhibited by cellulose tributyrate (19) in tributyrin and MEK. The value of $(\bar{r}_0^2/\bar{M}_w)^{\frac{1}{2}}$ for cellulose tributyrate in MEK at 303K is quoted as 673 x 10^{-11}cm by Huppenthal (19) calculated using $\Phi_0 = 2.87 \times 10^{23}$, this is in keeping with the concept that cellulose derivatives are more extended in solution than the corresponding amylose derivatives (20).

An alternative technique, for estimating the unperturbed dimensions from data in good solvents, has been proposed by Baumann (63) who based his relation on the equation of Stockmayer and Fixman (54) (equation (21)). Baumann took the Fixman (49) closed expression for α to be exact and based his derivation on this assumption. The expression which he derived is

$$[\bar{r}^2/M]^{3/2} = [\bar{r}_0^2/M]^{3/2} + BM^{1/2} \qquad (36)$$

and a plot of $(\bar{r}^2/M)^{3/2}$ against $M^{\frac{1}{2}}$ will give $(\bar{r}_0^2/M)^{3/2}$ from the

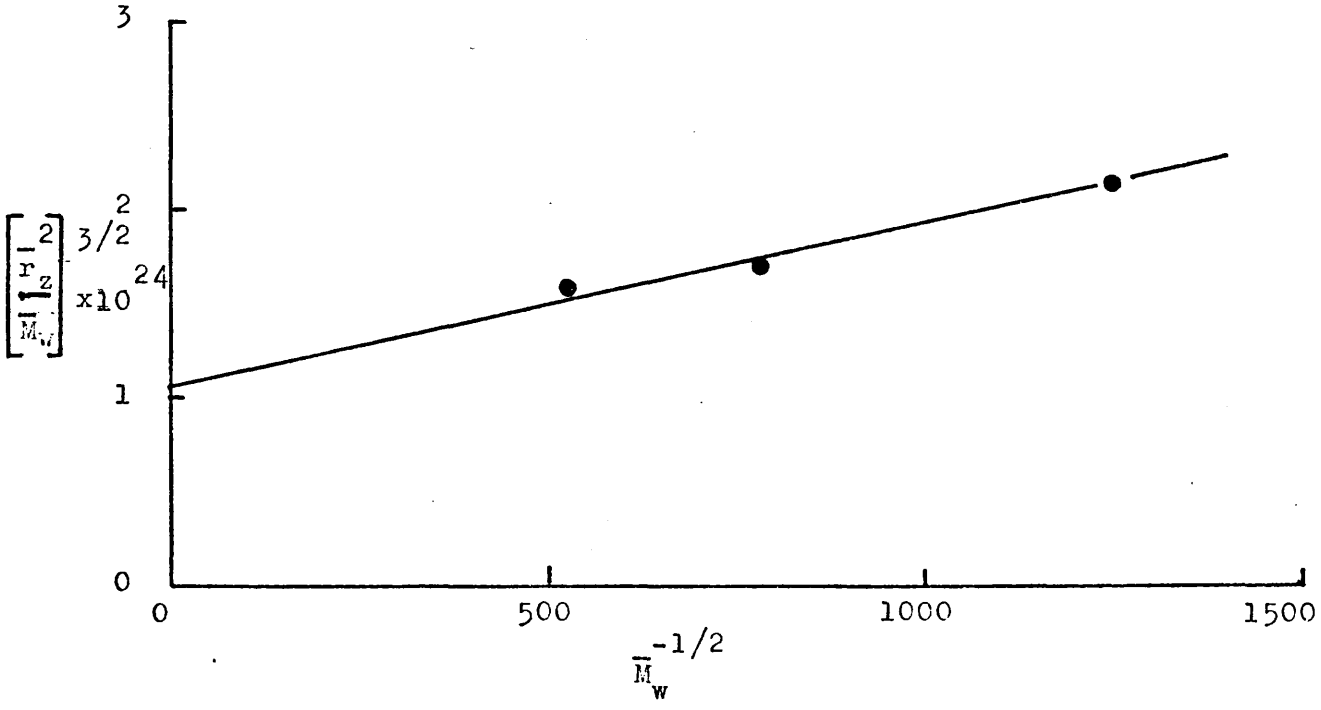

FIGURE 26 BAUMANN PLOT FOR ATB/MEK AT 298K.

intercept. Figure 26 shows that the Baumann plot gives an intercept of $1.04 \times 10^{-24} cm^3$ for $(\bar{r}_{O_2}^2/\bar{M}_w)^{3/2}$. When corrected for heterogeneity this corresponds to a value for $(\bar{r}_{Ow}^2/\bar{M}_w)^{\frac{1}{2}}$ of 878×10^{-11}cm. This value can be compared with that for the acetate measured by Banks and Greenwood (64) of 885×10^{-11}cm.

The value of $(\bar{r}_O^2/\bar{M}_w)^{\frac{1}{2}}$ calculated from viscosity data is considerably smaller than the value calculated from light-scattering but the uncertainty in the value calculated from light-scattering is fairly large and the data minimal.

Values of α calculated using the value of $(\bar{r}_O^2/M)^{\frac{1}{2}}$ from the Baumann plot are recorded in Table III.4. These values are very low and would, if true, indicate very little expansion in a very good solvent which is not born out by hydrodynamic considerations (see section on hydrodynamic considerations).

See corrections

Temperature dependence of the unperturbed dimensions

Data for ATB in EA at various temperatures was plotted according to equation (21) and (17). These plots are shown in Figure 27. The values of K_θ are tabulated in Table III.10.

Table III.10: Data for ATB in EA at various temperatures

Temperature ^oK	K_θ K-S	K_θ S-F	Average K_θ
289.8	0.059	0.063	0.061
298	0.059	0.056	0.058
307.9	0.046	0.042	0.044
313	0.046	0.042	0.044
317.5	0.048	0.046	0.047

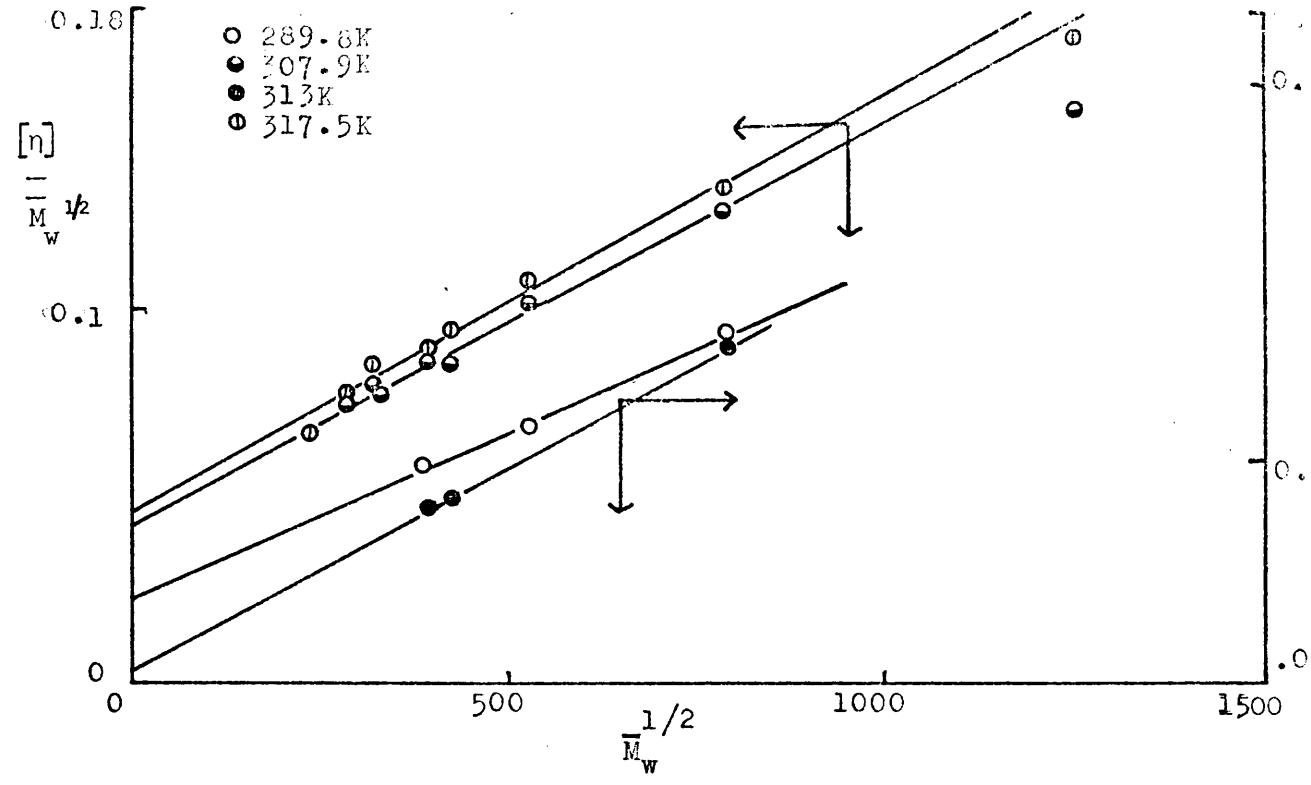

FIGURE 27a DATA FOR ATB/EA AT VARIOUS TEMPERATURES ACCORDING TO THE STOCKMAYER-FIXMAN EQUATION.

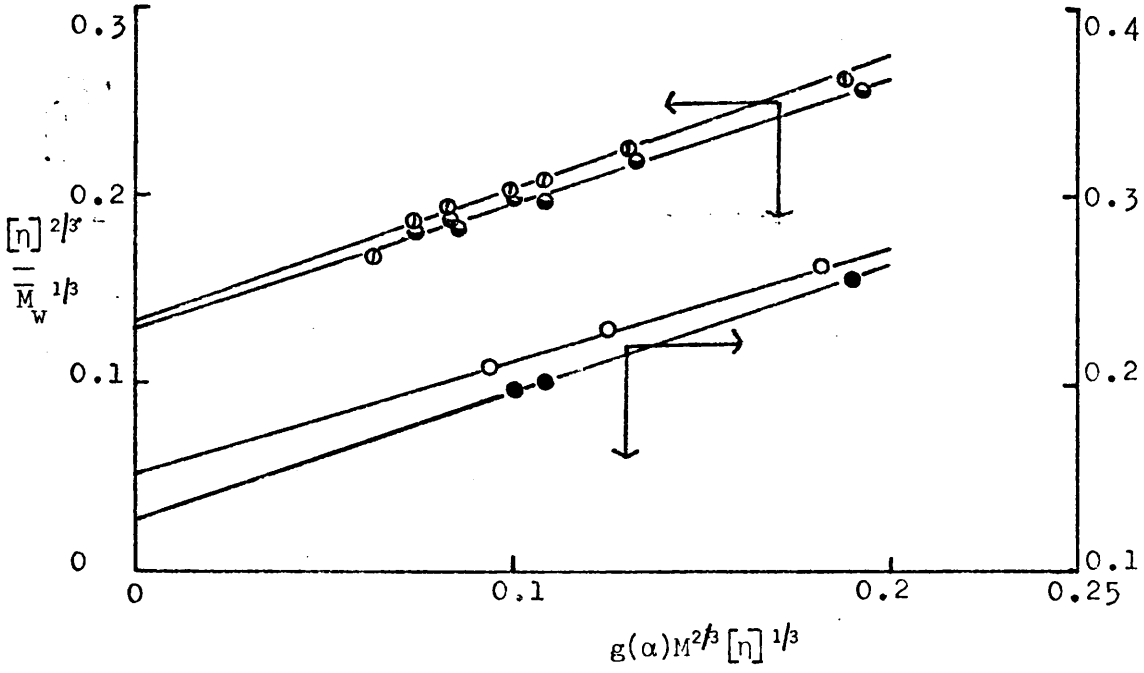

FIGURE 27b DATA FOR ATB/EA AT VARIOUS TEMPERATURES ACCORDING TO THE KURATA-STOCKMAYER EQUATION.

The variation of $[\eta]$ with temperature mentioned before is reflected as a similar variation in unperturbed dimensions with a minimum at about 310K. The minimum corresponds to a value of $(\bar{r}_0^2/M)^{\frac{1}{2}}$ of 531 x 10^{-11}cm, using $\Phi_0 = 2.87 \times 10^{23}$.

Expansion Coefficient, α_η

The expansion coefficients, α_η, have been computed using the average values of K_θ from Table III.8. These values are collected together in Table III.11. The variation of α_η with solvent follows the trend $\alpha_{THF} > \alpha_{CT} > \alpha_{MEK} > \alpha_{EA}$, which reflects the variation in solvent power shown by the exponent a.

The theories of Stockmayer and Fixman, Flory and Fox, Kurata and Stockmayer, and Ptitsyn predict various relationships between α and M, the molecular weight.

Table III.11: Values of α_η for ATB

ATB Sample	THF 298K α_η	CT 298K α_η	MEK 298K α_η	α_η EA 289.8K	298K	307.9K	313K	317.5K
B2			1.58		1.47			
B3	1.66	1.50	1.46	1.30	1.34	1.43	1.43	1.41
B4	1.51	1.39	1.35	1.21	1.25	1.33	1.35	1.32
B5	1.40	1.31	1.30	1.16	1.20	1.26	1.26	1.24
X9			1.29		1.19	1.25	1.27	1.26
X10b			1.24		1.20	1.21		
X11			1.25		1.17	1.22		1.22
X12			1.22		1.16	1.20		1.19
X13			1.17					1.12

Stockmayer and Fixman (54) predict

$$\alpha_\eta^3 - 1 = CM^{1/2} \qquad (37)$$

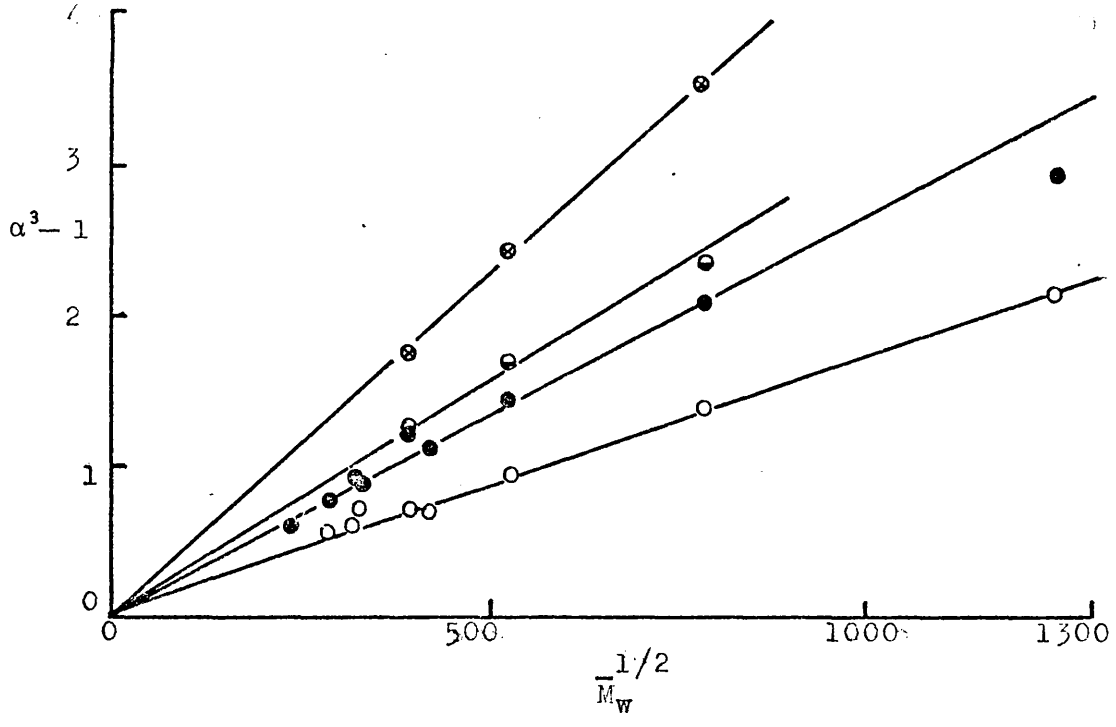

FIGURE 28a DATA FOR ATB ACCORDING TO THE STOCKMAYER-FIXMAN RELATION.

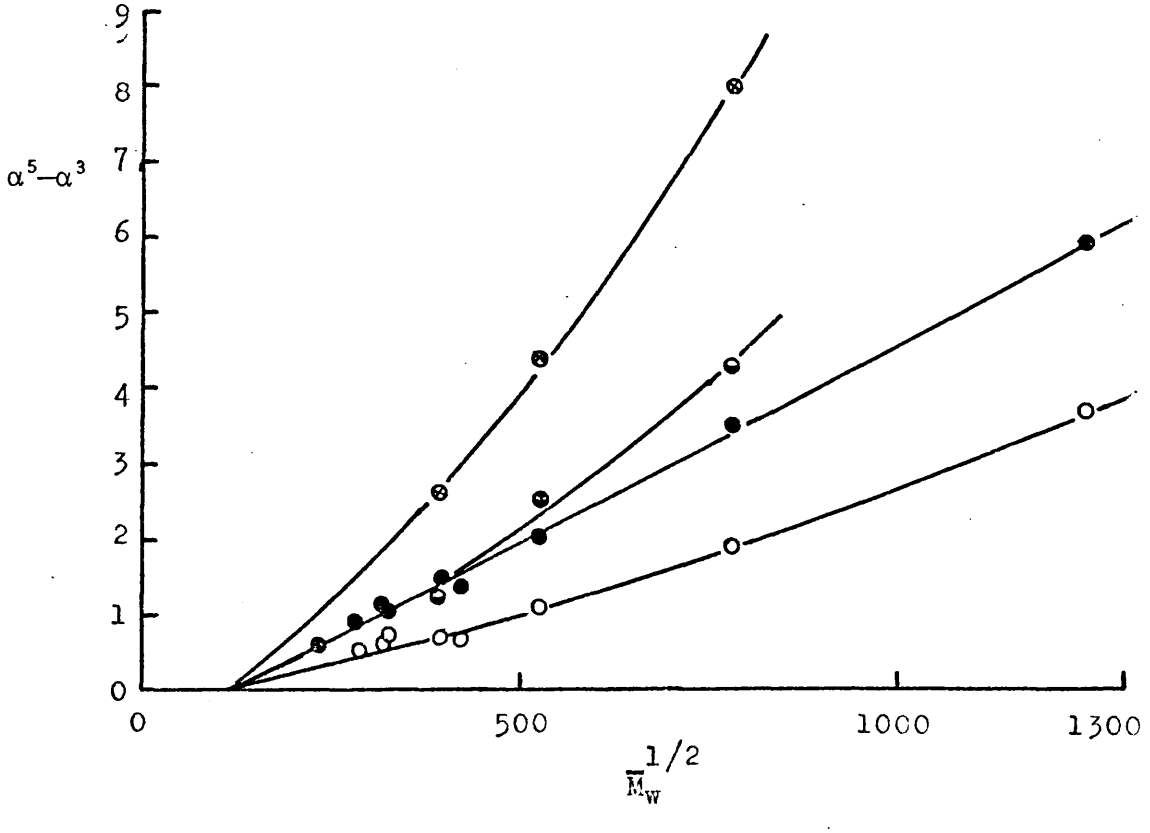

FIGURE 28b DATA FOR ATB ACCORDING TO THE FLORY-FOX RELATION.

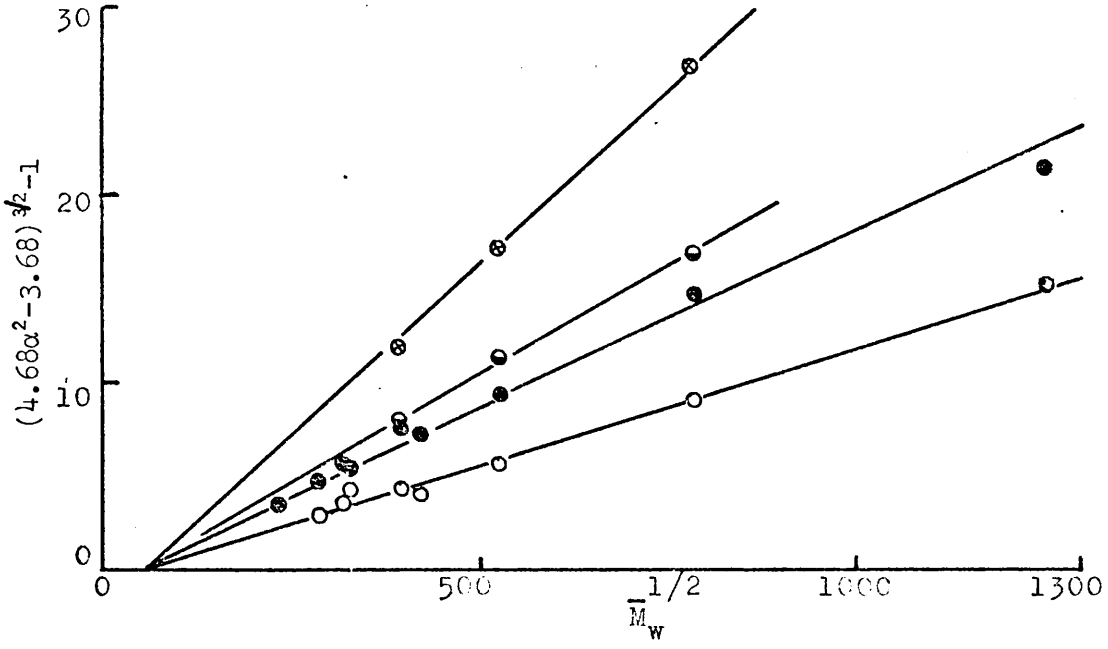

FIGURE 29a DATA FOR ATB ACCORDING TO THE PTITSYN RELATION.

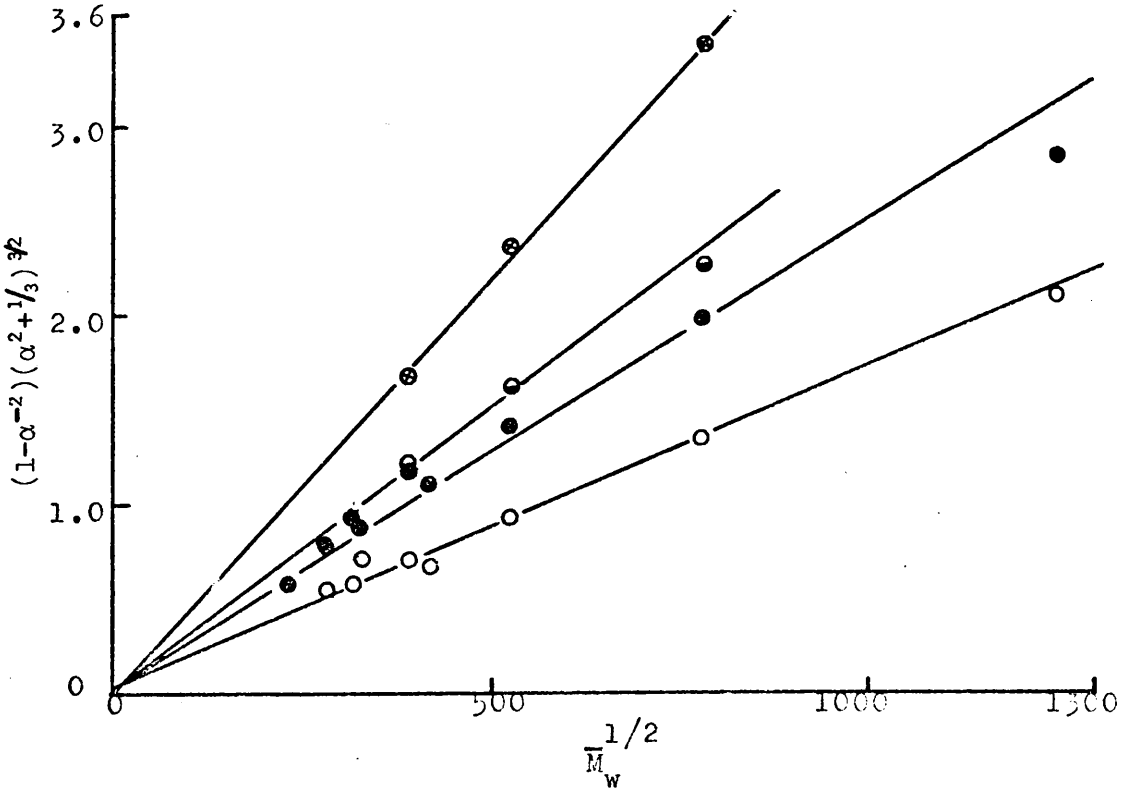

FIGURE 29b DATA FOR ATB ACCORDING TO THE KURATA-STOCKMAYER RELATION.

Kurata and Stockmayer (17)

$$(1 - \alpha_\eta^2)(\alpha_\eta^2 + 1/3)^{3/2} = C'M^{1/2} \qquad (38)$$

Flory and Fox (46a)

$$\alpha_\eta^5 - \alpha_\eta^3 = C''M^{1/2} \qquad (39)$$

and according to Ptitsyn (18)

$$(4.68\alpha_\eta^2 - 3.68)^{3/2} - 1 = C'''M^{1/2} \qquad (40)$$

where C, C', C'', and C''' are constants.

The data for ATB in the four solvents have been plotted according to equations (37), (38), (39) and (40) and are shown in Figures 28 and 29. It can be seen that the experimental data comply with both the S-F and K-S expressions, and are virtually numerically equivalent particularly to low α values. However the best fit seems to be the S-F expression because slight curvature can be seen in the data plotted according to equation (38). In the case of the Ptitsyn expression the lines intersect the abscissa at a point equivalent to a molecular weight of about 2500.

The data plotted according to the Flory-Fox expression show a slight upward curvature indicating that $(\alpha^5 - \alpha^3)/M^{\frac{1}{2}}$ is not independent of M a feature also found in other systems (17). The lines in the Flory-Fox plot also intersect the abscissa at a point corresponding to a molecular weight of about 10^4. Huppenthal (19) and Patel et al (8) have found similar behaviour in the case of cellulose tributyrate and amylose acetate. Patel proposed that the positive intercept

in the Flory-Fox relationship for α was due to the fact that α does not reach a limiting value at M = 0 but at a molecular weight when the chain can no longer coil. A molecular weight of 10^4 corresponds to a degree of polymerisation in ATB of about 27.

Table III.11 gives the values of α_η at the different temperatures. There is a slight tendency for α_η to increase generally with temperature, and a significant increase in α_η occurs between 298K and 307.9K. The values of α_η are not as high as those found for the cellulose derivatives indicating that ATB is not as highly expanded although an increase in temperature does cause expansion to occur. The normal behaviour for cellulose butyrate and vinyl polymers is for α to decrease with temperature.

Both K_θ and α_η show a variation with temperature which could account for the temperature dependence of $[\eta]$ but it is impossible to decide which of these two factors dominates. With the large variation in K_θ between 289.8 and 307.9K one might think this would dominate and bring about a large variation in $[\eta]$, but this is not so. It seems likely then that in this region α or the 'long' range forces contribute most to the decrease in $[\eta]$. At about 308K the unperturbed dimensions reach a minimum and then start to increase, this must be due to steric considerations or 'short' range forces. The expansion coefficient is also increasing and this seems to dominate again giving a larger $d \log [\eta]/dT$ than would be assumed by looking solely at K_θ.

Unfortunately due to lack of data it is impossible to say whether this unusual effect is solvent dependent or not.

The unperturbed dimensions are definitely solvent dependent and whether the interactions with solvent alone could cause the effect is a question which still has to be answered.

The Conformation of ATB from hydrodynamic considerations

The hydrodynamic behaviour of a polymer chain will be complex because of the many shapes that a linear flexible chain can adopt. These depend not only on the polymer itself but also on both solvent and temperature. The behaviour which is observed will depend on the average conformation dictated by long and short range forces. The short range effects will determine the bond angles and restrictions to free rotation and the long range effects such as solvent environment will also affect the conformation.

In the absence of long range effects the mean square end-to-end distance for a random coil with a large number of links will fit the relationship.

$$\bar{r}_0^2 = b_0^2 \bar{z} \qquad (41)$$

where b_0 is the length of the bonds and $\bar{z}$ their number. This means that $\bar{r}_0^2$ is directly proportional to the molecular weight of the polymer. The perturbed dimensions on the other hand are affected by long range interactions and the dimensions are proportional to some power of $\bar{z}$.

Several theories have been put forward to relate the unperturbed and perturbed dimensions of linear flexible polymers in dilute solution to the intrinsic viscosity. The perturbed dimensions have been calculated according to the theories of Kirkwood and Riseman (42a, 65) and Kuhn and Kuhn (66).

Kirkwood and Riseman Theory

The theory of Kirkwood and Riseman is based on a random coil model which takes into account inhibited fluid flow through the chain. Their expression for $[\eta]$ is

$$[\eta] = (N_A \zeta b^2 / 3600 \eta_0 M_0) \bar{Z} F(\lambda_0 \bar{Z}^{1/2}) \qquad (42)$$

where N_A is Arogadro's number, $\bar{Z}$ is the degree of polymerisation, b is the effective bond length, η_0 is the viscosity of the solvent, M_0 is the monomer molecular weight, ζ is the friction constant per monomer unit and $\lambda_0 = \zeta/(6\pi^3)^{1/2}\eta_0 b$.

The effective bond length, b, is given by the expression

$$b^3 = \frac{3600 M_0}{(6\pi^3)^{1/2} N_A} \frac{[\eta]}{\bar{Z}^{1/2}} (1/xF(x)) \qquad (43)$$

where $x = \lambda_0 \bar{Z}^{1/2}$. The function xF(x) tends to 1.48 as $\bar{Z} \to \infty$ and therefore equation (43) can be written as

$$b^3 = \frac{2435 M_0}{(6\pi^3)^{1/2} N_A} \lim_{Z \to 0} \frac{[\eta]}{\bar{Z}^{1/2}} \qquad (44)$$

The parameter b can be seen as the bond length of a hypothetical random coil having the same mean square end-to-end distance but a greater overall length. Therefore b is a measure of the flexibility of the chain. For such a molecule

$$\bar{r}^2 = b^2 \bar{Z} \qquad (45)$$

The values of b for ATB in the four solvents were obtained by plotting $[\eta]/\bar{Z}_w^{\frac{1}{2}}$ against $\bar{Z}_w^{-\frac{1}{2}}$, the intercept on the ordinate at $\bar{Z}_w^{-\frac{1}{2}} = 0$ gives the value of $\lim_{Z \to \infty} [\eta]/\bar{Z}_w^{1/2}$ from which b can be calculated. These plots are shown in Figure 30.

Kuhn and Kuhn Theory.

Kuhn and Kuhn (66) considered the polymer molecule to

consist of N_m straight line segments each of length A_m and hydrodynamic thickness d_h, statistically connected so that the orientation of each segment is independent of its neighbours. For such a chain

$$\bar{r}^2 = N_m A_m^2 \qquad (46)$$

A further assumption was made that the chain has the same contour length as the real chain, so that r_{max}, the end-to-end distance of the fully stretched molecule is given by

$$r_{max} = N_m A_m = \Sigma b_o \qquad (47)$$

Kuhn, Kuhn and Silberberg (67) have deduced the following relation between $[\eta]$, A_m and d_h.

$$[\eta] = \frac{N b_o^2 A_m}{100 M_o} \cdot \frac{0.43\Sigma}{\left[-1.6 + 2.3\log_{10}(A_m/d_m) + (\Sigma b_o/A_m)^{1/2}\right]} \qquad (48)$$

To obtain A_m, $\Sigma/[\eta]$ was plotted against $\Sigma_w^{\frac{1}{2}}$ as shown in Figure 31 and A_m obtained from the slopes of the straight lines obtained.

Weight average molecule weights and degree of polymerisation have been used when examining the theories of Kirkwood and Riseman and Kuhn and Kuhn, therefore the root mean square end-to-end distance calculated will be a weight average. In order to compare the light-scattering values of $\bar{r}_z^2$ with those calculated from the theories they must be corrected for heterogeneity using the relation

$$(\bar{r}_z^2)^{1/2}/(\bar{r}_w^2)^{1/2} = \left[(h+2)/(h+1)\right]^{1/2} \qquad (49)$$

FIGURE 31 DATA FOR ATB ACCORDING TO THE KUHN-YUHA EQUATION.

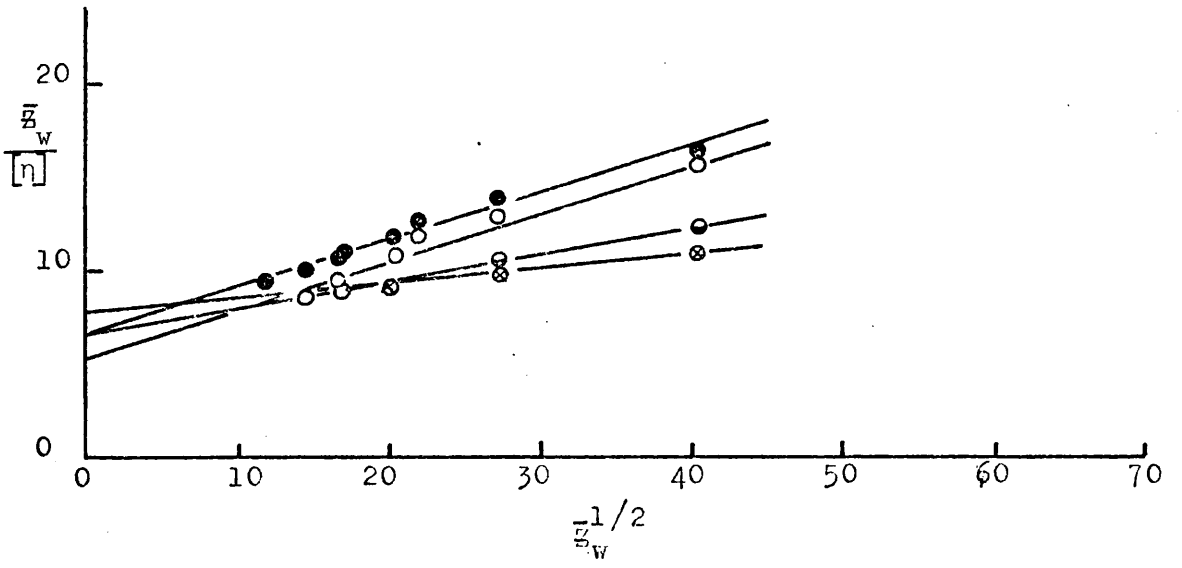

FIGURE 30 DATA FOR ATB ACCORDING TO THE KIRKWOOD-RISEMAN EQUATION

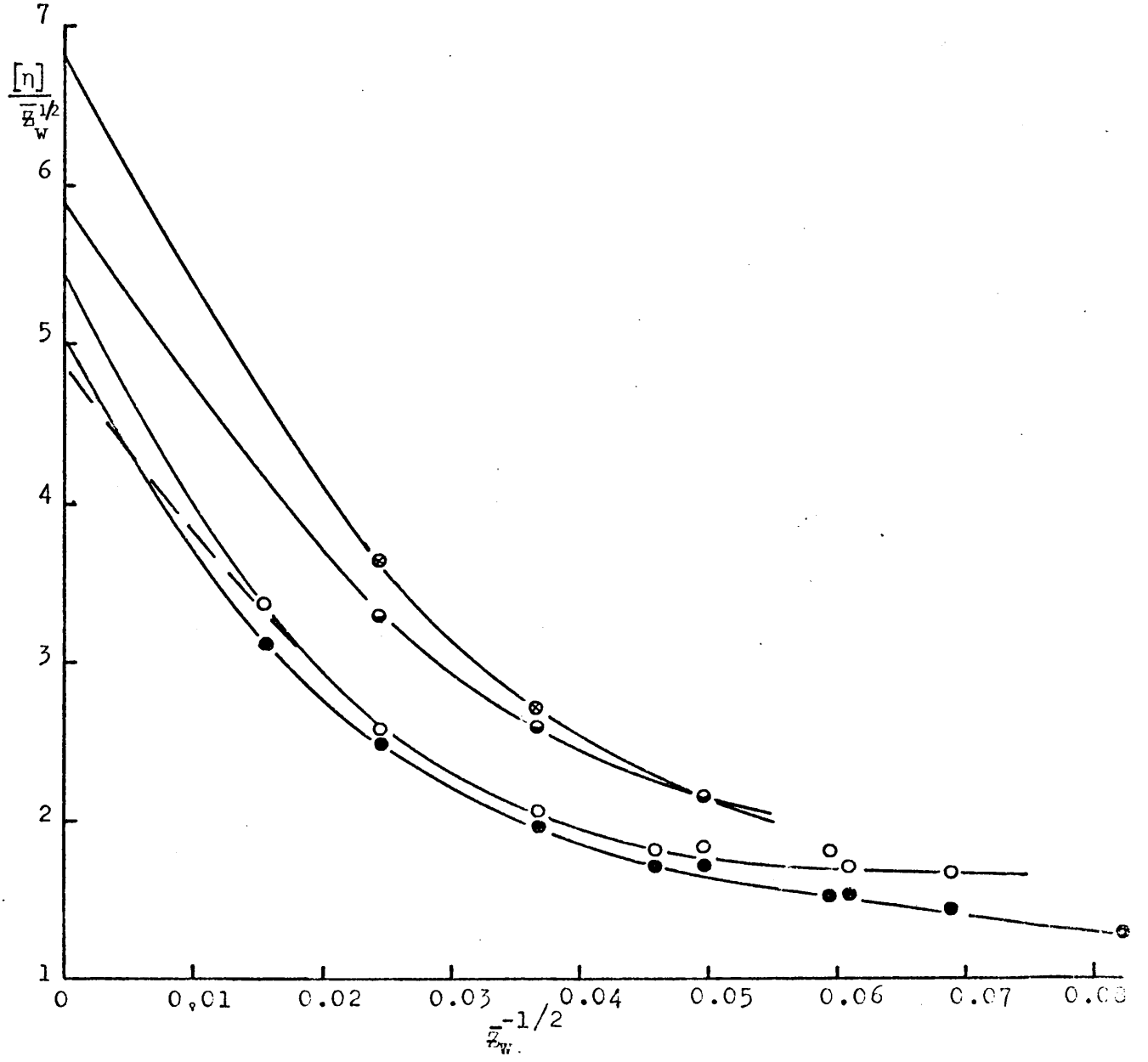

The values of b and A_m are given in Table III.12. The values of b are highest in THF and decrease in the order CT, EA and MEK that is almost the same order as the Mark-Houwink exponent a. This could mean that ATB is more expanded in THF than in CT, less expanded in EA and least expanded in MEK. Values of α_η calculated using derived K_θ values indicate that the order should be THF, CT, MEK and EA. However, the extrapolations are long and some uncertainty does appear in the values of b. Thus, it is possible to draw a line through the values for EA such that b is 17.4 which would bring the values of b into line with the order for α and a.

The values of b for ATB in EA decrease with increasing temperature which might explain the negative temperature coefficient of $[\eta]$ in terms of flexibility but not the positive coefficient.

Comparison of b with values found for other polymers indicates that ATB is more flexible than the cellulose derivatives but slightly less-flexible than the synthetic polymers.

Table III.12: Values of b and A_m calculated using the Kirkwood-Riseman and Kuhn-Kuhn theories.

Solvent	Temperature K	b x 10^8cm	A_m x 10^8cm
EA	289.8	17.8	
	298	18.0 or (17.4)	69.6
	307.9	16.7	
	313	17.0	
	317.5	15.5	
MEK	298	17.7	71.7
THF	298	19.5	182
CT	298	18.6	101.6

Table III.13: Comparison of $(\bar{r}_w^2)^{\frac{1}{2}}$ values for ATB using the Kirkwood-Riseman theory and light scattering

ATB Fraction	EA $(\bar{r}_w^2)^{\frac{1}{2}} \times 10^8$cm VISC	EA $(\bar{r}_w^2)^{\frac{1}{2}} \times 10^8$cm L-S
B2	1145	1395
B3	719	807
B4	482	542

Table III.13 shows a comparison of values of the perturbed dimensions of ATB in MEK calculated using b and equation (45) with those from light scattering. Considering the uncertainties in the b values the agreement is very good. The calculated values are between 11 - 18% lower than the experimental values.

Table III.14: Comparison of $(r_w^2)^{\frac{1}{2}}$ values for ATB using Kuhn-Kuhn theory and light scattering

ATB Fraction	EA $(\bar{r}_w^2)^{\frac{1}{2}} \times 10^8$cm VISC	EA $(\bar{r}_w^2)^{\frac{1}{2}} \times 10^8$cm L-S
B2	1149	1395
B3	755	807
B4	483	542

Values of A_m calculated according to the Kuhn-Kuhn theory are shown in Table III.12. ATB in THF has the largest value and A_m decreases in the order CT, MEK and EA which follows the trend in Mark-Houwink exponents. The value in THF is virtually twice the value in EA and MEK showing the molecule

to be considerably extended in this solvent.

The perturbed dimensions calculated using A_m are shown in Table III.14 taking b_o to be 4.4×10^{-8}cm (25). The correlation is as good as that found for the Kirkwood-Riseman theory. Both theories would seem to hold for ATB to a certain extent.

For the polymer in the unperturbed state b and A_m can be calculated from the following equations

$$b = (\bar{r}_0^2/z)^{1/2} = (\bar{r}_0^2/M)^{1/2} M_0^{1/2} \qquad (50)$$

and

$$A_m = \bar{r}_0^2/b_o z = (\bar{r}_0^2/M)(M_o/b_o) \qquad (51)$$

Table III.15: b and A_m for the unperturbed polymer

Solvent 298K	b x 10^8cm (a)	A_m x 10^8cm (a)	b x 10^8cm (b)	A_m x 10^8cm (b)	b x 10^8cm (c)	A_m x 10^8cm (c)
EA	11.1	28.1	15.5	53.3	12.8	37.4
MEK	10.1	23.1	13.9	43.8	11.8	31.8
CT	10.8	26.4	14.8	50.0	13.0	38.4
THF	10.1	23.1	13.9	43.8	12.4	35.2

(a), (b) and (c) see legends for Table III.9.

Table III.15 gives the values of b and A_m calculated using $(\bar{r}_0^2/\bar{M}_w)^{\frac{1}{2}}$ values from Table III.9. In the unperturbed state the values of A_m for THF and CT are very much lower than the perturbed values and also the large difference in A_m values shown in Table III.12 is not seen. This might indicate that stiffness in the perturbed state is due to solvent interactions

not short-range forces. Both b and A_m indicate that ATB is a flexible polymer in the unperturbed state, more flexible than the cellubsic polymers but stiffer than the synthetic polymers (see Table IV.6).

Another useful quantity for characterising the stiffness of the chain is the persistence length, q, introduced by Kratky and Porod (68). It equals the mean length of projection of an infinitely long chain along the direction of the first link. Benoit and Doty (69) derived the following equation between $\bar{s}_0^2$ and q.

$$\bar{s}_o^2 = q^2\{(x/3) - 1 + (2/x) - 2(1 - e^{-x})/x^2\} \qquad (52)$$

where X is the number of Kratky-Porod lengths defined as

$$X = r_{max}/q$$

When X is large equation (52) may be written as

$$\bar{s}_0^2 = r_{max}\, q/3 \qquad (53)$$

For B2 in MEK one obtains the value $q = 11.6 \times 10^{-8}$cm for $\Phi_0 = 2.87 \times 10^{23}$, which means again that ATB is considerably less stiff than the cellulose derivatives but stiffer than most non-cellulosic polymers which have values of q in the region $8 - 10 \times 10^{-8}$cm.

The steric factor, σ, is another measure of the flexibility of a polymer chain and is expressed in terms of the ratio

$$\bar{r}_\theta^2/\bar{r}_{0f}^2 = \sigma^2 \qquad (54)$$

where $\bar{r}_{0f}^2$ is the mean square end-to-end distance of the equivalent freely jointed chain. The value of σ is thus a measure of the hindrance to rotation about the bonds making

up the polymer chain. Burchard (70) has calculated the value of $(\bar{r}^2_{0f}/M)^{\frac{1}{2}}$ for an amylosic chain (and thus its derivatives) whose monomer units are in the C1 configuration. This configuration is energetically most favourable and there is some evidence for its existence in polyglucosans. The value of $(\bar{r}^2_{0f}/M)^{\frac{1}{2}}$ is 295 x 10^{-11}cm, and that of $(\bar{r}^2_{0f}/M)^{\frac{1}{2}}$, 3.755 x 10^{-8}cm.

Using values of $(\bar{r}^2_0/M)^{\frac{1}{2}}$ in Table III.9, calculated using Φ_0 = 2.87 x 10^{23}, σ was calculated and these are shown in Table III.16. The steric factors for ATB are found to be comparable with those quoted for cellulose butyrate (19) and cellulose tricarbanilate (18) but considerably lower than those found for cellulose trinitrate and some other cellulose derivatives (18).

Table III.16: Steric factors for ATB in various solvents

Solvent 298K	σ
EA	2.96
MEK	2.71
CT	2.88
THF	2.71

ATB seems to behave as a typical random coil polymer which is more flexible than most cellulosic polymers but stiffer than the synthetic polymers. Variation of the unperturbed dimensions with solvent has been found which has also been seen in the case of cellulose tributyrate (19) and other derivatives of cellulose.

SECTION II HYDRODYNAMIC PROPERTIES OF AMYLOSE TRIPROPIONATE RESULTS AND DISCUSSION

1. NUMBER AVERAGE MOLECULAR WEIGHT, $\bar{M}_n$

Values on $\bar{M}_n$ were measured in MEK at 295.5K for fractions P12, P34, P55, P6 and P78 in the membrane osmometer. Fractions with lower molecular weights could not be measured using the membrane osmometer due to permeation of low molecular weight material through the membrane, this shows itself as a gradual drift downwards of the recorder trace. All low molecular weight fractions were measured in EA at 303.6K using the vapour pressure osmometer. The techniques used for both these osmometers have been described previously in Chapter I. The plots of π/C against C are shown in Figure 32 and plots of V/C against C in Figure 33. The values of $(\pi/C)_0$, $(V/C)_0$, $\bar{M}_n$ and A_2 obtained from these plots are shown in Table III.17. The values of the molecular weight are very low, much lower than those found in previous studies of amylose and its derivatives (6, 31, 25). No explanation is put forward for this since the extraction procedure for amylose was essentially the same as that used by Banks and Greenwood (2). Also the reactions conditions for the preparation of the ester were mild and should not have caused excessive degradation of the amylose.

The second virial coefficient, A_2, appears to exhibit no particular trend with molecular weight and this occurs for amylose tripropionate (ATP) in both EA and MEK. The reproducibility of A_2 is rather poor, especially those values

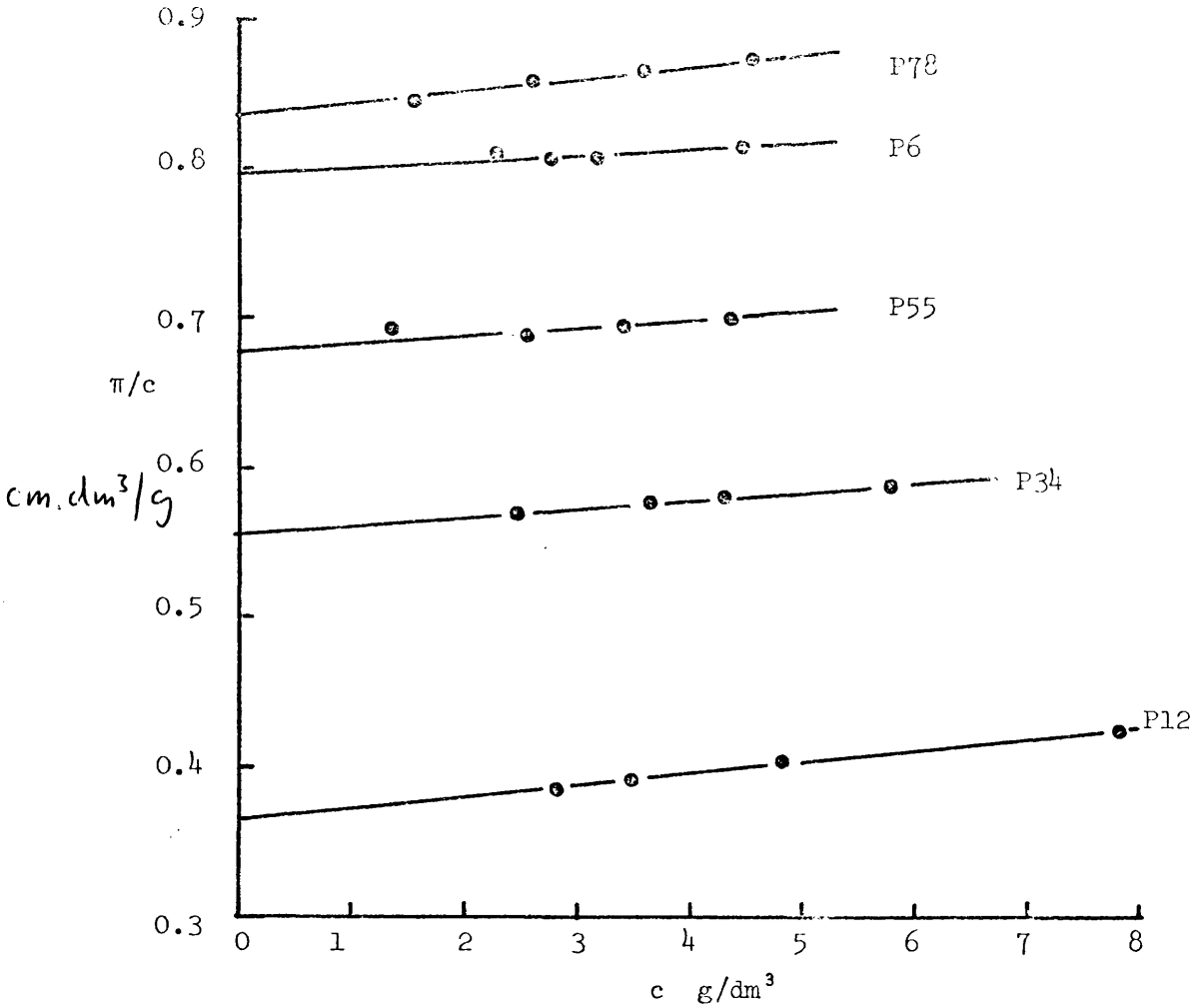

FIGURE 32 PLOT OF π/c AGAINST c FOR ATP/MEK AT 295.5K.

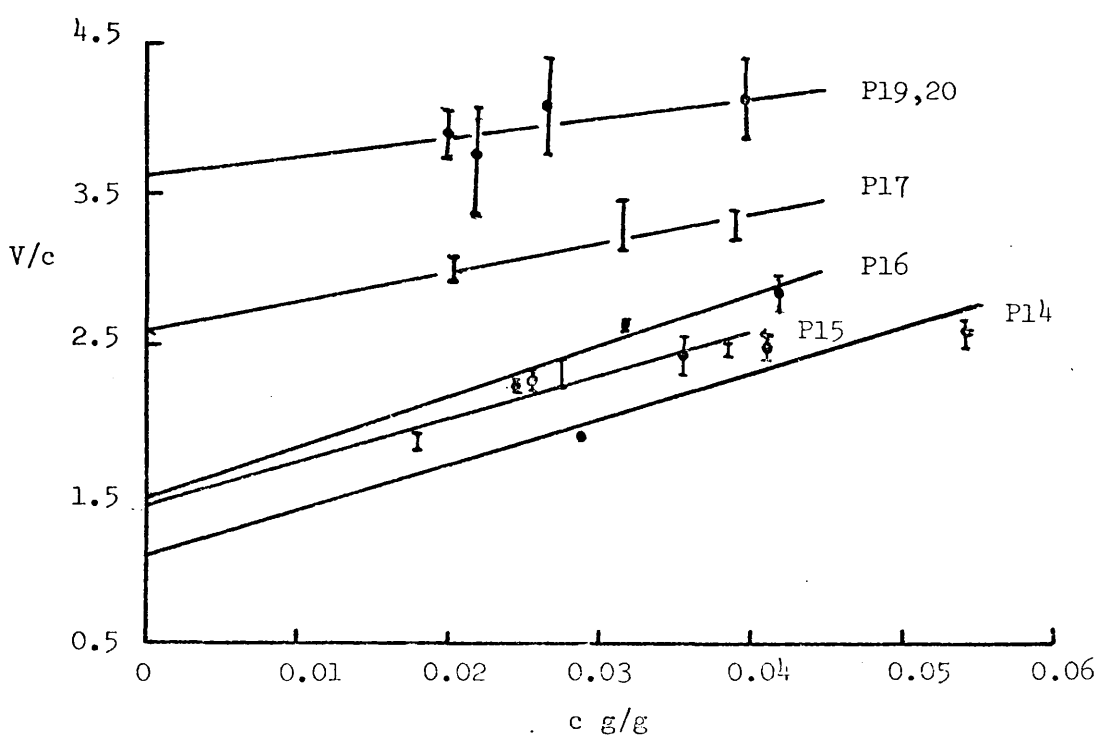

FIGURE 33 PLOTS OF V/c AGAINST c FOR ATP/EA AT 303.6K.

measured by VPO due to uncertainties in its determination. The plots of log A_2 against log $\bar{M}_n$ are shown in Figure 34. The lines drawn through the data correspond to slopes in equation (2) of 0.55 and 0.07 for ATP in EA and MEK respectively, however the scatter on the data is very large and lines with positive slopes could also be drawn.

According to Kurata et al (41) the variation of A_2 with molecular weight can be described by equation (3). The scatter on the data for ATP plotted according to equation (3) was such that no linear relationship was followed. According to present theories the ratio $A_2 M/[\eta]$ should be a function of the expansion

Table III.17: Data for ATP in EA and MEK from measurements of $\bar{M}_n$

ATP Sample	$\bar{M}_n \times 10^{-4}$	$(\frac{\Pi}{C})_0$ cm g^{-1} dm^3	$(\frac{V}{C})_0$ μV	$A_2^{(a)} \times 10^4$ cm^3 mol g^{-2}	$A_2^{(b)} \times 10^4$ cm^3 mol g^{-2}
P12	6.07	0.364		3.59	
P34	3.97	0.557		2.46	
P55	3.28	0.674		2.71	
P6	2.78	0.795		1.95	
P78	2.65	0.833		4.17	
P14	1.42		1.06		2.09
P15	1.07		1.40		1.70
P16	1.02		1.48		2.32
P17	0.579		2.60		1.80
P19,20	0.410		3.66		4.76

(a) Measured in MEK at 295.5K

(b) Measured in EA at 303.6K

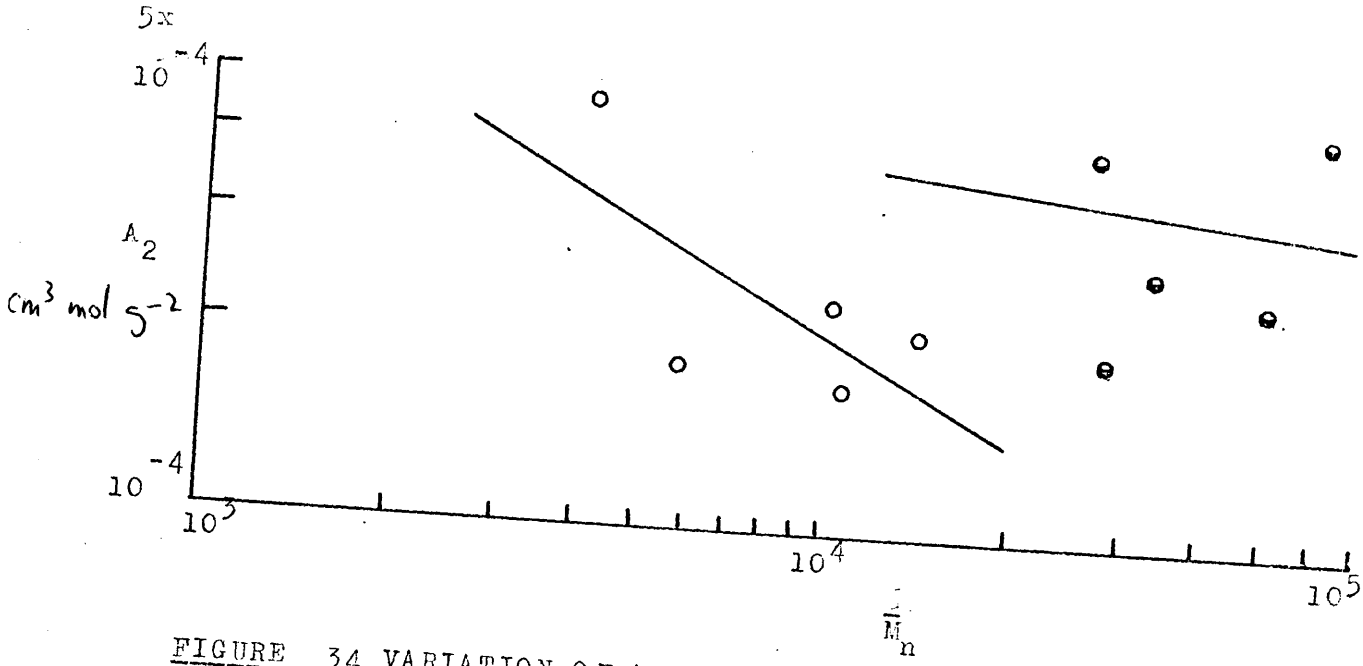

FIGURE 34 VARIATION OF A_2 WITH $\bar{M}_n$ FOR ATP IN EA AND MEK.

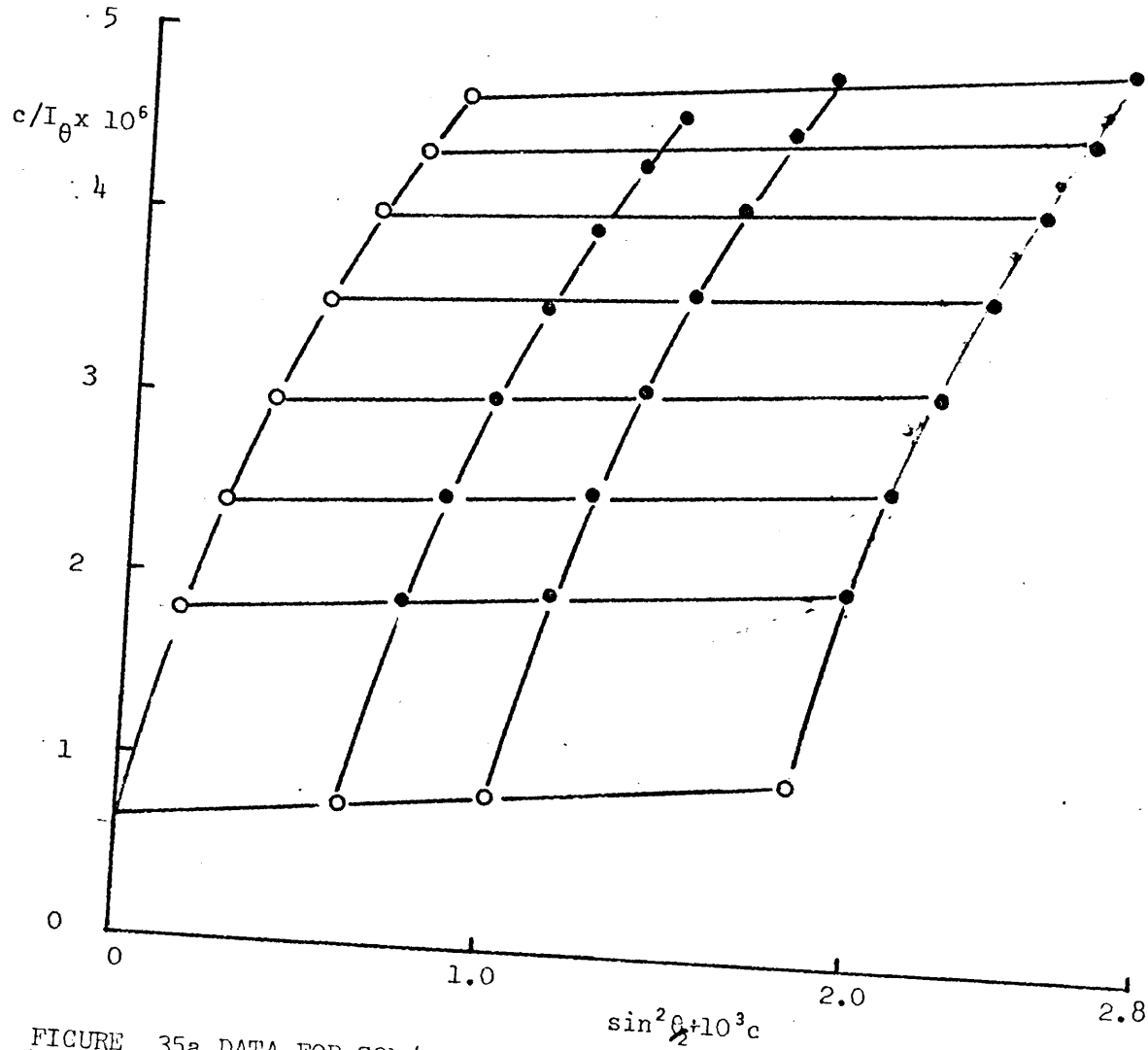

FIGURE 35a DATA FOR S2b/MEK AT 298K PLOTTED ACCORDING TO THE METHOD OF ZIMM.

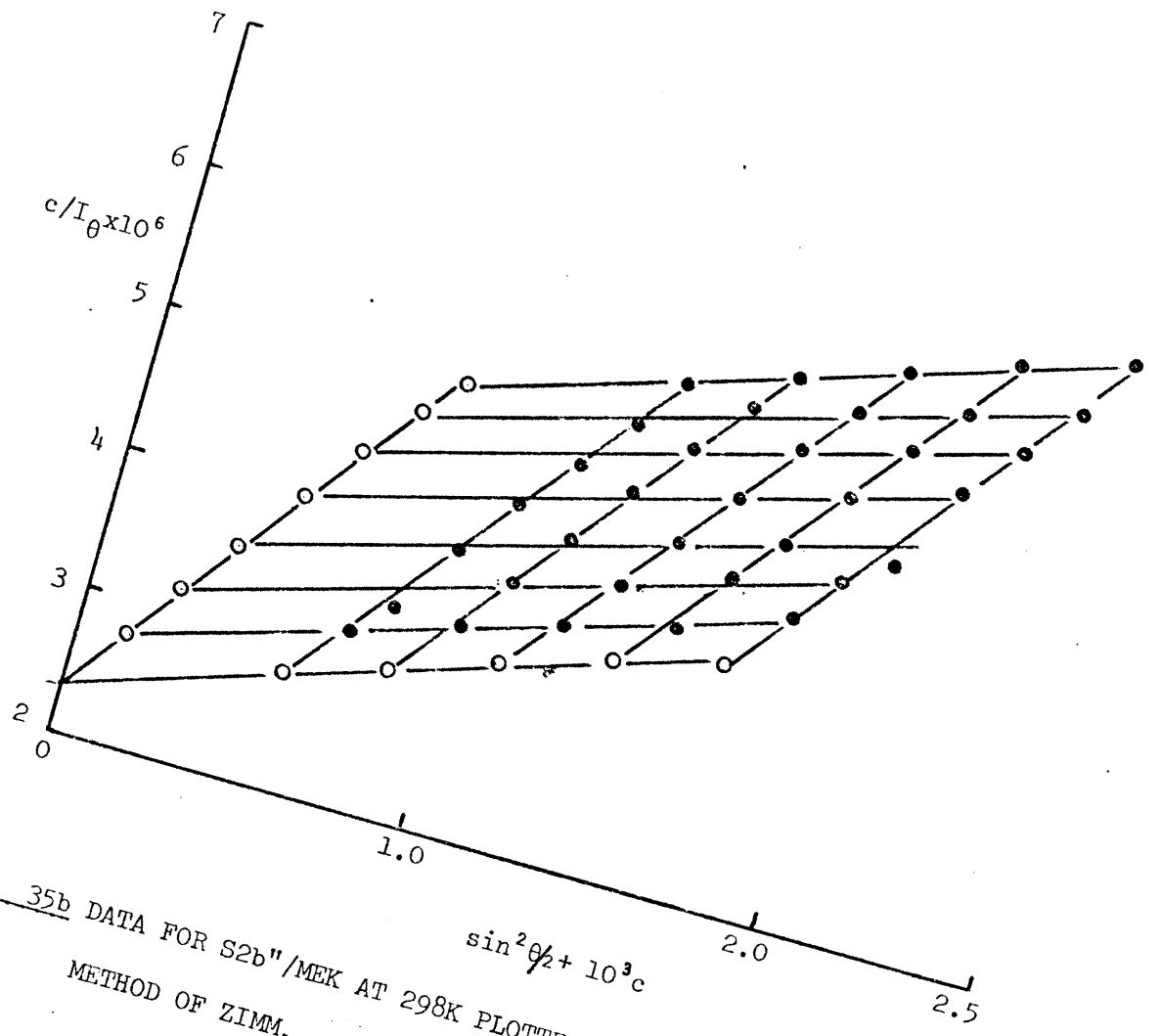

FIGURE 35b DATA FOR S2b"/MEK AT 298K PLOTTED ACCORDING TO THE METHOD OF ZIMM.

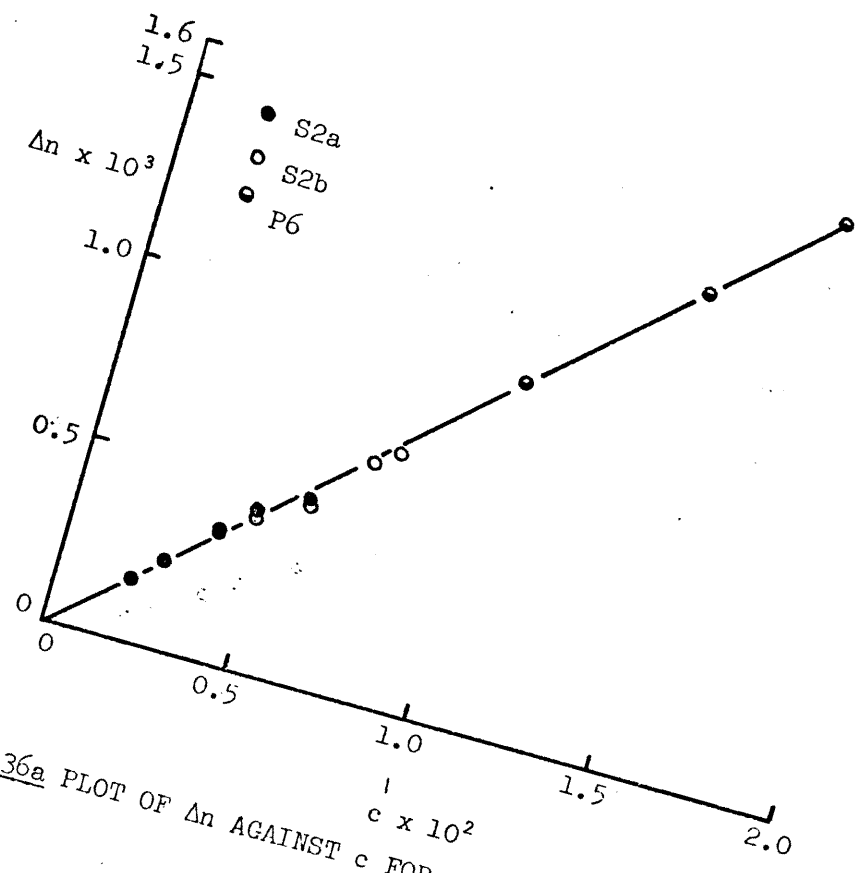

FIGURE 36a PLOT OF Δn AGAINST c FOR ATP/MEK. λ EQUALS 436nm.

coefficient, α. Orofino and Flory (74) have put forward the expression for $f(\alpha)$ given in equation (5). The expansion coefficient, α, has been calculated using experimental values of A_2, $\bar{M}_n$ and $[\eta]$ in EA and MEK. Since the variation with temperature of A_2 is small and uncertainties in A_2 large, values of $[\eta]$ at 298K in MEK and EA have been used. The values of α calculated using Φ_0 equal to 2.87×10^{23} (42) are recorded in Table III.18 along with values of α_η determined from viscosity measurements. The values of α are overestimated using the

Table III.18: Values of α and α_η for ATP in EA and MEK

ATP Sample	Solvent	α from A_2	α_η
P34	MEK	1.35	1.09
P6	MEK	1.26	1.08
P14	EA	1.16	1.09
P15	EA	1.12	1.08
P16	EA	1.18	1.07
P17	EA	1.09	1.13
P19,20	EA	1.21	1.12

Orofino-Flory expression. The dominant factor in the expression appears to be the virial coefficient and since there are large variations in A_2 this affects the values of α.

2. WEIGHT AVERAGE MOLECULAR WEIGHT, $\bar{M}_w$

Measurements of $\bar{M}_w$ were made by light-scattering using unpolarised blue light at 298K on the fractions labelled S. Solutions made up in EA and MEK would not filter through a G5

filter but would pass through a G4 filter. The values of $\bar{M}_w$ were exceedingly large and viscosity measurements made on the samples indicated, on examination of $[\eta]$ - M plots, that either branching or aggregation was being encountered in the samples. Branching could only occur if the original amylose was not linear but this is ruled out by the method of preparation and the enzymic analysis described in Chapter I. The alternative suggestion of aggregation was considered to be more likely.

G.P.C. measurements (see Appendix) made on these samples in THF indicated very broad distributions with a high molecular weight tail. The broad distributions agreed with the idea put forward of aggregation. The light-scattering data plotted according to the method of Zimm had a slight curvature of the lines of equal concentration for some of the samples. The lines in most of the plots were virtually linear which is considered normal for polymers having a distribution of about 1.5. According to the light-scattering data the samples had a reasonable distribution of about 1.5 - 2. This is not consistent with the exceedingly high molecular weights found for two of the samples in particular, S1 and S2a, of 30 x 10^6 and 150 x 10^6, respectively. S1 was found to have the same molecular weight in MEK and EA, but S2a had a higher $\bar{M}_w$ in EA than in MEK. If these molecular weights were correct the molecular weight of amylose would be approximately 75 x 10^6 or 15 x 10^6. Amylose has been found to have a molecular weight in the region of 1 x 10^6 which is considerably less than that indicated by light-scattering on the tripropionate. Table III.19 shows the values of $\bar{M}_w$, $(\bar{s}_z^{-2})^{\frac{1}{2}}$ and Γ_2 for S in EA and MEK.

Table III.19. Data for ATP samples S in EA and MEK

ATP sample	$(\bar{s}^2_z)^{\frac{1}{2}} \times 10^8$ cm	EA Γ_2 cm^{3}g^{-1}	$\bar{M}_w \times 10^{-6}$	$(\bar{s}^2_z)^{\frac{1}{2}} \times 10^8$ cm	MEK Γ_2 cm^{3}g^{-1}	$\bar{M}_w \times 10^{-6}$
S1	1635	0.401	31.1	1429	0.345	28.1
S2a	2511	1.5	186.6	1803	1.023	103.7
S2b				1707	0.188	5.28
S3				1260	0.225	13.47
S4				650	0.0260	1.53

As solutions of the tripropionate would not pass through G5 filters without blocking them this was used as a method of removing the high molecular weight material in the fractions which it was hoped would contain the anomalous material. Solutions were made up of the ATP fractions in EA and filtered under pressure through millipore filters and subsequently G5 filters. The fractions collected after filtration were labelled S'. Light-scattering measurements were made on these filtered fractions in MEK and EA. If the molecular weights of a fraction measured in both solvents were not within about 10% a further filtration was carried out. S1 and S2c were filtered once and renamed S1' and S2c', S2b and S4 had to be filtered twice and were relabelled S2b" and S4". Using this technique the molecular weights dropped considerably. If the aggregation was solvent dependent, as indicated by the values of $\bar{M}_w$ found for S2a in EA and MEK, then by checking the molecular weights of the fractions in two solvents it was assumed that any aggregation had been removed. Table III.20 shows the data for the filtered fractions. An average of the values of $\bar{M}_w$ in the two solvents was used in subsequent calculations involving $\bar{M}_w$.

Table III.20: Data for ATP fractions after filtration

ATP samples	EA $\bar{M}_w \times 10^{-6}$	EA $(\bar{s}_z^{-2})^{\frac{1}{2}} \times 10^8$ cm	EA Γ_2 cm^3/g	EA $A_2 \times 10^8$ cm^3 g^{-2} mol	MEK $\bar{M}_w \times 10^{-6}$	MEK $(\bar{s}_z^{-2})^{\frac{1}{2}} \times 10^8$ cm	MEK Γ_2 cm^3/g	MEK $A_2 \times 10^8$ cm^3 g^{-2} mol
S1'	2.31	466	0.236	10.22	2.64	507	0.205	7.77
S2b"	1.37	461	0.213	15.6	1.43	471	0.163	11.46
S2c'	0.657	307	0.100	15.28	0.653	292	0.0725	11.11
S4"	0.926	449	0.130	14.04	0.972	395	0.0352	3.62

Values of A_2 increase slightly with decreasing molecular weight and are higher for solutions in EA than those in MEK, this correlates with a higher Mark-Houwink exponent for ATP in EA than in MEK (see subsequent sections). Zimm plots for S2b and S2b" are shown in Figure 35. A comparison of data in Table III.19 and Table III.20 shows that not only the molecular weights but also the root mean square radii of gyration have also dropped considerably. However the values for $(\bar{s}_z^2)^{\frac{1}{2}}$ in EA and MEK of S1' and S2b" indicate that MEK is the better solvent although A_2 values show the opposite.

The refractive index increment, (dn/dc), was measured in EA and MEK at 298K. Initially S2a and S2b were used for the measurements but because of the possible aggregation the measured value of (dn/dc) in MEK was checked using a low molecular weight fraction, P6, which according to GPC has a narrow distribution. The data for P6 fitted on the plot for S2a and S2b. According to Elias (71) aggregation should not affect (dn/dc). The values of (dn/dc) were 0.0856 cm^3 g^{-1} for ATP in MEK and 0.0920 cm^3 g^{-1} for ATP in EA. The plots of Δn against C are shown in Figure 36.

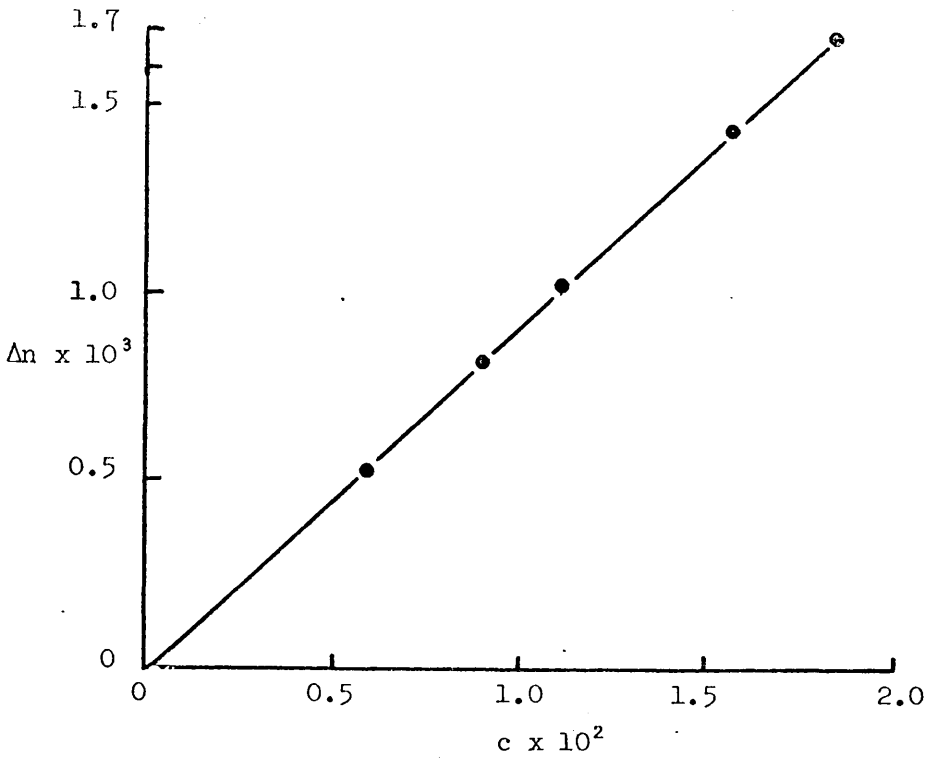

FIGURE 36b PLOT OF Δn AGAINST c FOR S2b/EA AT 298K. λ EQUALS 436nm.

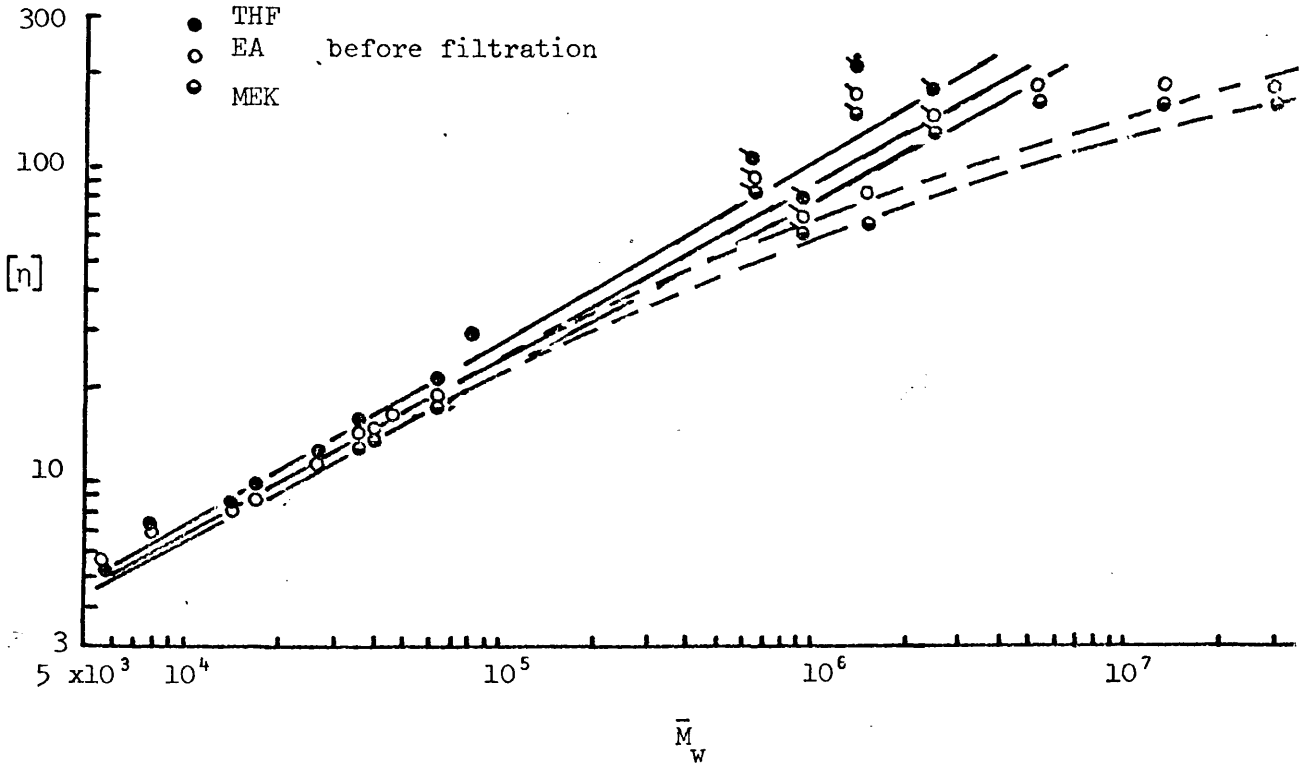

FIGURE 37 $[\eta]-\bar{M}_w$ DATA FOR ATP SHOWING THE EFFECTS OF FILTRATION ON THE SAMPLES.

G.P.C. Results

The distributions $\bar{M}_w/\bar{M}_n$ measured by G.P.C. were assumed to be correct and were used in conjunction with values of $\bar{M}_n$ measured by osmometry to calculate $\bar{M}_w$. The values of $\bar{M}_w^{GPC}$ and $\bar{M}_n^{GPC}$ are listed in Table A.1. in the Appendix and show that according to G.P.C. the values of $\bar{M}_w$ for the apparently anomalous high molecular weight fractions increases after filtration and also the distributions become even broader. However, light-scattering shows $\bar{M}_w$ to have decreased. Obviously something unusual is happening to these fractions but further investigations are needed to elucidate this problem.

2. VISCOSITY MEASUREMENTS

Measurements of the limiting viscosity number, $[\eta]$, were made in tetrahydrofuran (THF), methyl ethyl ketone (MEK) and ethyl acetate (EA) at 298K. The temperature dependence of $[\eta]$ was also examined in EA.

Viscosity - Molecular Weight Relationships

The viscosity-molecular weight data for ATP in the three solvents is shown in Table III.21, included is the data for the ATP fractions prior to filtration. Log - log plots of the data are shown in Figures 37 and 38. The behaviour of the S fractions prior to filtration is shown by the dashed lines, in Figure 37, as mentioned earlier in this section this type of curve is indicative of branching or aggregation (72). After filtration the values of the molecular weights are such that there is still quite a large scatter. A line drawn through the low molecular weight data points also passes through the point for S1'. This was taken as the correct

Table III.21: $[\eta]$ - M data for ATP

ATP Sample	$\bar{M}_n \times 10^{-5}$	$\bar{M}_w \times 10^{-5}$	$[\eta]$ cm³/g THF 298K	MEK 298K	EA 289.8K	EA 298K	EA 313K
P12	0.607		29.3	24.7			24.6
P34	0.397	0.639	21.2	17.8	19.1	18.5	16.8
P55	0.328	0.466				16.3	
P6	0.278	0.361	15.3	13.0	13.6	14.3	13.0
P78	0.265			13.5		14.6	
P14	0.142	0.257	12.1			11.3	
P15	0.107	0.168	9.4		8.6	8.8	8.2
P16	0.102	0.140	8.2		8.2	8.0	
P17	0.0579	0.0780	7.3			6.9	
P19,20	0.0410	0.0537	5.1			5.6	
S1		295		160		181.3	
S2a		145		292.7		340.2	
S2b		52.8		167.5		185.8	
S3		134.7		159.1		180.2	
S4		15.3		66.2		73.1	
S1'		24.8	175.8	131.6	146.9	147.8	132.7
S2b"		14.0	208.1	147.3	177.0	168.9	160.1
S2c'		6.55	106.0	82.8	90.9	90.3	82.3
S4"		9.48	79.5	61.6	69.3	67.8	64.1

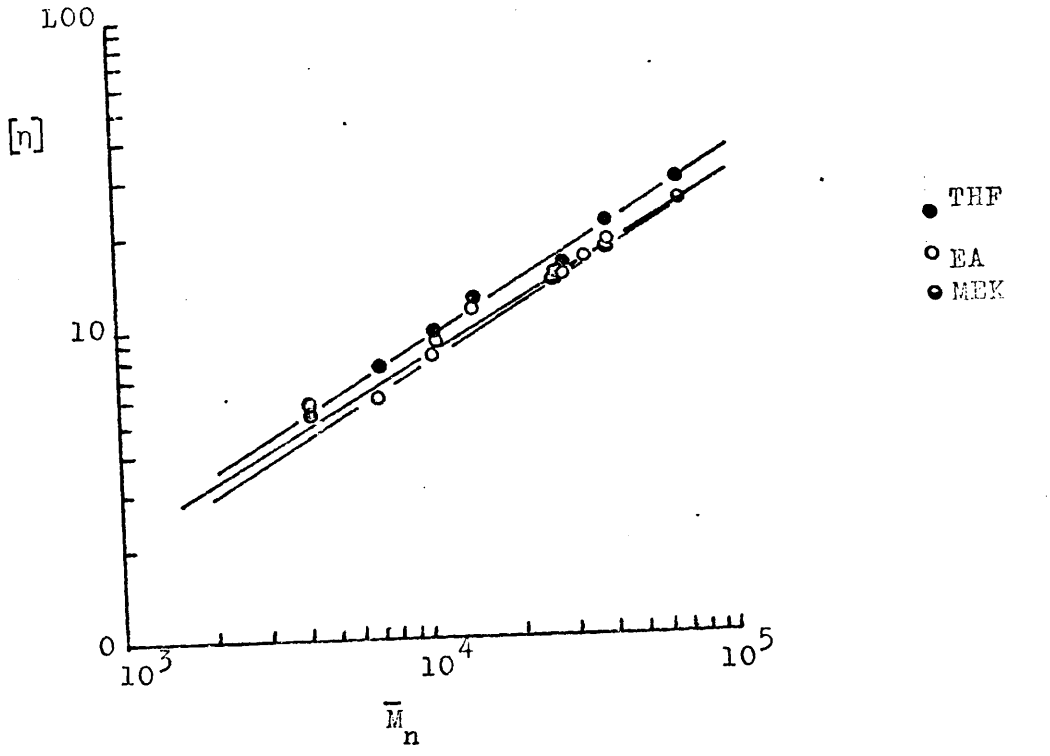

FIGURE 38 VISCOSITY-$\bar{M}_n$ DATA FOR ATP AT 298K.

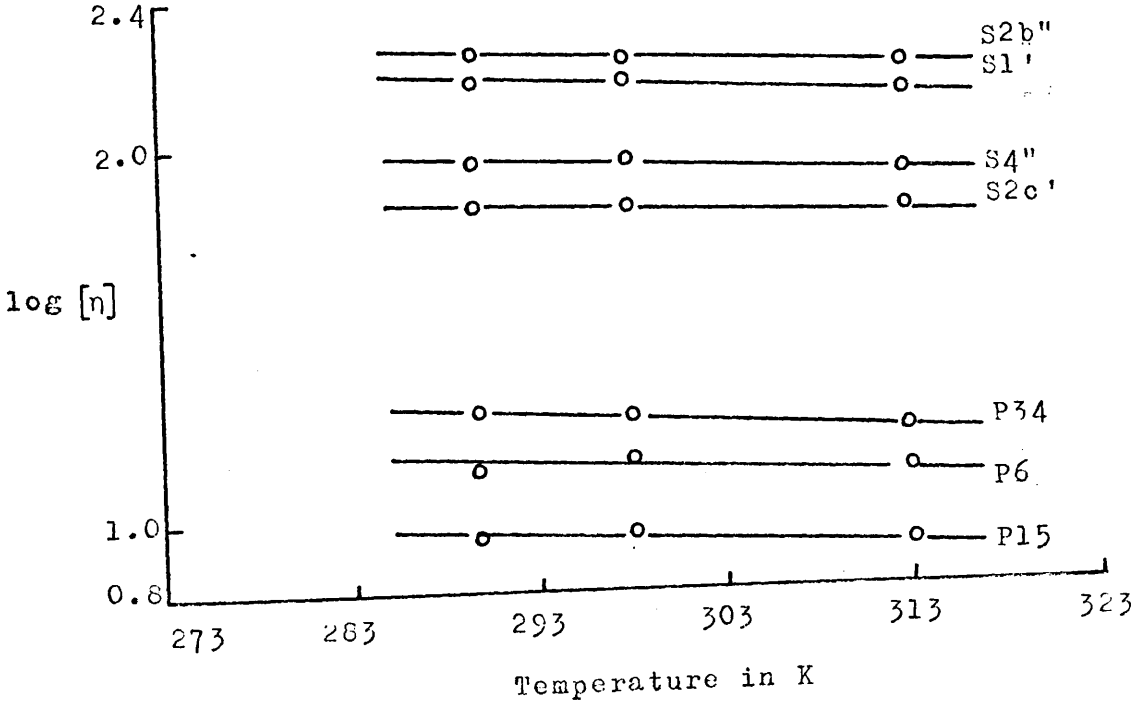

FIGURE 39 TEMPERATURE DEPENDENCE OF VISCOSITY OF ATP IN EA

$[\eta]$ - M relationship. Data for S4" falls below this line, possibly there is still anomalous material contained in it. The two sets of data which lie above the line belong to S2b" and S2c'. These could be explained if a different $[\eta]$ - M relationship existed above about $\bar{M}_w$ equal to 2×10^5, in which case both S1' and S4" would possibly contain anomalous material. It is difficult to say which is correct, if any, by looking at the $[\eta]$ - $\bar{M}_w$ plot. The use of this data will be discussed again in later sections.

The $[\eta]$ - M relationships at 298K are

EA $[\eta] = 3.96 \times 10^{-2} \bar{M}_w^{0.56}$

$[\eta] = 3.49 \times 10^{-2} \bar{M}_n^{0.59}$

MEK $[\eta] = 4.56 \times 10^{-2} \bar{M}_w^{0.54}$

$[\eta] = 3.03 \times 10^{-2} \bar{M}_n^{0.60}$

THF $[\eta] = 3.78 \times 10^{-2} \bar{M}_w^{0.58}$

$[\eta] = 3.18 \times 10^{-2} \bar{M}_n^{0.61}$

Temperature dependence of $[\eta]$

The equations describing the temperature dependence of $[\eta]$ were given in the section on the tributyrate. Amylose tripropionate in EA shows a negative temperature dependence of $[\eta]$ between 289.8K and 313K. Plots of $\log[\eta]$ against T are shown in Figure 39. The values of $-\Delta \log[\eta] / dT$ are recorded in Table III.22, these show no dependence on molecular weight. The dependence on temperature is about a factor of 10^2 smaller than that shown by cellulose derivatives (18, 19)

Table III.22: Temperature dependence of $[\eta]$ for ATP in EA

ATP Sample	$-\Delta \log[\eta] / dT \times 10^3$
P34	3.0
P6	2.0
P15	2.0
S1'	2.0
S2b"	2.5
S2c'	2.0
S4"	2.0

and the same order of magnitude as the butyrate.

In Table III.23 are the values of the Mark-Houwink exponents at the different temperatures, very little change with temperature can be detected.

Table III.23: Mark-Houwink constants for ATP in EA

Temperature K	$K \times 10^2$	a
289.8	3.79	0.56
298	3.96	0.56
313	3.10	0.57

Unperturbed dimensions from viscosity measurements

Unfortunately as in the case of the tributyrate no θ-solvent was established for amylose tripropionate. It has therefore been necessary to apply again the theories outlined in the section on the tributyrate.

The data for ATP in EA, MEK and THF was treated according to the theories of Flory and Fox, Stockmayer and Fixman, Kurata

and Stockmayer, Inagaki, Suzuki and Kurata, Berry and Cowie. The graphs plotted according to equations (14), (17), (21), (25), (28) and (32) are shown in Figures 40 - 45.

(a) Flory-Fox

The data plotted according to this theory are shown in Figure 40. Lines through the data for the three solvents can be made to pass through the same intercept without strain. At molecular weights below about 10^4 there is evidence of a possible tail-off where the equation is no longer valid. Also included in the plot are the data points for S4", S2b" and S2c'. The point S4" is low and those for S2b" and S2c' high. Both sets would cause fairly drastic curvature in the plot if used. Use of the high data in particular would mean that the Flory-Fox relationship was invalid below molecular weights of about 2×10^5 and would lead to K_θ values which were very low or negative. However, the Flory-Fox treatment is valid near the theta point, as is the case for ATP in the three solvents, so that such spurious values of K_θ are unlikely. K_θ is recorded in Table III.24.

(b) Kurata-Stockmayer-Roig

The data plotted according to equation (17) are shown in Figure 41. The lines pass without strain through a common intercept if the high molecular weight data is ignored. The difference between K_θ values on the second and third trials was less than 2%. The K_θ value is recorded in Table III.24.

(c) Stockmayer-Fixman

The data plotted according to equation (21) are shown in Figure 42. Once again a common intercept can be found by

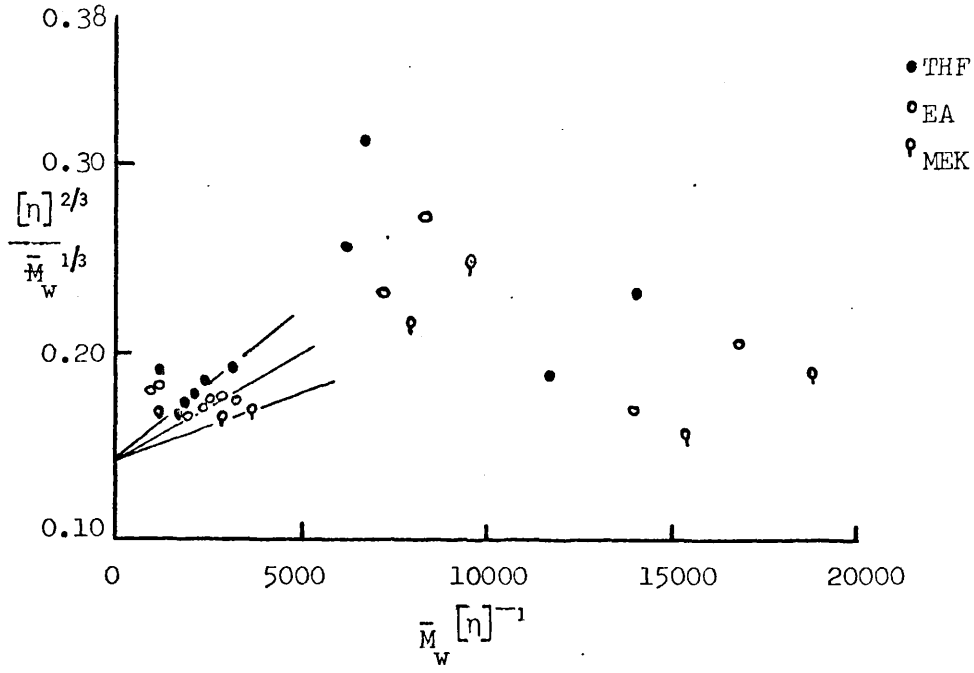

FIGURE 40 DATA FOR ATP PLOTTED ACCORDING TO THE FLORY-FOX EQUATION.

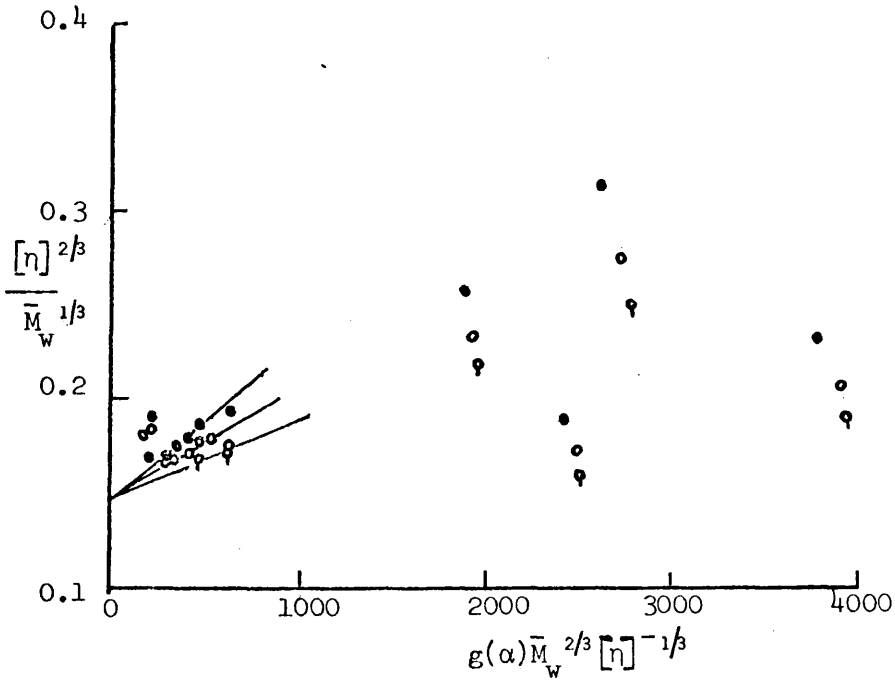

FIGURE 41 DATA FOR ATP PLOTTED ACCORDING TO THE KURATA-STOCKMAYER EQUATION.

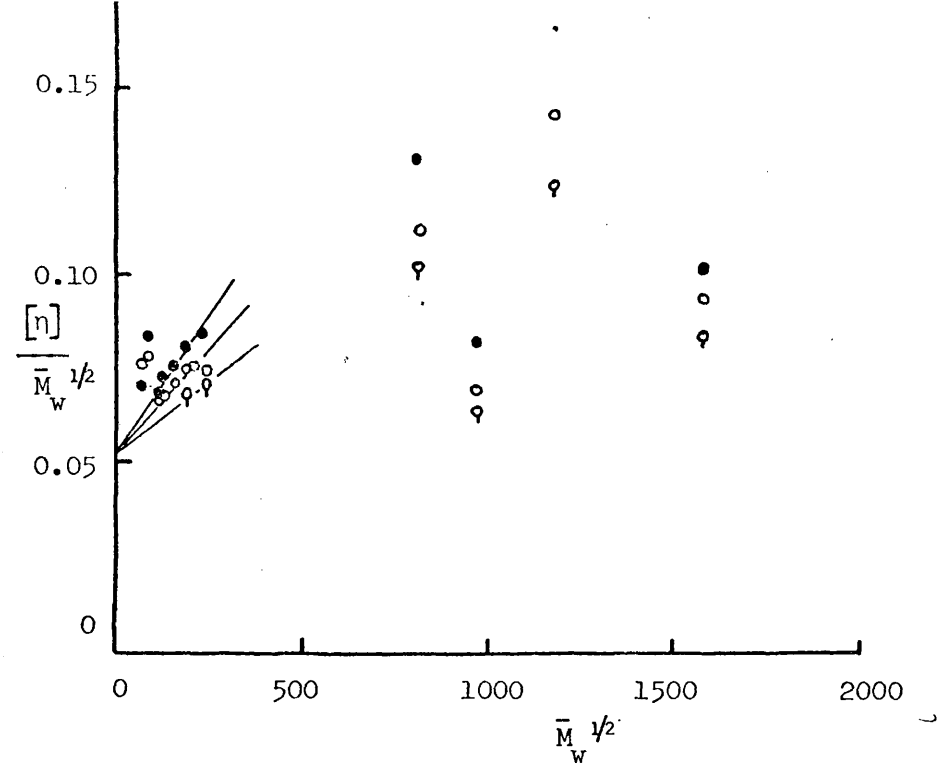

FIGURE 42 DATA FOR ATP PLOTTED ACCORDING TO THE STOCKMAYER-FIXMAN EQUATION AT 298K.

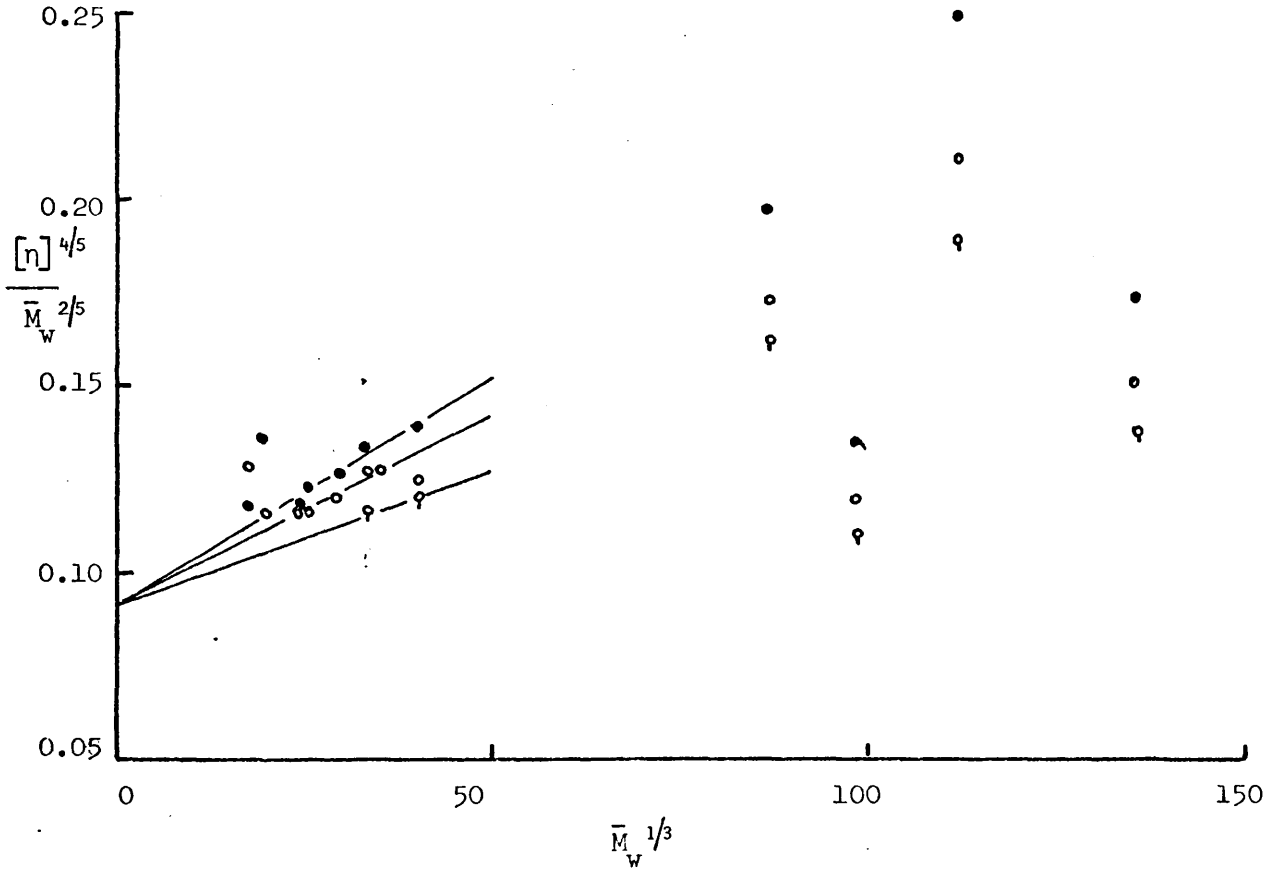

FIGURE 43 DATA FOR ATP PLOTTED ACCORDING TO THE INAGAKI-SUZUKI-KURATA EQUATION

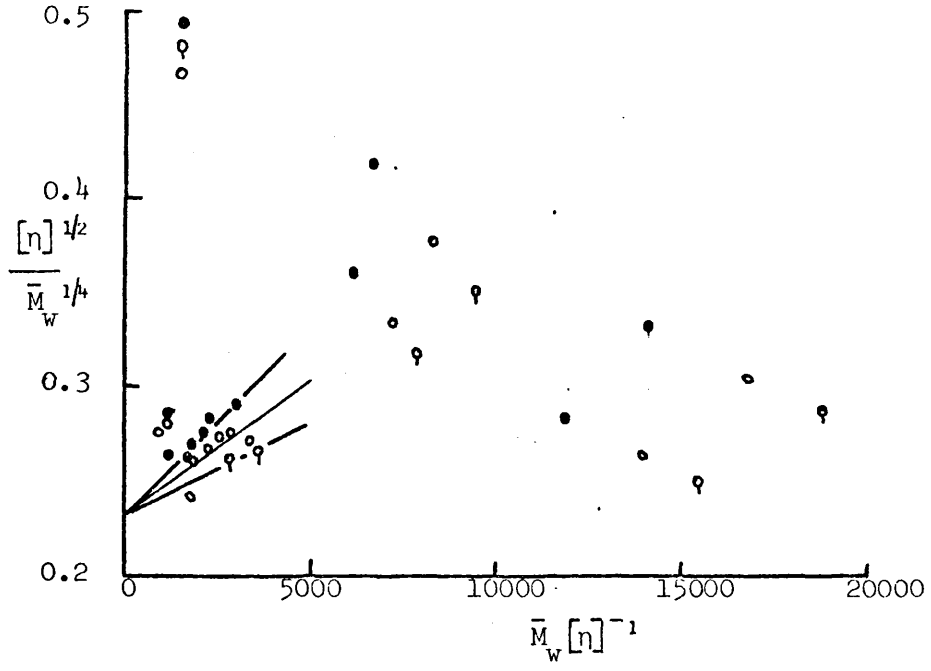

FIGURE 44 DATA FOR ATP PLOTTED ACCORDING TO THE BERRY EQUATION.

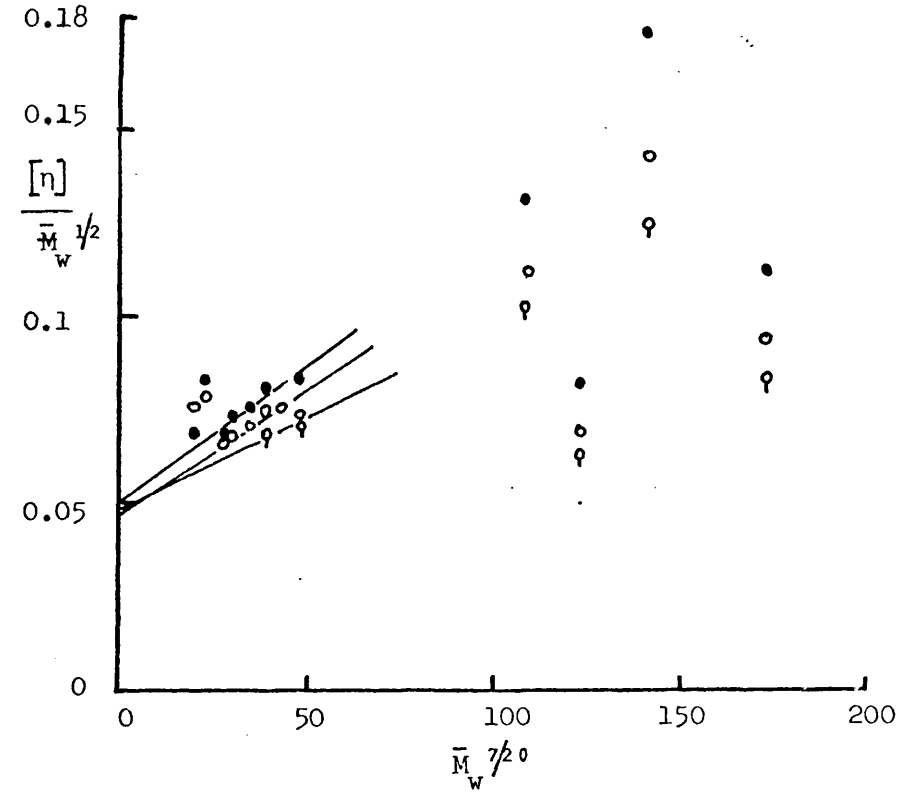

FIGURE 45 DATA FOR ATP PLOTTED ACCORDING TO THE MODIFIED BOHDANECKY EQUATION, AT 298K.

drawing lines through the three sets of data. Use of the high molecular weight data would give low and varying intercepts. The value of K_θ is recorded in Table III.24.

(d) Inagaki-Suzuki-Kurata

The data plotted according to equation (25) are shown in Figure 43. Lines can be drawn through the three sets of data which intercept the abscissa at the same point. The value for K_θ is shown in Table III.24. Once again use of the high molecular weight points cause varying intercepts.

(e) Berry

The data plotted according to the theory of Berry given by equation (28) is shown in Figure 44. A common intercept was found for lines drawn through the three sets of data. Use of the higher molecular weight data would leads to spurious results. K_θ is recorded in Table III.24.

The expression proposed by Bohdanecky and modified by Cowie was also tested using the data for ATP. The plot of data treated according to equation (32) is shown in Figure 45. The values of K_θ are shown in Table III.24. Very little variation of K_θ with solvent was found.

Table III.24: K_θ values according to the various theories

ATP Solvent	K_θ F-F	K_θ S-F	K_θ K-S	K_θ Berry	K_θ Cowie	K_θ I-S-K
EA	0.055	0.053	0.056	0.054	0.053	0.068
MEK	"	"	"	"	0.056	"
THF	"	"	"	"	0.054	"

Table III.24 shows that apart from the value for K_θ derived from the Inagaki-Suzuki-Kurata treatment the values of K_θ only vary by about 2.5% from a mean of 0.0545. Inagaki et al (55) have suggested that equation (25) is only valid for $\alpha_\eta > 1.4$ thus none of the data falls within this category since $\alpha_\eta < 1.3$.

The consistency of the K_θ values seems to point to the fact that, apart from the Inagaki-Suzuki-Kurata treatment, all the treatments are valid for systems near the theta-point which have low Mark-Houwink exponents and α_η values. The Flory-Fox treatment, in particular, is invalid for data away from the theta-point, as shown by the data for the tributyrate where increasing solvent power causes the value of K_θ to drop.

Using values for Φ_0 of 2.87×10^{23} and $\Phi(\varepsilon)$ (as defined by equation (33)) $(\bar{r}_0^2/\bar{M}_w)^{\frac{1}{2}}$ was calculated from the value for K_θ found above. Values of $(\bar{r}_0^2/\bar{M}_w)^{\frac{1}{2}}$ of 575×10^{-11}cm and 576×10^{-11}cm were found using Φ_0 and $\Phi(\varepsilon)$ respectively, which are considerably smaller than the value found for amylose acetate in nitromethane by Banks, Greenwood, and Hourston (25) but similar to the values found for some cellulose derivatives (19, 45).

Temperature dependence of the unperturbed dimensions

Data for ATP in EA at 289.8K and 313K were plotted according to equations (21) and (17) and are shown in Figure 46. The average values of K_θ were 0.060 at 289.8K and 0.053 at 313K. The unperturbed dimensions therefore decrease with temperature, but not smoothly.

Expansion coefficient, α_η

The expansion coefficients have been calculated using the

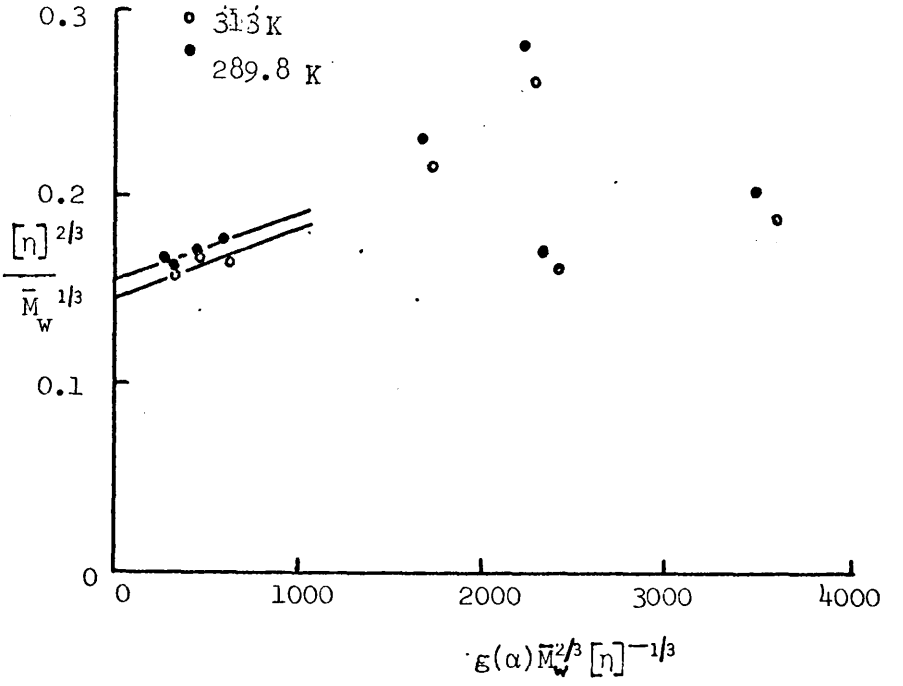

FIGURE 46a TEMPERATURE DEPENDENCE OF K_θ. DATA FOR ATP/EA PLOTTED ACCORDING TO THE KURATA-STOCKMAYER EQUATION.

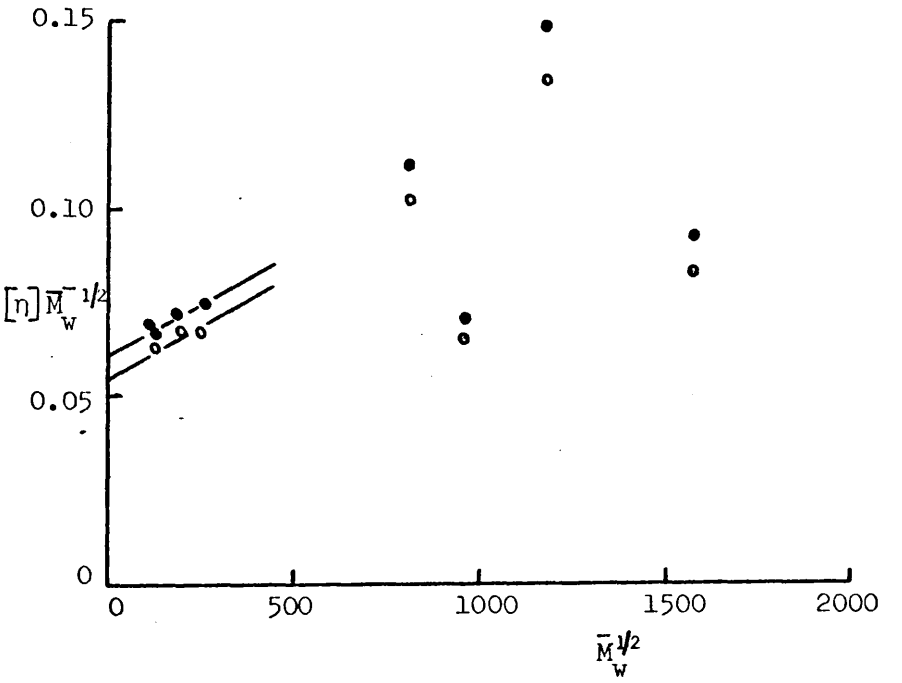

FIGURE 46b TEMPERATURE DEPENDENCE OF K_θ. DATA FOR ATP/EA PLOTTED ACCORDING TO THE STOCKMAYER-FIXMAN EQUATION.

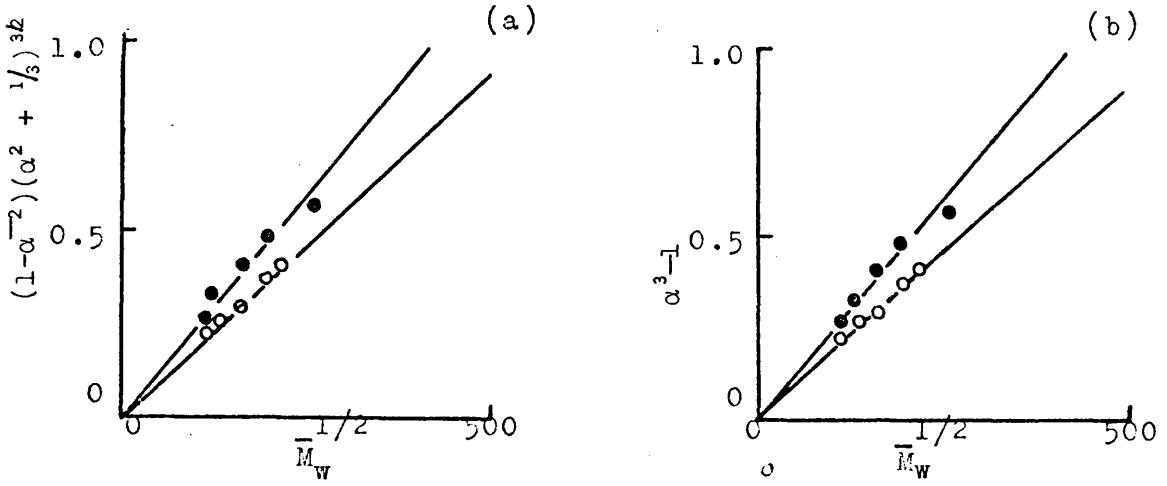

FIGURES 47a&b DATA FOR ATP IN THF AND EA ACCORDING TO THE STOCKMAYER-FIXMAN AND KURATA-STOCKMAYER EQUATIONS, RESPECTIVELY.

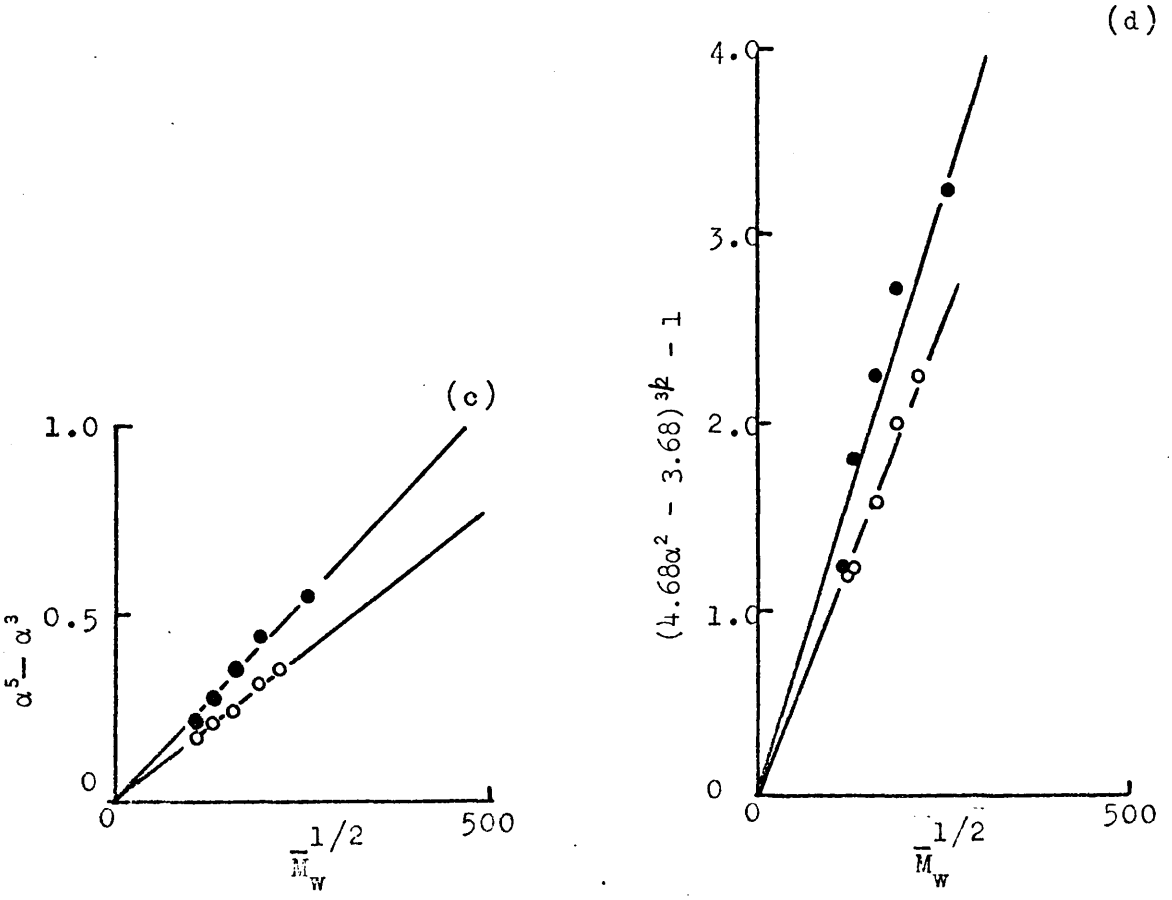

FIGURES 47c&d DATA FOR ATP IN THF AND EA ACCORDING TO THE FLORY-FOX AND PTITSYN EQUATIONS, RESPECTIVELY.

average values of K_θ and are recorded in Table III.25. The variation of α_η with solvent follows the trend $\alpha_{THF} > \alpha_{EA} > \alpha_{MEK}$ which is mirrored in the variations of Mark-Houwink exponents. The values of α_η decrease slowly with decreasing molecular weight and are smaller than the values for ATB which is to be expected because the solvents are better solvents for ATB.

The variation of α_η with temperature shows an increase followed by a decrease from 298K. The temperature coefficient of $[\eta]$, d log $[\eta]$/dT, is small and is determined by the expansion coefficient which dominates the unperturbed dimensions causing a small regular decrease in $[\eta]$. 'Long' range forces and not 'short' range forces therefore dominate the temperature coefficient of $[\eta]$.

The data for ATP in EA and MEK were treated according to the theories of Stockmayer and Fixman, Kurata and Stockmayer, Flory and Fox, and Ptitsyn using the relationships given in equations (37), (38), (39) and (40). The plots are shown in Figure 47. For each equation the data is linear with $M^{\frac{1}{2}}$ and lines can be drawn to pass through the origin. The Stockmayer-Fixman and Kurata-Stockmayer expressions are numerically equal when the values of the expansion coefficient are low but at higher values of α_η the expressions diverge.

4. THE CONFORMATION OF ATP FROM HYDRODYNAMIC CONSIDERATIONS

In section I on amylose tributyrate the Kirkwood-Riseman and Kuhn-Kuhn models for describing the hydrodynamic behaviour of a polymer chain were discussed. These theories have been applied to the data for ATP using equations (44) and (48). The

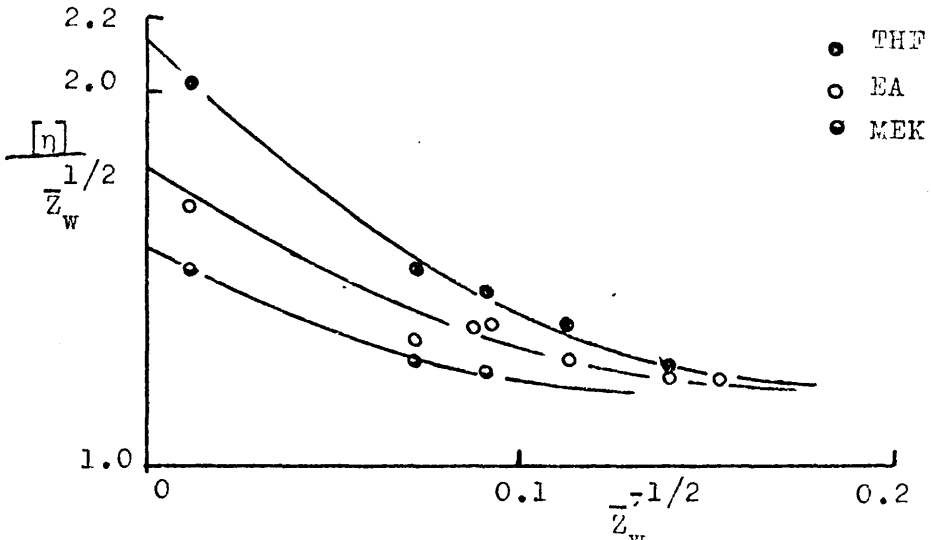

FIGURE 48 DATA FOR ATP IN THF, EA AND MEK ACCORDING TO THE KIRKWOOD-RISEMAN EQUATION.

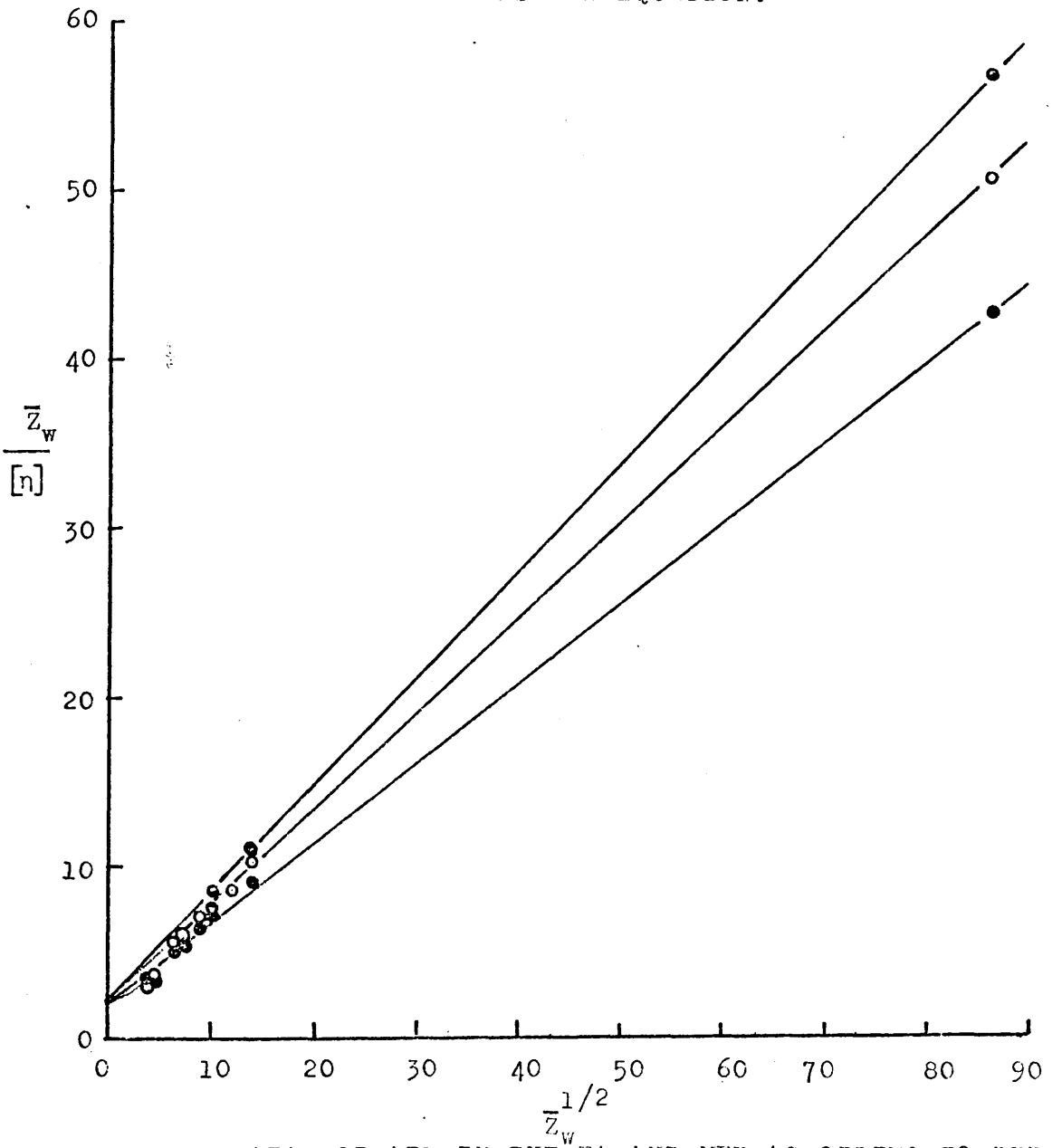

FIGURE 49 DATA FOR ATP IN THF, EA AND MEK ACCORDING TO THE KUHN-KUHN EQUATION.

Table III.25: α_η for ATP in THF, EA and MEK

ATP Sample	α_η THF 298K	α_η MEK 298K	α_η EA 298K	α_η EA 289.8K	α_η EA 313K
P34	1.16	1.09	1.10	1.08	1.07
P55			1.12		
P6	1.14	1.08	1.11		1.08
P14	1.12		1.09		1.05
P15	1.10		1.08	1.03	
P16	1.08		1.07	1.05	
P17	1.15		1.13		
P19,20	1.08		1.12		

plots showing the data according to these equations are shown in Figures 48 and 49. The values of b and A_m calculated from these plots are shown in Table III.26.

Table III.26: Values of b and A_m calculated according to theories in the text for ATP

Solvent	Temperature (K)	b x 10^8cm	A_m x 10^8cm
EA	289.8	12.0	36.0
	298	12.1	38.9
	313	11.5	34.8
THF	298	13.0	44.1
MEK	298	11.5	36.1

The values of b and A_m indicate that ATP is a flexible polymer but again as in the case of the tributyrate less flexible

than the synthetic polymers. The effective length b decreases slightly with increasing temperature indicating that the molecule is becoming increasingly flexible. The slight increase in b and A_m between 289.8K and 298K might well be due to uncertainties in the extrapolations. More data would help to clarify this situation. Both b and A_m are largest in THF which agrees with the value of the Mark-Houwink exponent which is largest for ATP in THF. The persistence length, q, calculated for ATP using equations (52) and (53) is 12.4×10^{-8}cm which again shows that ATP is relatively flexible but more rigid than the synthetic polymers.

For the polymer in the unperturbed state b and A_m can be calculated using equations (50) and (51). The values of b and A_m calculated in this way are 10.4×10^{-8}cm and 24.8×10^{-8}cm, respectively, which again indicate a flexible polymer. The values of b and A_m in the perturbed state only increase slightly over the unperturbed values. The presence of solvent seems to have little effect on the flexibility as would be expected because of the poor quality of the solvents. The steric factor, σ, has a value of 2.78.

All the parameters discussed above indicate that ATP is a normal flexible chain polymer more rigid that the synthetic polymers and less rigid than the cellulosic polymers. The magnitude of the unperturbed dimensions approaches that of many synthetic polymers.

More data is required particularly about high molecular weight ATP so that fractions can be studied with a wider range of molecular weights. It would also be useful to carry out further research on the present high $\bar{M}_w$ ATP samples to try to elucidate the exact nature of the anomalous behaviour.

SECTION III HYDRODYNAMIC PROPERTIES OF AMYLOSE TRIACETATE RESULTS AND DISCUSSION

1. NUMBER AVERAGE MOLECULAR WEIGHT, $\bar{M}_n$

Measurements of $\bar{M}_n$ were carried out on all the amylose triacetate (ATA) fractions. Fractions F4, F5 and F6 had to be run in the VPO due to permeation of low molecular weight species through the membranes of the membrane osmometer. Measurements in the VPO were made in ethyl acetate (EA) at 303.6K and those in the membrane osmometer in nitromethane (NO_2Me) at 295.5K. The techniques used are described in Chapter I. Graphs of π/C against C and V/C against C are shown in Figures 50 and 51. In Table III.27 are recorded the values of $\bar{M}_n$, $(\pi/C)_0$, $(V/C)_0$ and A_2 for the acetate in EA and NO_2Me. From Table III.27 it can be seen that the values of $\bar{M}_n$ are very low, as in the case of the propionate. Banks, Greenwood and Hourston (25) for their study of ATA had a range of molecular weights from $\bar{M}_w$ of 0.148×10^6 to 3.11×10^6 so that the range of molecular weight fractions in the present study should provide data at the low molecular weight end.

The values of A_2 tend to increase rapidly with increasing molecular weight. If a log-log plot is made of A_2 against $\bar{M}_n$ according to equation (2) the slope, γ, should not exceed 0.15 or in the case of very good solvents 0.25. In fact as can be seen in Figure 52 a line drawn through the data for ATA in NO_2Me corresponds to a slope of 1.1. If the data for F4b and F3 is ignored a value for γ of 0.24 is found which is just within the limit for very good solvents. A value for γ

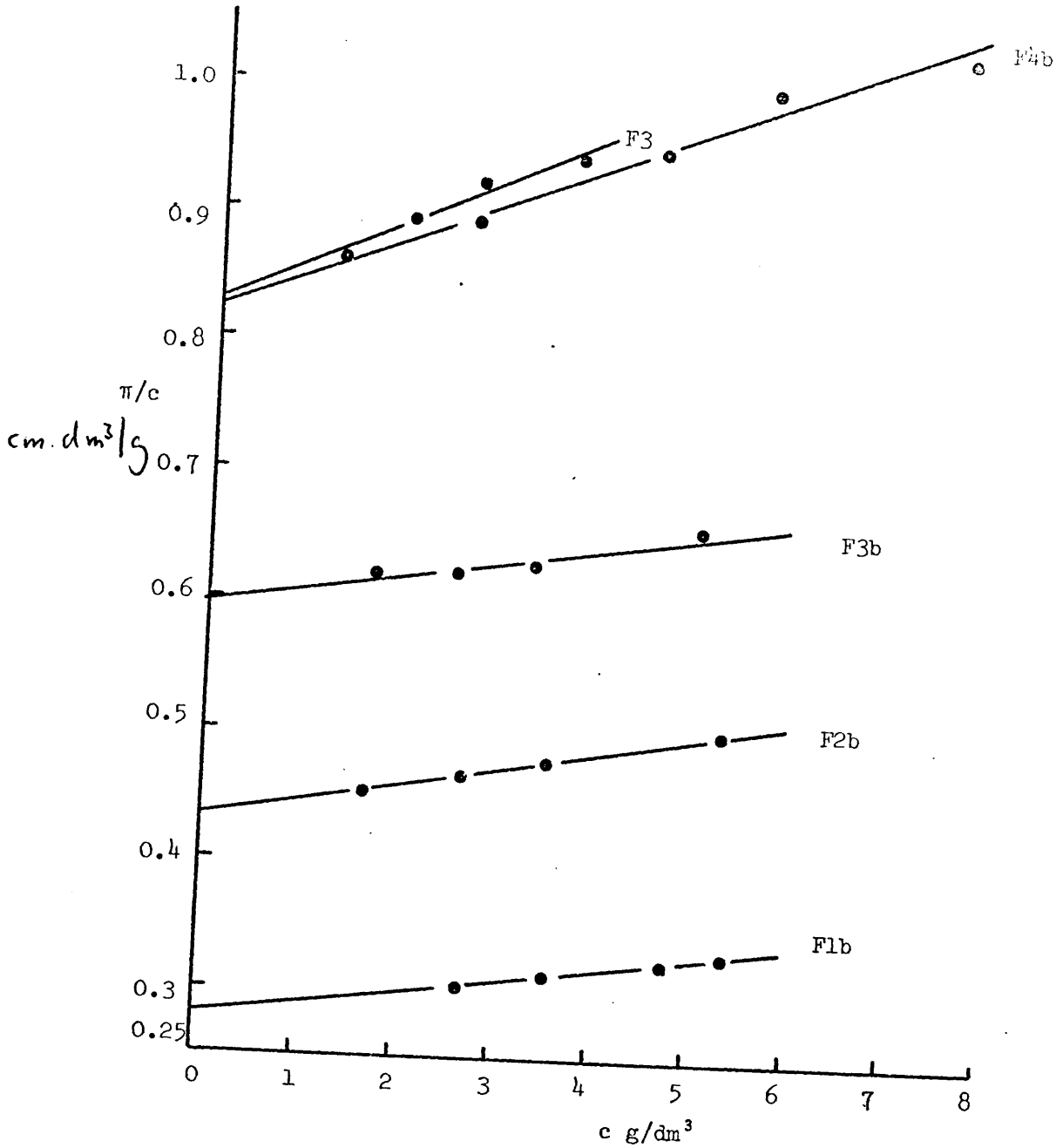

FIGURE 50 PLOTS OF π/c AGAINST c FOR ATA/NO_2ME AT 295.5K.

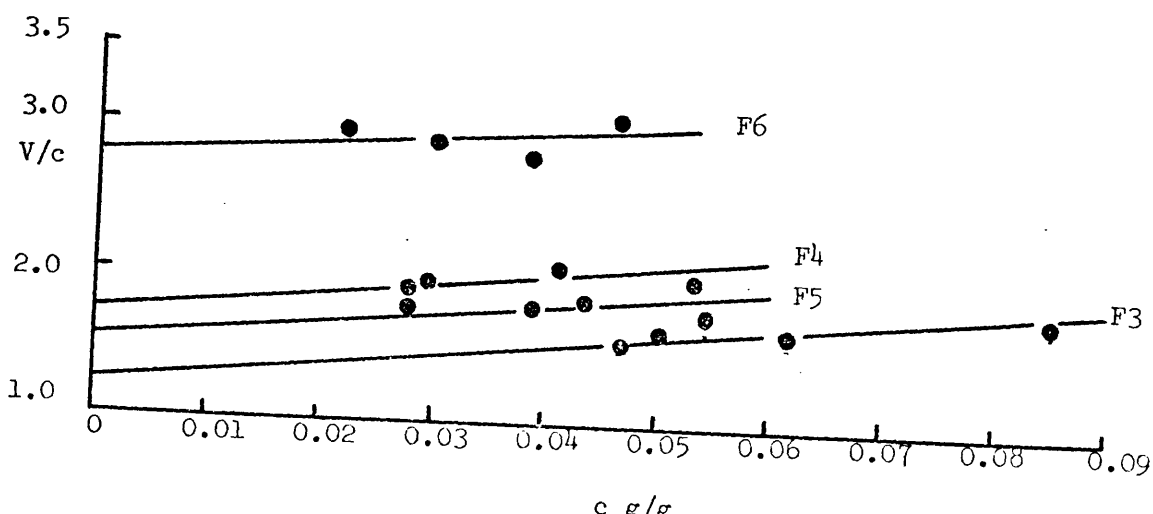

FIGURE 51 PLOTS OF V/c AGAINST c FOR ATA/EA AT 303.6K.

Table III.27: Data from $\bar{M}_n$ measurements of ATA in NO_2Me and EA

ATA Fractions	$\bar{M}_n \times 10^{-5}$	$(\frac{\pi}{C})_0$ cm g^{-1} dm^3	$(\frac{V}{C})_0$ μV	(a) $A_2 \times 10^4$ $cm^3 g^{-2} mol$	(b) $A_2 \times 10^4$ $cm^3 g^{-2} mol$
F1b	0.798	0.277		4.50	
F2b	0.515	0.429		6.25	
F3b	0.370	0.597		5.2	
F4b	0.267	0.829		14.50	
F3	0.268	0.825		12.71	
F4	0.088		1.72		4.76
F5	0.0983		1.53		3.30
F6	0.0574		2.62		6.90

(a) Measured in NO_2Me at 295.5K

(b) Measured in EA at 303.6K.

of 1.4 was calculated from the data for ATA in EA which is well above the limit. The values of A_2 are prone to large errors but they still exhibit a tendency to increase with decreasing molecular weight which was not found by Banks and Greenwood (73).

Table III.28: Data for ATA in NO_2Me using the Flory-Orofino expression

ATA Fraction	α from A_2	α_η
F1b	1.48	1.25
F3b	1.68	1.18
F4b	2.73	
F3	2.43	1.15

The data for A_2 plotted according to equation (3) give negative slopes and intercepts corresponding to very large unperturbed dimensions, because of the rapid increase in A_2. Again as in the case of the Kurata-Stockmayer (17) equation, that of Kurata and coworkers (41) does not fit the experimental values of A_2.

The Flory-Orofino expression (74) was used to determine values of α and these are recorded in Table III.28. The limiting value (42) for Φ_0 of 2.87×10^{23} was used in the calculations. The large variation in A_2 also causes large variations in α, as seen in Table III.28. Because of the uncertainties in the values of A_2 it is difficult to draw any conclusions regarding the agreement between theoretical and experimental values of α.

Temperature variation of A_2

Using the membrane osmometer A_2 was measured at 279.5K, 287.8K, 308.2K and 295.5K for F1b and F2b in NO_2Me. The values of A_2 are recorded in Table III.29. The variation with temperature is small and follows no definite trend particularly in the case of F2b. The method of measurements was obviously not sensitive or accurate enough to get any information from it other than there is little variation over the temperature range studied. This is in keeping with the idea that NO_2Me is a good solvent for ATA. (see section on $[\eta]$ - M relationships and ref. (25)).

Table III.29: Variation of A_2 with temperature for ATA in NO_2Me

ATA Fraction	279.8K $A_2 \times 10^4$	287.8K $A_2 \times 10^4$	295.5K $A_2 \times 10^4$	308.2K $A_2 \times 10^4$
F1b	3.4	3.5	4.50	4.5
F2b	5.0	4.4	6.25	3.4

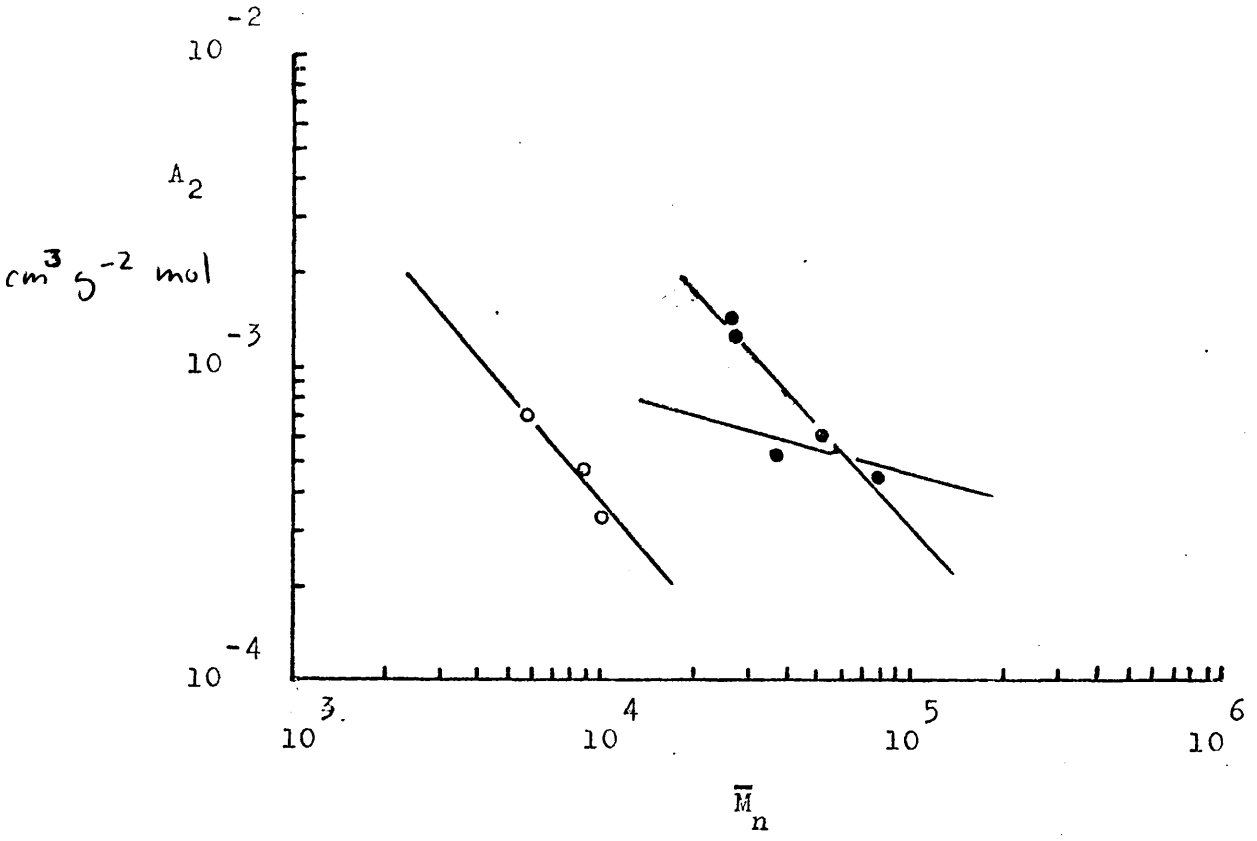

FIGURE 52 VARIATION OF A_2 WITH $\bar{M}_n$ FOR ATA IN ● NO_2ME AND ○ EA.

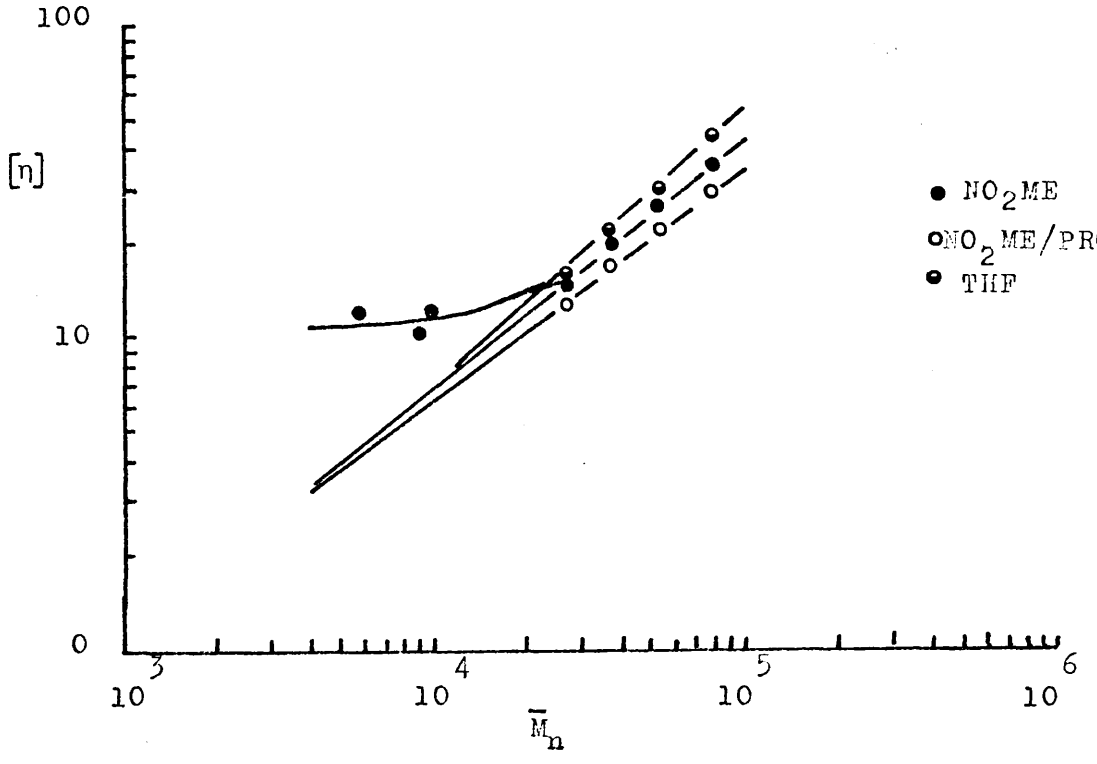

FIGURE 53a VISCOSITY-$\bar{M}_n$ DATA FOR ATA AT 298K.

2. WEIGHT AVERAGE MOLECULAR WEIGHT, $\bar{M}_w$

Measurements of $\bar{M}_w$ were made in NO_2Me at 298K on fractions F1b, F3b, F4b and F3. The values of $\bar{M}_w$ are shown in Table III.30 together with A_2 and values of $\bar{M}_w$ calculated using the distribution from GPC. Apart from F1b for which $\bar{M}_w^{GPC}$ is exceedingly high due to a very broad distribution value, the correlation between G.P.C. and light-scattering data is excellent. The difference between the experimentally measured distribution and that measured by G.P.C. is of the order of 1 - 6%. Use of the GPC distribution and measured $\bar{M}_n$ values will give $\bar{M}_w^{GPC}$ values which are 1 - 6% different from experimental values, which is within the error in molecular weight measurements. Thus use of the GPC distributions is justified.

Table III.30: Data from light-scattering and GPC

ATA Fraction	$\bar{M}_w^{LS} \times 10^{-6}$	$\bar{M}_w^{GPC} \times 10^{-6}$	$A_2^{LS} \times 10^4 cm^3 g^{-2} mol$
F1b	0.137	0.708	1.22
F3b	0.0584	0.0603	3.90
F4b	0.0428	0.0456	3.11
F3	0.0380	0.0375	0.95

The values of A_2 recorded in Table III.30 are smaller than those measured by osmometry shown in Table III.27 by up to a factor of 10 for F3 which had a particularly high value of A_2 according to osmotic pressure measurements. Banks and Greenwood (73) found little, if any, variation in A_2 measured by light-scattering. A_2 is this study is prone to large uncertainties and varies erratically.

3. VISCOSITY MEASUREMENTS

Measurements of the limiting viscosity number $[\eta]$ were made in nitromethane (NO_2Me), 50/50 V/V nitromethane / propan - 1 - ol and tetrahydrofuran (THF) at 298K and in NO_2Me at 303K and 295.5K.

No high molecular weight fractions had been prepared and it was felt desirable to have some. Two samples A2 and A3 were provided by Dr. J.M.G. Cowie, these samples had values of $\bar{M}_w$ of 1.00×10^6 and 0.82×10^6, respectively. Viscosity measurements were also made in methyl ethyl ketone and ethyl acetate on the low molecular weight fractions. The high molecular weight fractions were found to be insoluble in MEK, EA and THF. Table III.31 contains all the viscosity-molecular weight data for ATA.

Figure 53 records plots of log $[\eta]$ against log M for ATA in NO_2Me, 50/50 NO_2Me/propan-1-ol and THF at 298K, for both $\bar{M}_n$ and $\bar{M}_w$. The graph for THF is included because although high molecular weight material is insoluble, this relationship was used in the GPC calibration for the low molecular weight fractions with reasonable success.

The $[\eta]$ - M relationships at 298K are

Nitromethane $[\eta] = 3.58 \times 10^{-3} \bar{M}_w^{0.78}$

$[\eta] = 4.34 \times 10^{-3} \bar{M}_n^{0.8}$

50/50 nitromethane/propan-1-ol $[\eta] = 4.63 \times 10^{-3} \bar{M}_w^{0.74}$

$[\eta] = 6.91 \times 10^{3} \bar{M}_n^{0.74}$

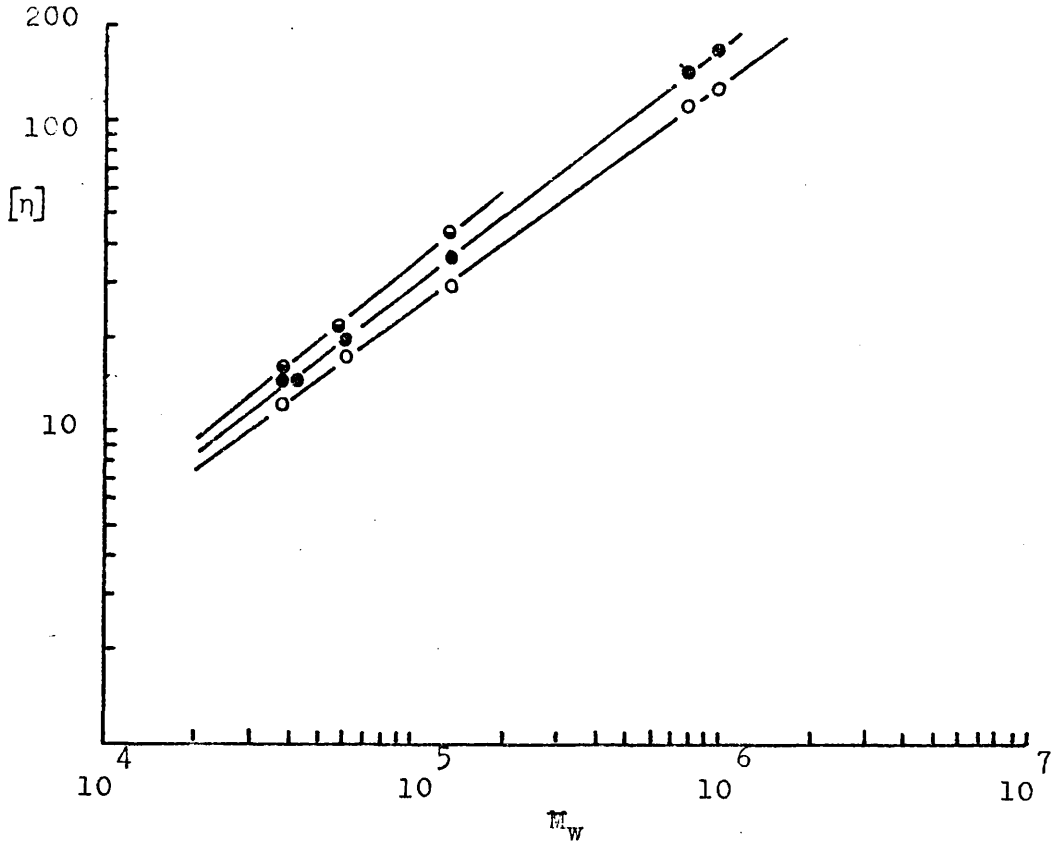

FIGURE 53b VISCOTY-$\bar{M}_w$ DATA FOR ATA AT 298K.

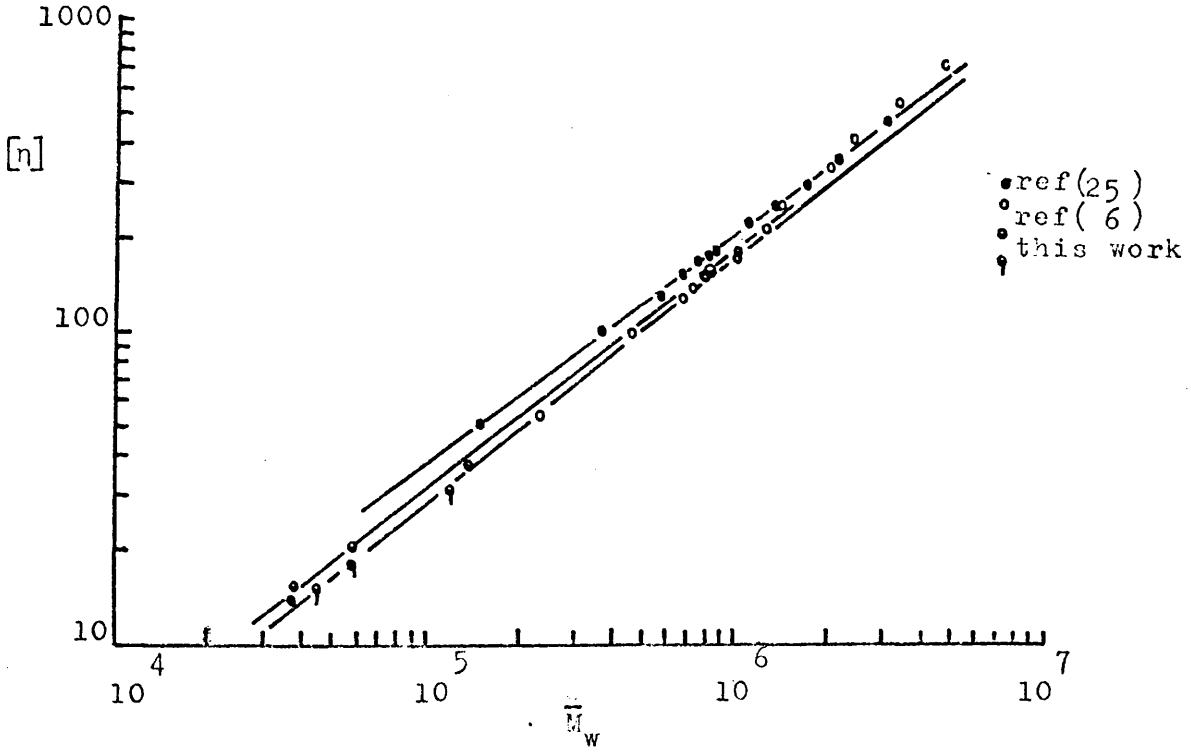

FIGURE 54 DATA FOR ATA/NO_2ME ACCORDING TO REF.(25) AND REF.(6) AND THIS STUDY.

THF (applicable only for $\bar{M}_w < 2 \times 10^5$)

$$[\eta] = 3.42 \times 10^{-3} \bar{M}_w^{0.8}$$

$$[\eta] = 1.71 \times 10^{-3} \bar{M}_n^{0.9}$$

Both nitromethane and the mixed solvent are good solvents shown by quite high Mark-Houwink exponents. For ATA in NO_2Me Banks and Greenwood (25) found a value for a of 0.73 at 295.5K and Cowie (6) a value of 0.87 at 303K. The data from references (25) and (6) have been plotted together with data from this study in Figure 54.

Table III.31: $[\eta]$ - M data for ATA

cm^3/g

ATA Fraction	$\bar{M}_n \times 10^{-5}$	$\bar{M}_w \times 10^{-6}$	$[\eta]$ NO_2Me 295.5K	$[\eta]$ NO_2Me 298K	$[\eta]$ NO_2Me 303K	$[\eta]$ 50/50 N/P 298K	$[\eta]$ THF 298K
A2		1.00	180.0	180.2	171.5	134.4	
A3		0.82	159.0	153.9	156	118.7	
F1b	0.798	0.137		36.2		29.3	44.0
F2b	0.515			26.2		22.2	29.5
F3b	0.370	0.0584		20.0	17.5	17.3	21.9
F4b	0.267	0.0428		14.7			
F3	0.268	0.0380		14.7	13.5	12.4	15.9
F4	0.088			10.2			
F5	0.0983			12.2			
F6	0.0574			12.2			

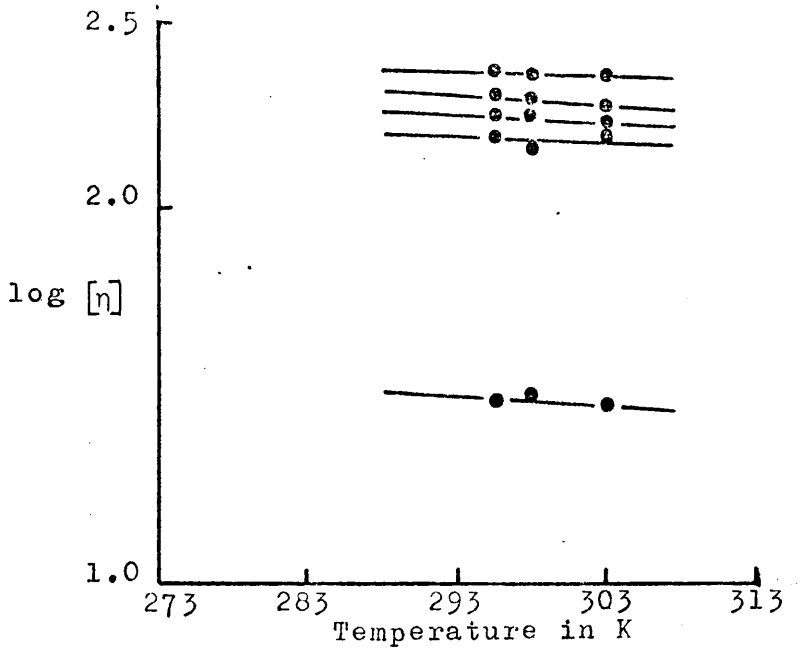

FIGURE 55 TEMPERATURE DEPENDENCE OF VISCOSITY OF VARIOUS FRACTIONS OF ATA, SUPPLIED BY Dr. J.M.G. Cowie, IN NO_2ME.

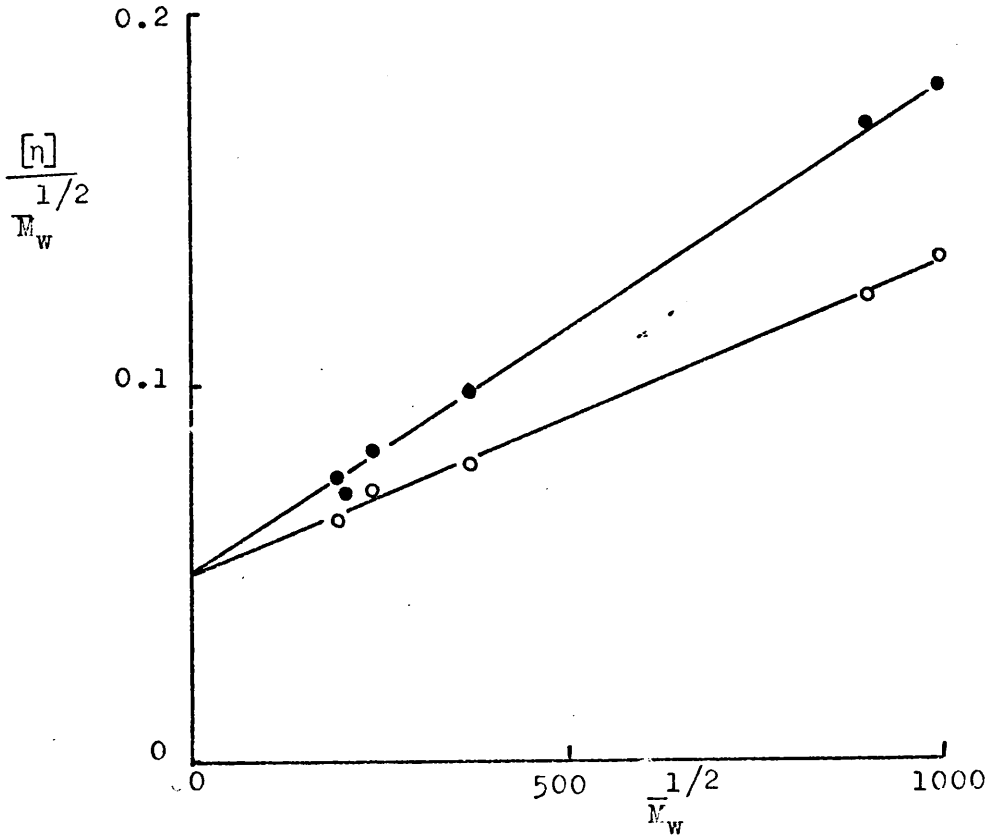

FIGURE 56 DATA FOR ATA IN NO_2ME AND NO_2ME/PROPANOL ACCORDING TO THE STOCKMAYER-FIXMAN EQUATION.

The data in Table III.31 at 303K can be fitted to a line drawn through Cowie's data which disregards the high molecular weight points giving a value for a of 0.8. There seems to be an upward trend shown by the highest fractions possibly due to overcorrection for shear effects. The temperature variation of viscosity is very low for the samples in this work. It was not possible to fit the Banks and Greenwood data with this work, possibly due to the samples having different heterogeneities which will affect the dependence of $[\eta]$ on $\bar{M}_w$. The temperature dependence of $[\eta]$ is shown in Figure 55 for 5 samples of amylose triacetate all of which were supplied by Dr. J.M.G. Cowie. The average value of $(-\Delta \log [\eta]/dT)$ is 2.2×10^{-3} K^{-1}, which is of the same order as that found for the propionate and the butyrate.

According to the Mark-Houwink plot there is a tail-off below about $\bar{M}_n$ equal to 2×10^4. Below this molecular weight it is possible that the molecule no longer behaves as a random coil.

Unperturbed dimensions from viscosity measurements

The data for ATA in NO_2Me and the mixed solvent at 298K were treated according to the theories of Stockmayer and Fixman (54), Kurata and Stockmayer (17), and Flory and Fox (46) outlined in the section of ATB. The graphs plotted according to the appropriate equations are shown in Figures 56, 57 and 58.The Stockmayer-Fixman and Kurata-Stockmayer plots are linear over the range of experimental molecular weights and the data for NO_2Me and NO_2Me/propan-1-ol extrapolates to the same intercept. Both of these plots give values for K_θ of 0.050.

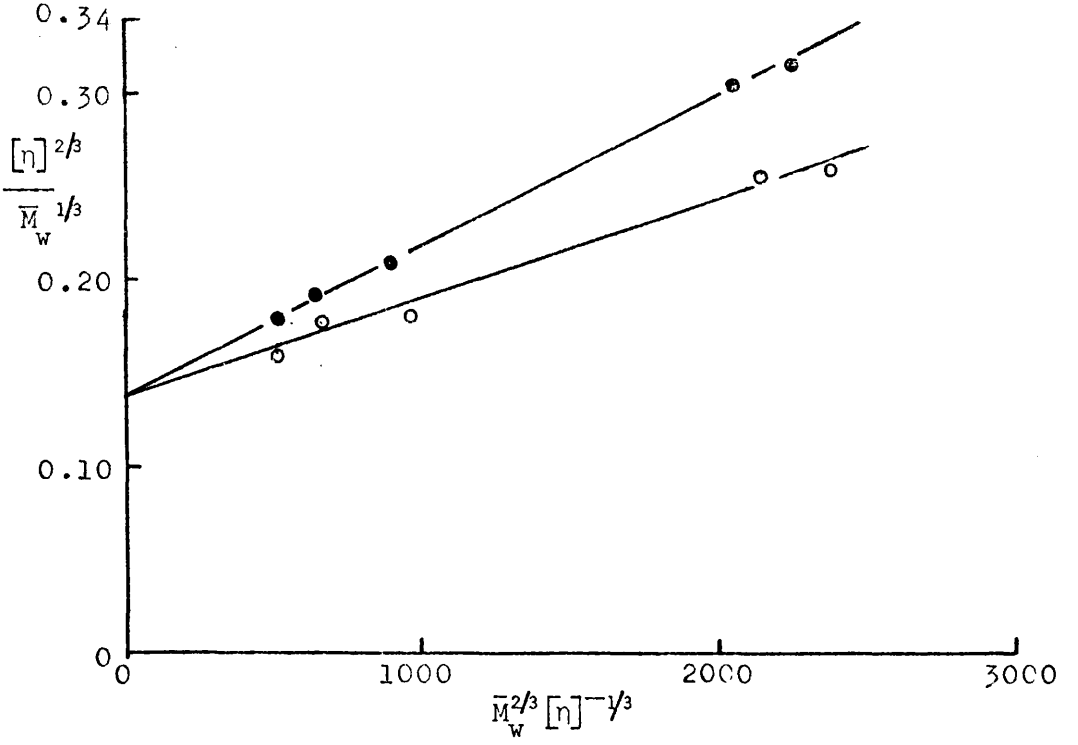

FIGURE 57 DATA FOR ATA IN NO_2ME AND NO_2ME/PROPANOL ACCORDING TO THE KURATA-STOCKMAYER EQUATION.

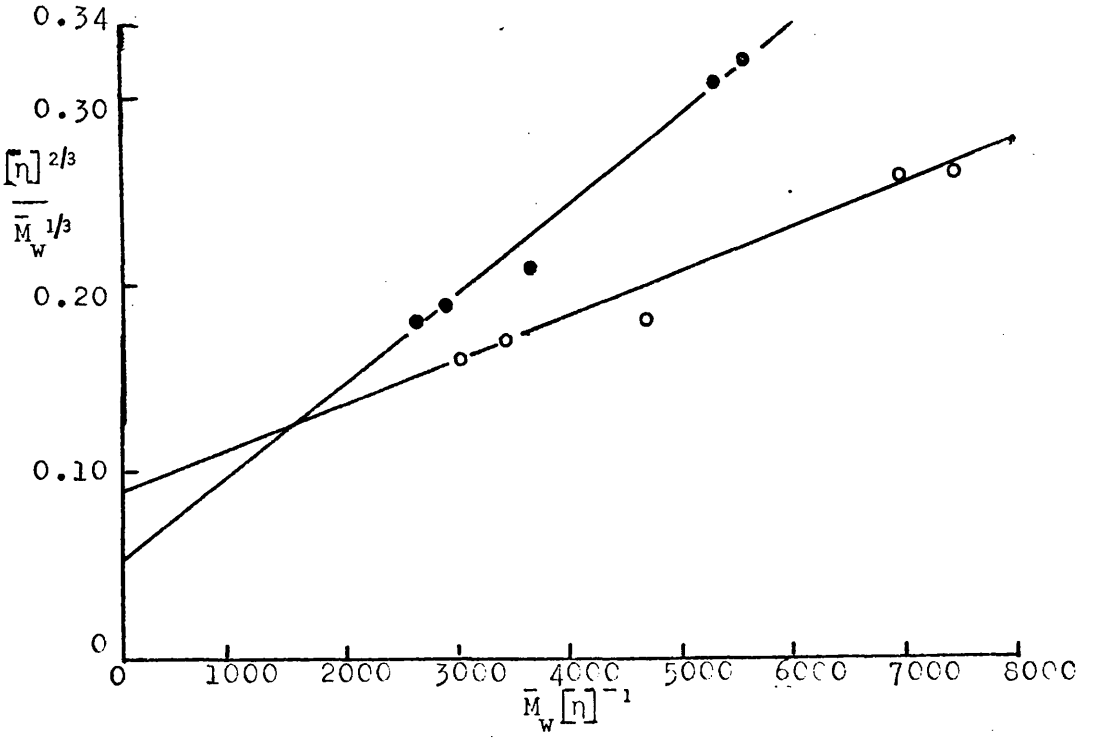

FIGURE 58 DATA FOR ATA IN NO_2ME AND NO_2ME/PROPANOL ACCORDING TO THE FLORY-FOX EQUATION.

Table III.33 Expansion coefficients for ATA.

ATA fractions	α_η NO_2Me	α_η NO_2Me/propanol
A2	1.53	1.39
A3	1.50	1.38
F1b	1.25	1.17
F3b	1.18	1.13
F3	1.15	1.09

Using the limiting value of Φ_0 of 2.87×10^{23} and $\Phi(\varepsilon)$, $(\bar{r}_0^2/\bar{M}_w)^{\frac{1}{2}}$ values were calculated and are shown in Table III.32. The values for $(\bar{r}_0^2/\bar{M}_w)^{\frac{1}{2}}$ are considerably lower than that found by Banks and Greenwood of 885×10^{-11}cm but closer to the value of $580 \pm 60 \times 10^{-11}$cm found by Cowie (6). Lines drawn through the data plotted according to the Flory-Fox theory give intercepts which vary as the solvent power varies, the better solvent has a lower K_θ value. This was also found with data for ATB and for many other systems (17).

Table III.32: $(\bar{r}_0^2/\bar{M}_w)^{\frac{1}{2}}$ values for ATA

Solvent	$(\frac{\bar{r}_0^2}{\bar{M}_w})^{\frac{1}{2}} \times 10^{11}$cm (a)	$(\frac{\bar{r}_0^2}{\bar{M}_w})^{\frac{1}{2}} \times 10^{11}$cm (b)
MO_2Me	559	659
50/50	559	644

(a) $\Phi_0 = 2.87 \times 10^{23}$

(b) $\Phi = \Phi(\varepsilon)$

The expansion coefficient, α_η

The expansion coefficients, α_η, were calculated using the value of K_θ found from the viscosity plots. These are recorded in Table III.33.

The variation in the expansion coefficient with molecular weight for ATA in NO_2Me is much greater than that found by Banks, Greenwood and Hourston (25). The variation of α_η with solvent reflects the variation in solvent power, $\alpha_{NO_2Me} > \alpha_{NO_2Me/propanol}$, also seen in the Mark-Houwink exponent. The size of the expansion coefficients are similar to those for flexible polymers.

The theories of Stockmayer-Fixman, Kurata-Stockmayer, Flory-Fox and Ptitsyn discussed earlier in this chapter were

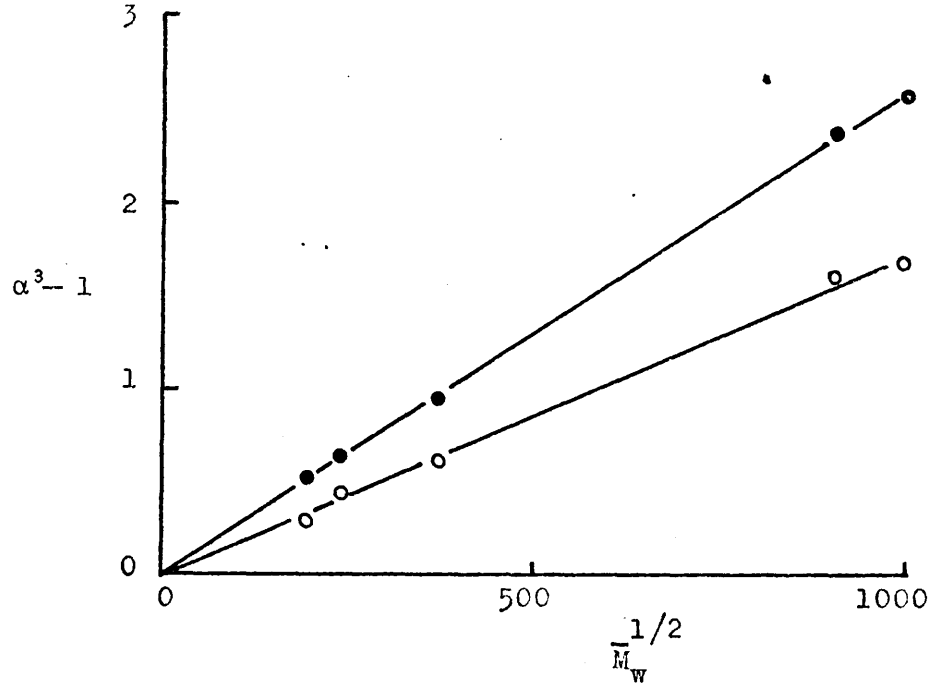

FIGURE 59a DATA FOR ATA IN NO_2ME AND 50/50 NO_2ME/PROPANOL ACCORDING TO THE STOCKMAYER-FIXMAN EQUATION.

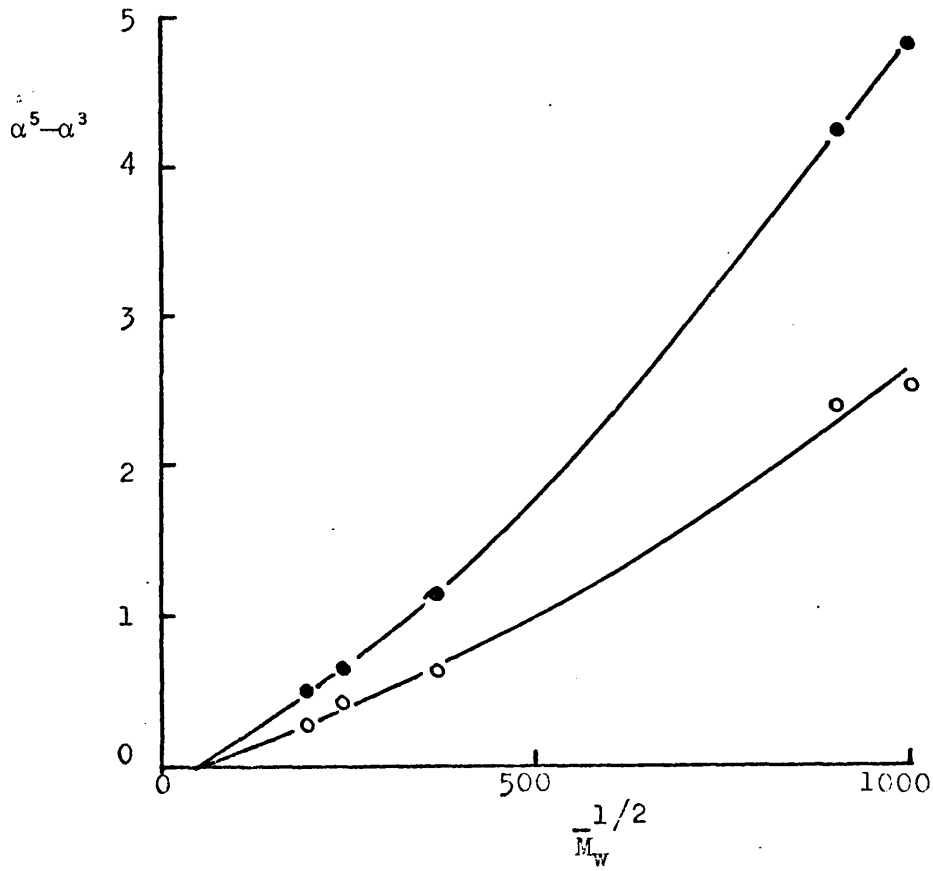

FIGURE 59b DATA FOR ATA IN NO_2ME AND 50/50 NO_2ME/PROPANOL ACCORDING TO THE FLORY-FOX EQUATION.

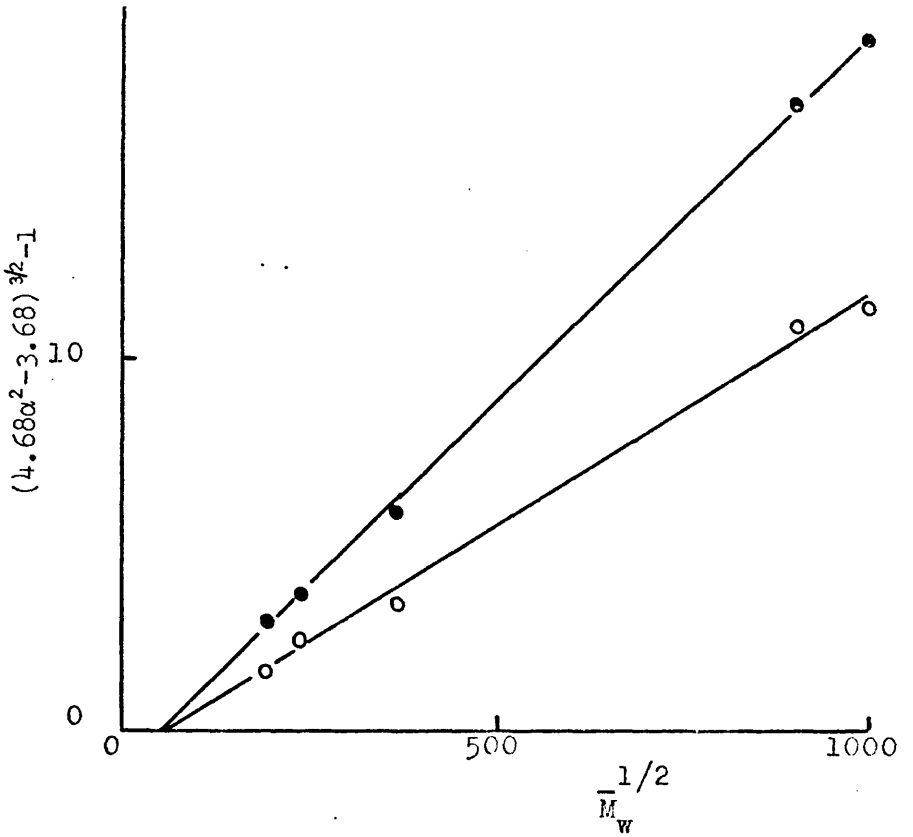

FIGURE 59c DATA FOR ATA IN NO_2ME AND 50/50 NO_2ME, PROPANOL ACCORDING TO THE PTITSYN EQUATION.

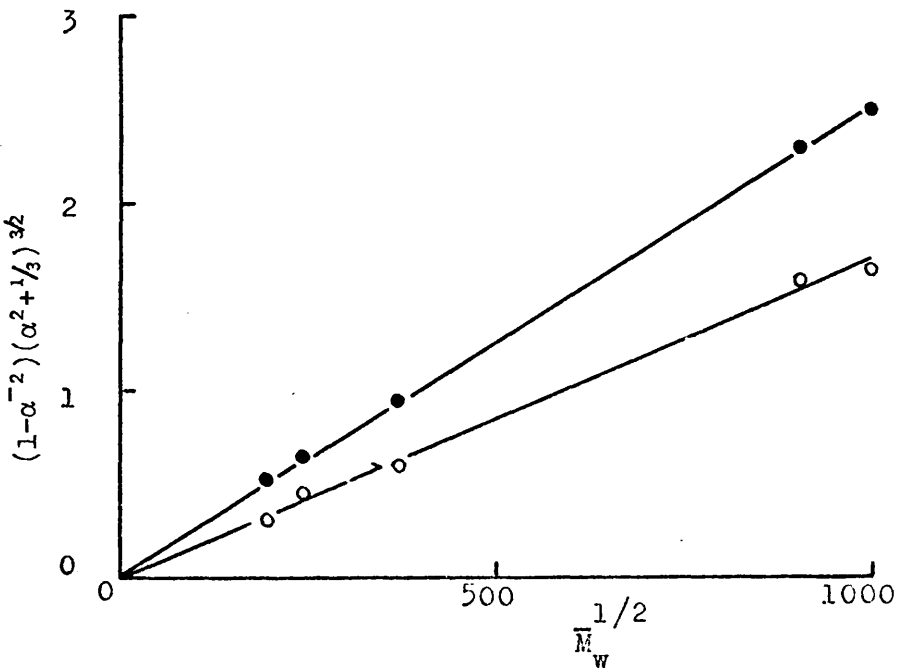

FIGURE 59d DATA FOR ATA IN NO_2ME AND 50/50 NO_2ME/PROPANOL ACCORDING TO THE KURATA-STOCKMAYER EQUATION.

tested using the data for α_η. Graphs plotted according to these theories are shown in Figure 59. The data comply with the Stockmayer-Fixman and Kurata-Stockmayer theories which are numerically equivalent at low values of the expansion coefficient. The Flory-Fox plot shows an upward curvature indicating, as has been found before, that $(\alpha^5 - \alpha^3)/M^{\frac{1}{2}}$ is not independent of molecular weight. The plot also intersects the abscissa at a value of M greater than zero. This behaviour was also found for amylose tributyrate. The intercept corresponds to a value of $\bar{M}_w$ equal to about 2.5×10^3. The data plotted according to the Ptitsyn theory also intersect the abscissa at a value of $\bar{M}_w$ of about 2.5×10^3. Huppenthal (19) and Patel (8) have found similar behaviour in the case of cellulose tributyrate and amylose acetate. Patel suggested that the intercept corresponds to the point at which the polymer chain can no longer coil, in the case of the acetate this corresponds to a degree of polymerisation of about 9.

4. THE CONFORMATION OF ATA FROM HYDRODYNAMIC CONSIDERATIONS

The Kirkwood-Riseman (65) and Kuhn-Kuhn (66) theories have been applied to data for amylose triacetate. Figure 60 shows the plots of $[\eta]/\bar{z}_w^{\frac{1}{2}}$ against $\bar{z}_w^{-\frac{1}{2}}$ and $\bar{z}_w/[\eta]$ against $\bar{z}_w^{\frac{1}{2}}$ for ATA in NO_2Me and 50/50 NO_2Me/propan-1-ol. Values of b and A_m derived from these plots according to equations (44) and (48) are recorded in Table III.34.

As in the case of butyrate and propionate, values of b and A_m indicate that although the acetate is more flexible than the cellulose derivatives it is not as flexible as the synthetic polymers. The value of A_m for ATA in NO_2Me is very

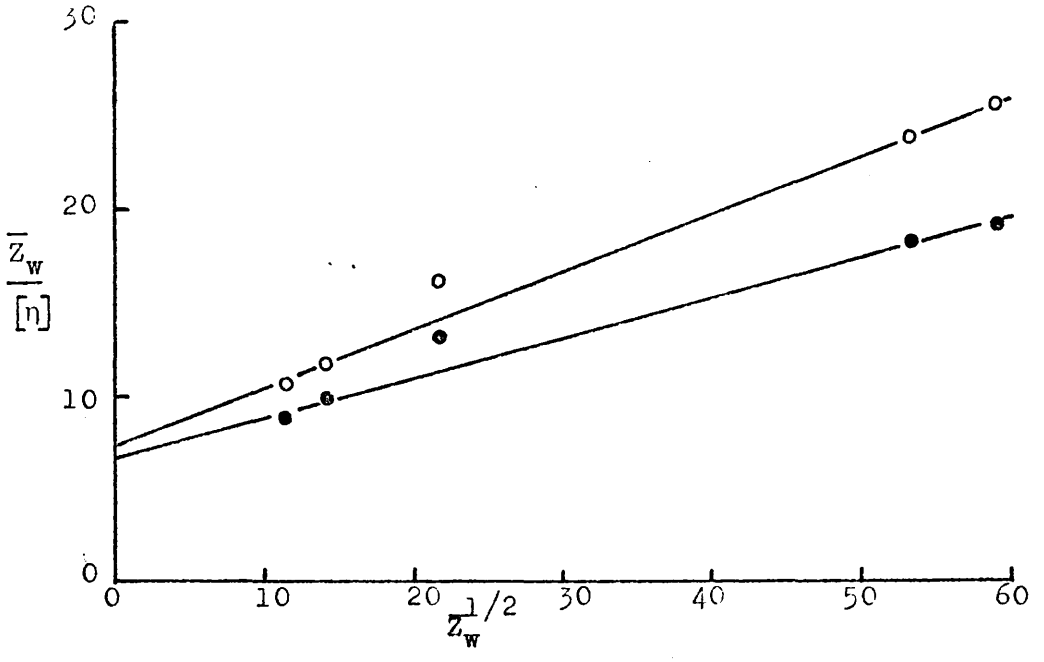

FIGURE 60 DATA FOR ATA IN NO_2ME AND 50/50 NO_2ME/PROPANOL ACCORDING TO THE KUHN-KUHN AND KIRKWOOD-RISEMAN EQUATIONS.

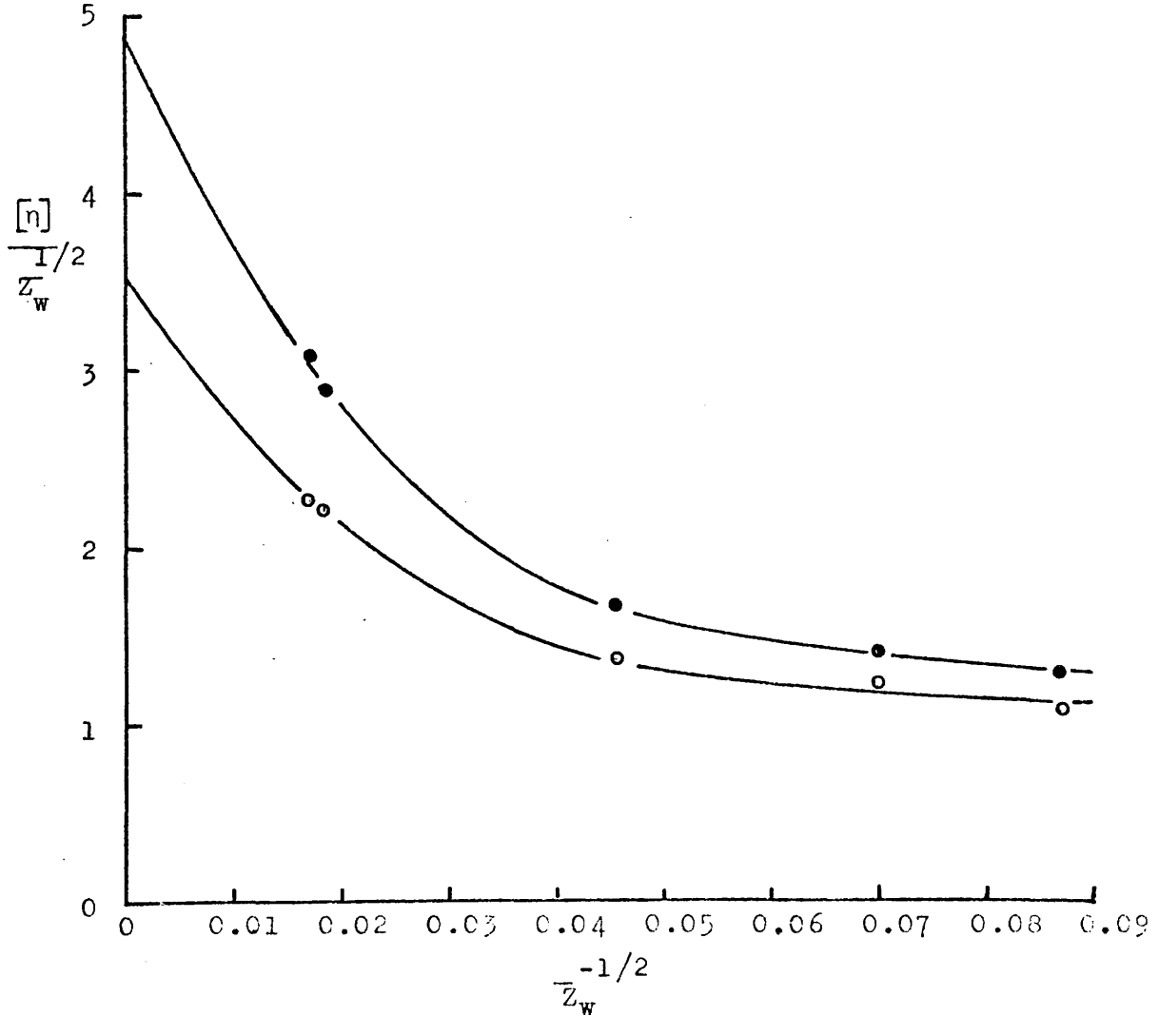

Table III.34: b and A_m for ATA in NO_2Me and NO_2Me/propanol

Solvent	b x 10^8cm	A_m x 10^8cm
NO_2Me	16.0	67.8
50/50	14.4	53.0

close to that found by Banks, Greenwood and Hourston (25) of 75 x 10^{-8}cm from viscosity data and 53 x 10^{-8}cm from sedimentation data.

The values of b and A_m calculated for the unperturbed polymer chain using equations (50) and (51) are recorded in Table III.35. They show ATA to be much less rigid in the unperturbed state as NO_2Me and NO_2Me/propan-1-ol are good solvents. Similar behaviour was observed for the butyrate.

The steric factor, σ, has also been calculated to give a value of 2.53 using Φ_0 equal to 2.87 x 10^{23}. All the flexibility parameters which have been calculated show ATA to be a flexible polymer which combined with previous results indicate that it behaves as a stiff coil in solution.

Table III.35: Values of b and A_m for the unperturbed ATA

Solvent	(a) b x 10^8cm	(a) A_m x 10^8cm	(b) b x 10^8cm	(b) A_m x 10^8cm
NO_2Me	9.5	20.5	11.2	28.4
50/50	9.5	20.5	10.9	27.1

(a) Using $\Phi_0 = 2.87 \times 10^{23}$

(b) Using $\Phi = \Phi(\varepsilon)$.

C H A P T E R IV

COMPARISON OF THE PROPERTIES OF AMYLOSE ESTERS

COMPARISON OF THE PROPERTIES OF AMYLOSE ESTERS

The addition of an ester side-chain to amylose is known to affect it's physical properties (75, 76). As mentioned in the introduction, the solubility of amylose changes completely when the ester side-chain is added to produce a polymer which is no longer soluble in water but soluble in a variety of organic solvents. Amylose esters will no longer complex with alcohols or retrograde, phenomena which both occur with the unsubstituted polymer. This change is reflected in the different values of δ_s, the Hildebrand solubility parameter, which is defined as

$$\delta_s = [\Delta E^v/V]^{1/2} \qquad (1)$$

where $\Delta E^v/V$ is the energy of vapourisation per unit volume of liquid and is often called the cohesive energy density. The solubility parameter varies with the length of the side-chain and Table IV.1. shows the values of δ_s for the three esters and amylose found by Cowie et al (76). There is a drastic reduction in δ_s when amylose is substituted and further reductions take place as the side-chain length is increased. The values of δ_s for various solvents are shown in Table IV.2. Ideally the closer the values of δ_s for solvent and solute the more likely they are to be compatible. Amylose is more soluble in dimethyl sulphoxide (DMSO) and ethylenediamine than in water as might be expected from the values of δ_s. However, it is not soluble in the other solvents listed in Table IV.2 even though δ_s for nitromethane is very close to the value for amylose and those for the other solvents closer than that for

Table IV.1: Values of δ_s and T_g from ref. (76)

Polymer	δ_s (cal $cm^{-3})^{\frac{1}{2}}$	T_g (K)
Amylose	12.4	590
Amylose Acetate	9.6	440
Amylose Propionate	9.26	390
Amylose Butyrate	9.20	352

Table Iv.2: Values of δ_s for various solvents (75)

Solvent	δ_s (cal $cm^{-3})^{\frac{1}{2}}$
methyl ethyl ketone	9.57
ethyl acetate	9.05
tetrahydrofuran	9.30
nitromethane	12.60
water	23
DMSO	13.00
ethylenediamine	11.50

water. The solubility parameter seems to act as a crude indication of the solubility of a particular polymer in a solvent. Obviously other factors must be important as well, such as the molar volume and polarity of the solvent.

Trends in solubility are exhibited by the esters. Table IV.3 records the Mark-Houwink exponents found for the esters in the 6 solvents used. The exponents for the esters in MEK, THF and EA decrease as the side-chain length decreases. These

Table IV.3: Values of the Mark-Houwink exponents a for the esters in various solvents at 298K

Solvent / Ester	nitro-methane	50/50 nitromethane/ propan-1-ol	tetra-hydro-furan	carbon tetra-chloride	methyl ethyl ketone	ethyl acetate
Acetate	0.78	0.74	(0.8)	n.s.	n.s.	n.s.
Propionate	S	-	0.58	S	0.54	0.56
Butyrate	n.s.	-	0.86	0.82	0.77	0.74

n.s. not soluble, S soluble.

three solvents are good solvents for the butyrate and poor solvents for the propionate. The solvent power decreases again in the case of the acetate where at 298K only the low molecular weight material is soluble. The opposite trend in the Mark-Houwink exponents is observed for the esters in NO_2Me which is a good solvent for the acetate but the butyrate will not dissolve in it until about 333K.

The variations of solubility in EA and NO_2Me would be expected from the relative values of δ_s for the solvents and the esters. The value of δ_s for NO_2Me is high and nearest to that for the acetate. Therefore from solubility parameter data the acetate would be most soluble and the butyrate least soluble in NO_2Me. A similar argument holds for EA which has δ_s closest to that for the butyrate and furthest from δ_s for the acetate. The solubility trends for these two solvents can therefore be predicted by examining δ_s data. However, the forgoing arguments do not hold for the other solvents. According to δ_s data the acetate should be most soluble in MEK but experimental evidence shows that the butyrate is most soluble. Again δ_s for THF indicates that the propionate should be most

soluble in it. Other factors must be important.

The observed solubilities in NO_2Me and EA can also be explained by the variation in dielectric constant or polarity of the solvents. NO_2Me is the most polar of all the solvents and the most favourable interactions should take place between it and the most polar ester, the acetate. EA, as well as CT and THF, is fairly non-polar. The butyrate has long hydrocarbon chains which will tend to shield the polymer thus creating a hydrocarbon environment which is more compatible with the non-polar solvents.

Of all the solvents MEK is the one which does not fit either the polarity or δ_s arguments, it has a fairly high dielectric constant and δ_s is closest to the acetate not the butyrate. Another factor which might well dominate in this case is that of molar volume which is largest in the case of MEK possibly making packing of the solvent molecules around the butyrate more favourable than around the acetate. No hard and fast rules can be applied to explain the solubilities of the esters though polarity and solubility parameter data can be applied with some success. However defined trends due to increasing side-chain are observed.

The glass transition temperature, T_g, is also affected by substitution in the anhydroglucose unit of amylose. Values of T_g measured by Cowie (76) are also recorded in Table IV.1. Again there is a drastic reduction in T_g between amylose and its derivatives, but as the side-chain length increases the relative decrease becomes smaller. Cowie (76) has proposed two possible reasons for the observed decrease in T_g, either there is a decreasein polarity or chain stiffness or, an

increase in the total free volume arising from the increasing molar volume of the ester group. Increasing free volume has been attributed to the large decrease in T_g shown by isotactic poly (methyl methacrylate) (PMMA) as compared with atactic PMMA (77). In this case the higher value of T_g for the atactic polymer is explained by more efficient packing because of its less extended unperturbed state compared with the isotactic polymer. This means that for PMMA the larger unperturbed dimensions in solution can account for the lower glass transition temperature in the solid state. By analogy with PMMA, an increase in total free volume of the amylose esters might manifest itself as an increase in the unperturbed dimensions of the esters as the side-chain length increases, and thus account for the observed decrease in T_g. However, deductions made by analogy between solid state and solution properties are tenuous.

Ideally unperturbed dimensions should be measured in theta-solvents. Attempts were made to find theta-solvents for the esters but the results obtained could not be used with any confidence. All the solvents for ATP used in this study are thermodynamically poor and by adding non-solvent it should be possible to obtain mixtures which are theta-solvents. The systems tried included EA/n-hexane and MEK/propan-2-ol at 298K. Measurements of the second virial coefficient, A_2, at various temperatures were made on the system ATP/MEK but the theta-temperature was not found. Attempts were made to find the theta-temperatures of the systems ATB/nitromethane, ATB/nitroethane and ATB/nitropropane at temperatures above ambient with no success. Banks and Greenwood (26) found that NO_2Me/propan-1-ol was a theta-solvent for ATA at 295.5K. This mixture

was used for ATA at 298K but the results were prone to errors. Estimates of the unperturbed dimensions have therefore had to be made using indirect techniques involving good-solvents.

The unperturbed dimensions of amylose are solvent dependent and the values of K_θ, according to various authors (13) vary from 0.138 to 0.087. The highest values of K_θ were calculated by Burchard (13) who applied a drainage correction to the Stockmayer-Fixman relation. Burchard attributed the non-linearity of the Stockmayer-Fixman plots to partial draining in the molecule. It seems more likely that non-linearity was due to the expression not being valid at the high molecular weights because of the relation used between α and z. Banks and Greenwood (26) believe that a drainage correction is unnecessary for amylose and amylose acetate. Due to lack of data this aspect has not been investigated in this study. K_θ for amylose is larger than those for the esters as shown in Table IV.4. There is a large decrease in K_θ, and consequently $(\bar{r}_o^2/\bar{M}_w)^{\frac{1}{2}}$, as the side-chain is substituted onto the amylose chain, but a small increase occurs as the side-chain is lengthened further to form the propionate. Further substitution to form the butyrate causes the unperturbed dimensions of the polymer to become solvent dependent. The values of K_θ, and $(\bar{r}_o^2/\bar{M}_w)^{\frac{1}{2}}$, vary from 0.041 to 0.055 for the butyrate in the solvents studied. Polymer solvent interactions must take place which do not occur with the shorter side-chains causing changes in the conformation of the unperturbed polymer. Also included in Table IV.4 are values of the unperturbed dimensions of cellulose, cellulose acetate and cellulose tributyrate. The unperturbed dimensions of the cellulosic chains are larger than those of

Table IV.4. Comparison of unperturbed dimensions for cellulose and amylose and their derivatives.

Polymer	K_θ	$\left[\frac{r_o^2}{M_w}\right]^{1/2}$ x 10"cm	$\left[\frac{r_o^2}{Z_w}\right]^{1/2}$ x 10^8cm	Polymer	$\left[\frac{r_o^2}{M_w}\right]^{1/2}$ x 10"cm	$\left[\frac{r_o^2}{Z_w}\right]^{1/2}$ x 10^8cm	Ref
Amylose	0.087-0.138	672-783	8.6 - 9.97	Cellulose	1020	12.98	(22)
"Acetate	0.050	559	9.49	"Acetate	735	12.47	(78)
"Propion-ate	0.0545	575	10.45	-	-	-	-
"Butyrate	0.041-0.055	527-576	10.17 -11.11	"Butyrate	673-730	11.42-12.39	(19)

the corresponding amylosic chains. A trend in values of $(\bar{r}_0^2/\bar{M}_w)^{\frac{1}{2}}$ similar to that for the amylosic polymers is shown by the cellulosic polymers, namely a large decrease as the chain is substituted, but possibly the unperturbed dimensions decrease slightly as the side-chain is lengthened further. The larger unperturbed dimensions shown by the cellulosic polymers are to be expected since the β - (1 → 4) glycosidic links impart a much more extended structure to the chain (70).

A more realistic comparison of the unperturbed dimensions can be made by looking at the value of $(\bar{r}_0^2/Z_w)^{\frac{1}{2}}$ which shows the variation of the unperturbed dimensions with the number of monomer units and not the molecular weight. The values for the amylosic and cellulosic polymers are shown in Table IV.4. The amylosic polymers show a gradual increase in $(\bar{r}_0^2/Z_w)^{\frac{1}{2}}$ as the side-chain is lengthened, as might be expected, because of the increasing molar volume of the side-chains which will tend to expand the molecule. The polymers are therefore becoming more extended and not less extended as might be thought from a comparison of $(\bar{r}_0^2/\bar{M}_w)^{\frac{1}{2}}$ values. If this solution property can be transferred to the solid state this might explain the decrease in T_g in terms of increased free volume.

The cellulosic polymers exhibit a slight decrease in $(\bar{r}_0^2/Z)^{\frac{1}{2}}$ as the side-chain is lengthened so that, in this case, the substitution causes the backbone to become more flexible but still less flexible than the amylosic chains. The differences in flexibility between the two polyglucans can be measured in a number of ways. The following criteria have been used in the present study to look at the flexibility of the amylosic

chains and the values obtained will be compared with those for cellulosic polymers;

1. the Kirkwood-Riseman effective bond length, b, which in the unperturbed state is $(\bar{r}_0^2/Z)^{\frac{1}{2}}$;
2. the Kuhn-Kuhn statistical segment, A_m, which has also been calculated for the perturbed and unperturbed state;
3. the Kratky-Porod persistence length, q, and
4. the steric factor, σ .

The parameters for the three amylose esters are collected together in Table IV.5. The values of A_m (unperturbed) and q show variations with side-chain length as discussed above with regard to b (unperturbed) or $(\bar{r}_0^2/Z)^{\frac{1}{2}}$.

The perturbed values of b and A_m vary according to the quality of the solvent. CT and THF are very good solvents for ATB, indicated by the value of their respective Mark-Houwink exponents, and consequently ATB has a much more expanded configuration in these solvents than in the unperturbed state. EA and MEK are also good solvents for ATB but the Mark-Houwink exponents are lower than for ATB in CT and THF, consequently ATB is not as extended or rigid in EA and MEK. The flexibility of ATP in the three poor solvents does not decrease much more from that found in the unperturbed state because of the virtual lack of polymer-solvent interaction in such solvents. In the case of ATA both solvents are good solvents and the increase in b and A_m over the unperturbed values reflects this fact.

The steric factor, σ , is another measure of flexibility which considers the hindrance to rotation caused by steric interactions and compares the unperturbed dimensions and dimensions

Table IV.5. Various stiffness parameters for amylose esters and amylose.

Polymer	Solvent 298K	$b \times 10^8$ cm	$A_m \times 10^8$ cm	$b \times 10^8$ cm unperturbed	$A_m \times 10^8$ cm unperturbed	$q \times 10^8$ cm	σ'	σ
Amylose Acetate	NO_2Me	16.0	67.5	9.5	20.5	10.3	1.89	2.53
	50/50	14.4	53.0	"	"	"	"	"
Amylose Propionate	EA	12.1	38.9	10.4	24.8	12.4	1.95	2.78
	THF	13.0	44.1	"	"	"	"	"
	MEK	11.5	36.1	"	"	"	"	"
Amylose Butyrate	EA	17.4	69.6	11.1	28.1	14.1	1.95	2.96
	MEK	17.7	71.7	10.2	23.1	11.6	1.77	2.71
	THF	19.5	~~18.2~~ 182.0	10.8	26.4	13.2	1.89	2.88
	CT	18.6	101.6	10.2	23.1	11.6	1.77	2.71
Amylose	$DMSO/H_2O$	-	-	8.6	-	-	2.28	2.29

of the freely rotating chain. The steric factor increases steadily as the side-chain length is increased with a slight decrease in the case of ATB in MEK and CT below the value of that for ATP. The steric factor, σ, has been calculated using the expression

$$\sigma = (\bar{r}_0^2/Z)^{1/2}/(\bar{r}_{0f}^2/Z)^{1/2} \qquad (2)$$

which is the correct way of estimating σ since the flexibilities of the hindered chain and the freely rotating chain are compared in terms of the number of units in the chain not their molecular weights.

Also recorded in Table IV.5 along with σ is σ' which is defined as

$$\sigma' = (\bar{r}_0^2/M_1)^{1/2}/(\bar{r}_{0f}^2/M_2)^{1/2}$$

where M_1 is the molecular weight of the ester, M_2 is molecular weight of amylose, and is often used as a way of calculating σ but is incorrect.[3] Comparison of the values of σ' give a different idea of the relative flexibilities of amylose and its derivatives. The steric factor, σ', indicates that the derivatives are much more flexible than amylose which might lead to erroneous views about the amylose chain.

Values of various stiffness parameters for the cellulosic polymers and some synthetic polymers are shown in Table IV.6. The parameters for the cellulosic polymers indicate greater rigidity or extension in the unperturbed state than the amylosic polymers. However the values for the synthetic polymers are slightly lower indicating that the amylosic chain is more rigid than these. All the stiffness parameters together with

Table IV.6: Various Stiffness Parameters for Non-Amylosic Polymers

Polymer	Solvent	b x 10^8 cm	A_m x 10^8 cm	σ	σ'	ref.
Cellulose	Cadoxen	19	70	2.20	2.20	(22)
Cellulose Acetate		12.5	28	2.11	1.58	(78)
Cellulose Butyrate	MEK	13.0	31	2.50	1.65	(19)
Cellulose Caproate	DMF	22-24	105	4.44	2.65	(80)
Cellulose Carbanilate	Cyclohexanone	15.7	44	3.56	1.99	(45)
Polystyrene	Toluene	8.6	33	2.20	2.20	(60)
PMMA		5.5	12	1.82	1.82	(81)

the viscosity data indicate that the amylose polymers behave as stiff coils i.e. random coils which are less flexible than the synthetic polymers.

The values of the steric factor, σ, for the cellulose esters are lower than those for the amylose esters which would seem to indicate less repulsive contacts between substituents in the cellulosic chains, however the freely rotating state is smaller for amylose. Although amylose and cellulose are considered to be the isotactic and syndiotactic forms of the same polymer they can also be considered as cis and trans isomers across a "double bond", which in this case is the anhydroglucose ring. The cis- and trans-diene polymers show differences in their solution properties which are also exhibited by amylose and cellulose polymers. Cis-dienes have smaller unperturbed dimensions than trans-dienes (17), but the trans-dienes have smaller steric factors showing that there are fewer repulsive contacts between chain substituents. Amylosic polymers have smaller unperturbed dimensions than cellulosic polymers and, as mentioned above, the steric factors are larger than those for the cellulose chains. This difference between the two isomers was shown quite clearly in a comparative study by Burchard and Husemann (20) of amylose and cellulose tricarbanilates. The vinyl polymers only show distinguishable differences in unperturbed dimensions between the different tactic forms when an α - methyl group is present, and only then when dissolved in poor or theta solvents. The 1,4 dienes show a marked difference between the different isomers even when dissolved in good solvents.

The steric factor has also been found to increase in a series of polystyrene derivatives (79) as the bulk of the side-group increases, indicating that σ is mainly determined by the repulsive contacts between side-groups. There is, of course, a slight decrease in σ shown by ATB in certain solvents. Although the side-chain is much bulkier it is also more flexible and because of this steric repulsions may be reduced by changes in conformation of the side-chains, stimulated by specific polymer-solvent interactions.

The viscosity and the unperturbed dimensions of ATB in ethyl acetate go through a minimum at about 307K, so that a change in interactions present in the polymer must take place causing expansion of the polymer unperturbed state. A model of ATB shows that the long side-chains are very bulky and also with increasing temperature will become more flexible. The normal configuration which the ring assumes is believed to be the C1 - configuration. As the temperature increases the unperturbed dimensions decrease due to decreased hindrance to rotation about the glycosidic link. A point must be reached where the increased repulsion between the bulky side-chains is such that, to be able to accommodate the increasing flexibility of the back-bone and side-chains, the configuration of the ring may well distort slightly from the C1 position. Both the 3B and B1 configurations (70) cause the chain to expand but a slight distortion from C1 towards either boat configuration would be sufficient to cause the observed expansion. Obviously this is only a tentative explanation for the observed phenomena and more data must be gathered before any definite explanation can be put forward.

The temperature coefficients of viscosity, d log $[\eta]$ /dT, for the triacetate and the tripropionate in nitromethane and ethyl acetate, respectively, are equal in the range of temperatures studied and smaller than the temperature coefficients found for cellulosic polymers (18, 19).

The expansion coefficient, α_η , increases slightly with increasing side-chain length but more data is required to fill in certain gaps. Values of α_η are smaller than those for the cellulosic polymers. Huppenthal (19) quotes a value of α_η for cellulose tributyrate in MEK of 1.44, the equivalent value for amylose tributyrate is 1.17. Once again the fact that cellulosic chains are more extended is reinforced. Various theories were tested using the α_η values calculated for the three derivatives. The triacetate and tributyrate show the same behaviour, conforming to the Stockmayer-Fixman (54) and Kurata-Stockmayer (17) theories but not to the Flory-Fox (46) or Ptitsyn (56) relations. Deviations from these two theories seem to indicate that the limiting value of α_η is not reached at M = 0 but at a higher molecular weight, possibly when the molecule can no longer coil (8). This limit corresponds to 9 monomer units for the triacetate and 27 monomer units for the tributyrate. Both the triacetate and tributyrate have large values of α_η , from 1.53 to 1.09 for ATA and from 1.66 to 1.12 for ATB. The values of α_η for the ATP are much smaller, since all the solvents are thermodynamically poor, and varied from 1.16 to 1.03. These data for the propionate conformed to all four theories.

Various theories have been put forward in an attempt to relate $A_2M/[\eta]$ to some function of the expansion coefficient. In the previous chapter experimental values $A_2\bar{M}_n/[\eta]$ were used

to calculate α according to the Orofino-Flory expressions (74). In general the theories for the second virial coefficient may be expressed in the form.

$$A_2 = Y.F(X) \tag{4}$$

where Y is independent of molecular weight, but dependent on temperature. The function F(X) decays monotonically from unity at $\alpha = 1$, but its exact form is unknown and various theoretical treatments have been used to interpret it. Flory (74, 82) defined Y as

$$Y = 1/2(1 - 2\chi_1)(\bar{v}^2/V_1) \tag{5}$$

where χ_1 is a solvent-solute interaction parameter, $\bar{v}$ is the partial specific volume of the polymer and V_1 the molar volume of the solvent. By writing equation (5) in terms of z and substituting expressions for $[\eta]_\theta$ and α_η the relation derived is

$$A_2M/[\eta] = (2\pi/3)^{3/2}N_A/2\Phi_0(z/\alpha_\eta^3)F(X) \tag{6}$$

Flory and Orofino (74) obtained the first closed expression for F(X), thus

$$F(X) = \ln(1 + (\pi^{1/2}/4)X).(\pi^{1/2}X/4) \tag{7}$$

where

$$X = 3^{3/2}z/\alpha^3 \tag{8}$$

Using the Flory (46) relation

$$\alpha^5 - \alpha^3 = C_1z$$

where $C_1 = 2.60$, Flory and Orofino derived the expression

$$A_2M/[\eta] = \log(1 + 0.885(\alpha^2 - 1))^{4.14} \qquad (9)$$

This form of equation (9) assumes $\Phi_0 = 2.2 \times 10^{23}$ and $\alpha = \alpha_\eta$. Stockmayer (83) later modified equation (9) on the grounds that both the expression for F(X) and z failed to give the theoretical numerical factor of z when expanded in series of small z. The modified equation was

$$A_2M/[\eta] = 1.65\log(1 + 4.50(\alpha^2 - 1)) \qquad (10)$$

The Flory theory is based on the model of the uniformly expanded chain having a symmetrical distribution of chain elements about the molecular centre of mass. Casassa and Markovitz (84) developed a second theory in which the uniformly expanded chain has a symmetrical distribution of segments about the locus of an initial interchain contact and obtained

$$F(X) = (1 - \exp(-1.093X))/1.093X \qquad (11)$$

which gives

$$A_2M/[\eta] = 0.731(1 - \exp(-4.45(\alpha^2 - 1))) \qquad (12)$$

All the forgoing theories are based on the "fifth-power law" because in the limit of high α, $\alpha^5 \propto z$. Other theoretical treatments are based on a "third-power law" one of which is Ptitsyn's (56) treatment. Ptitsyn has derived for F(X') the relation

$$F(X') = (1 - (1 + 0.856X')^{-0.286})/0.246X' \qquad (13)$$

where $X' = 3^{3/2} z/\alpha_2^3$ and α_2 is an expansion factor defined by

FIGURE 61 DATA FOR ○ ATA, ◒ ATP AND ● ATP, AND THEORETICAL CURVES ACCORDING TO THE THEORIES DISCUSSED IN THE TEXT. THE NUMBERS REFER TO EQUATIONS IN CHAPTER IV.

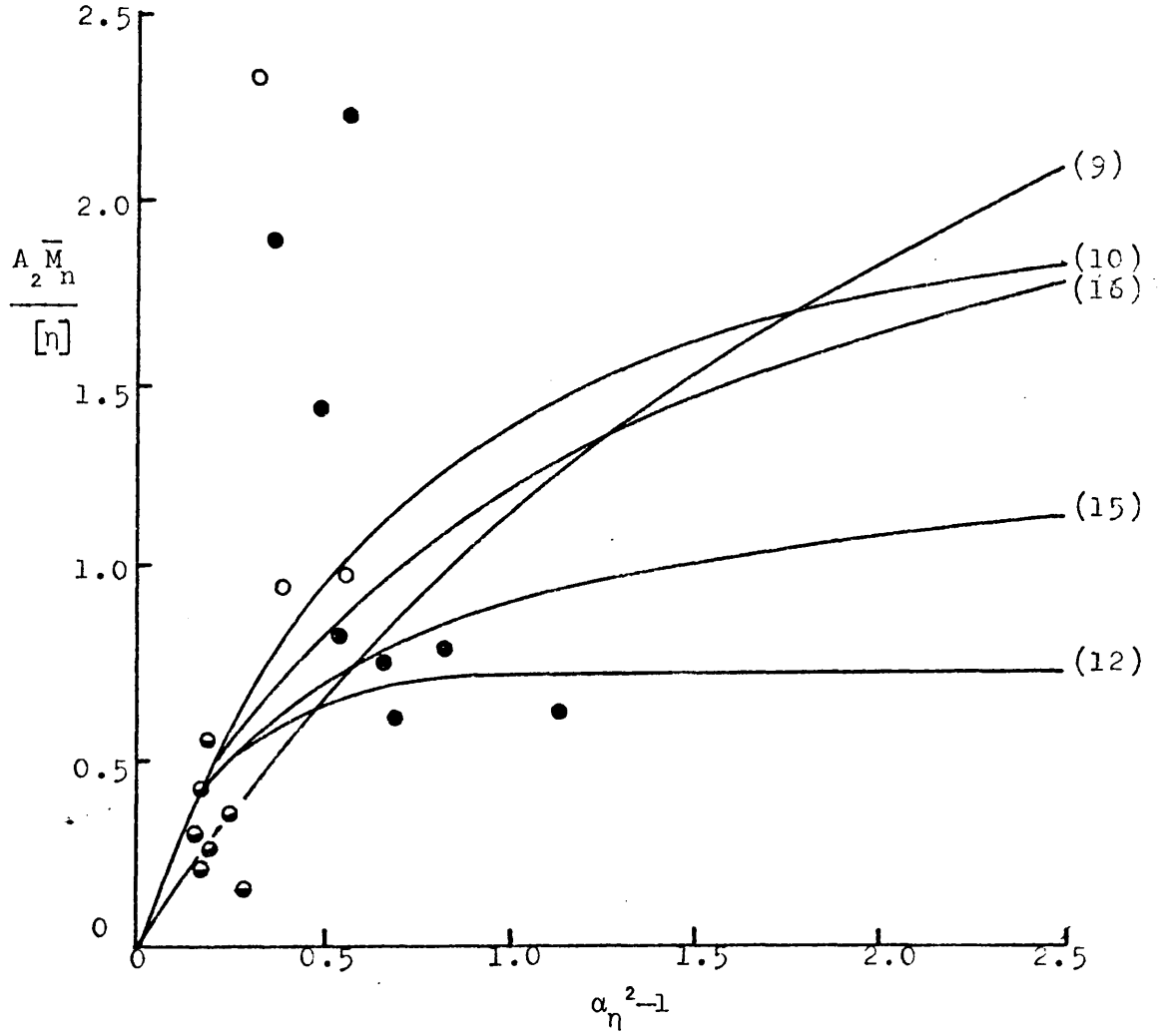

$b = \alpha_2 b_0$ where b_0 is the bond length of the polymer. The closed expression which Ptitsyn used for α was of the form

$$\alpha^2 = (3.68(1 + 9.362)^{2/3})/4.68 \qquad (14)$$

So that

$$A_2M/[\eta] = 3.26\{1 - (1 + 0.476\{(4.68 - 3.68\alpha^{-2})^{32} - \alpha^{-3}\})^{-0.286}\} \qquad (15)$$

The derivation of equation (15) assumes that $\alpha = \alpha_\eta = \alpha_2$. Krigbaum has suggested a semi-empirical relation (59)

$$A_2M/[\eta] = 2.17(1 - \alpha_\eta^{-3}) \qquad (16)$$

The value of $\Phi_0 = 2.2 \times 10^{23}$ has been used in all the forgoing equations, but Φ_0 could be varied to find the best fit between theory and experiment. Figure 61 shows a plot of $A_2\bar{M}_n/[\eta]$ as a function of $(\alpha_\eta^2 - 1)$ according to theory and experiment. The numbers on the theoretical curves correspond to equation numbers in this section. The data for the esters do not fit any one relationship. The butyrate data seem to fit the Casassa-Markovitz relation and the acetate and propionate possibly the Krigbaum expression. The uncertainties involved in measuring A_2 make it very difficult to fit the data to the theories especially if the low molecular weight butyrate data is considered. It seems as if there is a tendency for $A_2\bar{M}_n/[\eta]$ to go to an asymptotic limit in the case of the butyrate. Increasing Φ_0 causes the curves to shift downwards and vice versa but no one curve can be made to fit the data because of the scatter.

The interaction parameter, χ_1, in equation (5) can be

calculated if B is known, where

$$B = \bar{v}^2(1 - 2\chi_1)/V_1N_A \qquad (17)$$

The parameter B has been derived, for each ester/solvent pair, from the slope of the appropriate Stockmayer-Fixman plot. The values of B and χ_1 are recorded in Table IV.7. As the solvent power increases χ_1 decreases from a value of 0.5 for theta-solvents. The values of χ_1 are very close to 0.5 although the solvents, in the case of ATB and ATA, are good solvents. Banks and Greenwood (73) found a similar value of χ_1 for ATA in NO_2Me and explained this high value by saying that it refers to an already-solvated polymer system (85).

Table IV.7: Values of the interaction parameter χ_1 at 298K

Polymer	Solvent	B x 10^{27}	χ_1	$\bar{v}$	V_1 cm^3mol^{-1}
ATB	EA	0.663	0.472	0.844	98.5
	MEK	0.752	0.471	0.844	90.2
	CT	0.991	0.460	0.844	96.5
	THF	1.264	0.456	0.844	81.5
ATP	EA	0.0524	0.498	0.814	98.5
	Mek	0.0683	0.497	0.814	90.2
	THF	0.0888	0.497	0.814	81.5
ATA	NO_2Me	0.902	0.474	0.755	53.8
	50/50	0.560	0.475	0.755	85.4

Finally, in Figure 62 the infra-red spectra are shown for the three amylose esters. Each spectrum is almost identical to

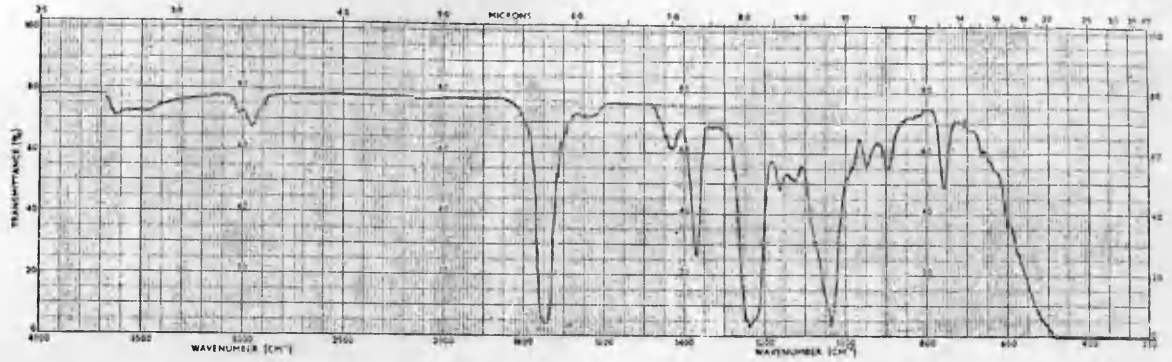

AMYLOSE TRIACETATE.

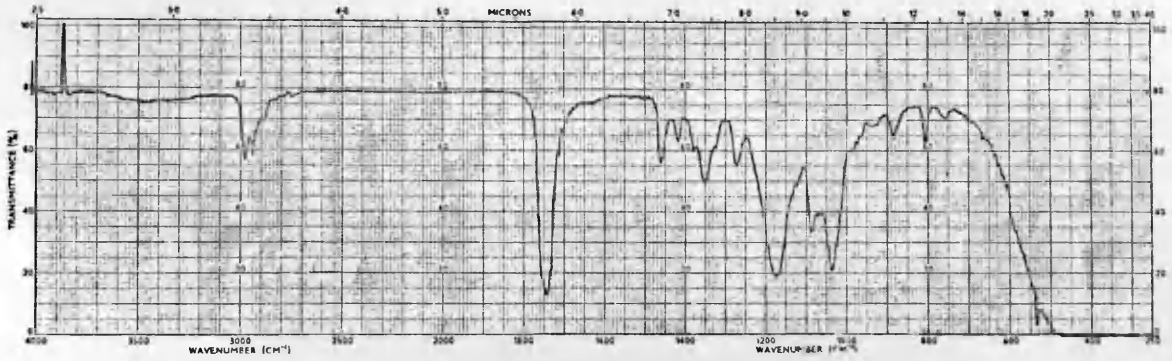

AMYLOSE TRIPROPIONATE.

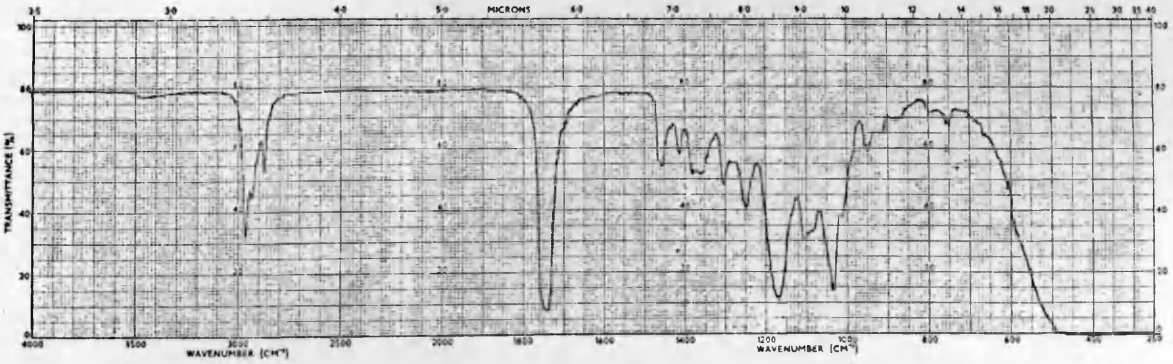

AMYLOSE TRIBUTYRATE.

FIGURE 62 INFRA-RED SPECTRA OF THE AMYLOSE ESTERS.

that of the corresponding cellulose ester (86) the only difference being in the region 1000cm^{-1} to 1100cm^{-1}. The spectrum for amylose triacetate has been assigned (87), the major differences in the other two spectra are, the shift to lower wave number of the C - O stretch band from ~1240cm^{-1} to ~1170cm^{-1}, and the appearance of the bands due to elongated hydrocarbon side-chain in the regions 2850 - 2980cm^{-1} and 1250 - 1470cm^{-1}.

The data presented in this study supports the idea that amylose (14) and its esters behave as stiff coils i.e. random coils which are less flexible than the synthetic polymers, and no results have been found to indicate any helical behaviour in solution. The values of the Kirkwood-Riseman effective bond length, b, and the Kuhn-Kuhn statistical segment, A_m, are equivalent to only 2 - 5 monomer units in the unperturbed state which is too small for helical behaviour (14).

IDEAS FOR FUTURE WORK ON THIS PROBLEM

Obviously the research into the solution properties of amylose esters is only just started. Two major questions have been raised, (a) will the temperature dependence of the unperturbed dimensions shown by ATB in EA also be shown in other solvents and by the other esters at higher temperatures? and (b) what causes the anomalous behaviour of the high molecular weight ATP material? Other questions have also

been raised but the two mentioned above seen to point to the most interesting problems. Further temperature studies are required, to include a greater range of molecular weights, combined with perhaps NMR as a tool for looking at conformational changes. Also a systematic light-scattering study of ATP at high molecular weight is required.

A P P E N D I X

GEL PERMEATION CHROMATOGRAPHY

APPENDIX

GEL PERMEATION CHROMATOGRAPHY (G.P.C.)

The experimental work involved in the GPC measurements was carried out at the Rubber and Plastics Research Association of Great Britain (RAPRA) by Dr. J. Evans.

G.P.C. (88) was used to establish the molecular weight distributions of the samples used in this study. The fundamental concept underlying the technique is, as the name suggests, one of permeation. The technique uses a column or columns packed with a gel containing pores which can vary in size. The larger polymer molecules which cannot permeate the gel phase of the column packing are rapidly eluted, but the smaller ones are retarded in their passage because they can penetrate into the gel network, are slowed down, and so eluted much later. The molecular weight of the material emerging from the column is a function of the elution valume. A calibration curve of molecular weight against elution volume has to be established so that the elution volume axes of the chromatograms can be related to the polymer molecular weight.

Benoit and co-workers (89) suggested that the hydrodynamic volume of the molecules in solution governs their elution volume. They found that plots of $[\eta]M$ against elution volume for a number of widely differing polymers, including comb and star branched polystyrene, fell on the same line. The actual calibration procedure used for the amylose esters involves calculating $[\eta]M$ values for the polymer and relating these to those for polystyrene. A primary calibration curve is established using polystyrene so that

$$\log M_1 = F(V_e) \qquad (1)$$

where V_e is the elution volume and M_1 is the molecular weight of polystyrene. The calibration curve for the ester is calculated using

$$\log M_1 [\eta]_1 = \log M_2 [\eta]_2 \qquad (2)$$

and the respective Mark-Houwink equations $[\eta]_1 = K_1 M_1^{a1}$ and $[\eta]_2 = K_2 M_2^{a_2}$ which yields

$$\log M_2 = \frac{1}{1 + a_2} \log \frac{K_1}{K_2} + \frac{1 + a_1}{1 + a_2} \log M_1 \qquad (3)$$

Using equations (1) and (3) the relation between M_2 and V_e is established.

The Mark-Houwink equations used in the calibration were

Polystyrene $[\eta] = 1.2 \times 10^{-2} M^{0.71}$

Amylose Acetate $[\eta] = 3.42 \times 10^{-3} \bar{M}_w^{0.80}$

Amylose Propionate $[\eta] = 3.78 \times 10^{-2} \bar{M}_w^{0.58}$

Amylose Butyrate $[\eta] = 1.66 \times 10^{-3} \bar{M}_w^{0.86}$

All calculations were carried out by computer.

Results

The chromatograph used a set of four columns with varying pore sizes: (1) 10^{-6} to 3.5×10^{-6}cm,

(2) 7×10^{-6} to 2×10^{-5}cm,

(3) 5×10^{-5} to 1.5×10^{-4}cm, and

(4) 7×10^{-3} to 5×10^{-2}cm.

THF was used as the solvent at ambient.

The results for each fraction are shown in Table A.2. No

corrections were made for peak broadening effects or for variation of refractive index with molecular weight at low molecular weight. Corrections for peak broadening were not considered to be important for the distributions involved which, according to Tung (90), are only important for narrow distributions.

Table A.1 shows the comparison between G.P.C. measurements and, osmometry and light-scattering measurements. Although the molecular weights measured by the different methods are not identical, the difference ranges from 46% to 1%, the errors in the distributions measured by GPC and, light-scattering and osmometry are $< 6\%$ in the cases where they have both been measured. It has therefore been assumed that the GPC distributions are correct and these have been used to calculate $\bar{M}_w$ and $\bar{M}_n$ has been measured by osmometry.

Table A.1 Comparison of $\bar{M}_n$ and $\bar{M}_w$ data.

Polymer sample.	$\bar{M}_n^{OS} \times 10^{-6}$	$\bar{M}_w^{GPC} \times 10^{-6}$	$\bar{M}_w^{LS} \times 10^{-6}$	$\bar{M}_w^{GPC} \times 10^{-6}$	$\frac{\bar{M}_w^{GPC}}{\bar{M}_n^{GPC}}$	$\frac{\bar{M}_w^{LS}}{\bar{M}_n^{OS}}$
B3	0.391	0.250	0.613	0.577	2.31	1.57
B4	0.188	0.136	0.275	0.209	1.53	1.46
B5	0.0898	0.0753		0.125	1.67	
X9	0.106	0.0871		0.145	1.66	
X10b	0.0671	0.0484		0.0759	1.57	
X11	0.0651	0.0467		0.0713	1.52	
X12	0.0488	0.0375		0.0599	1.60	
X13	0.0376	0.0282		0.0405	1.43	
F1B	0.0798	0.0504	0.137	0.403	8.00	1.72
F2b	0.0515	0.0391		0.0847	2.17	
F3b	0.0370	0.0309	0.0584	0.0503	1.63	1.58
F4b	0.0267	0.0145	0.0428	0.0248	1.71	1.61
F3	0.0268	0.0223	0.0380	0.0313	1.40	1.42
F4	0.0880	0.0147		0.0185	1.26	
F6	0.00574	0.00886		0.0267	3.01	
P34	0.0397	0.0405		0.0653	1.61	
P55	0.0328	0.0245		0.0348	1.42	
P6	0.0278	0.0244		0.0291	1.30	
P 14	0.0142	0.0115		0.0207	1.81	
P15	0.0107	0.0106		0.0167	1.57	

Table A.1 continued.

Polymer sample.	$\bar{M}_n^{OS} \times 10^{-6}$	$\bar{M}_w^{GPC} \times 10^{-6}$	$\bar{M}_w^{LS} \times 10^{-6}$	$\bar{M}_w^{GPC} \times 10^{-6}$	$\bar{M}_w^{GPC} / \bar{M}_n^{OS}$	$\bar{M}_w^{LS} / \bar{M}_n^{OS}$
P16	0.0102	0.00989		0.0135	1.37	
P17	0.00579	0.00845		0.0114	1.35	
P19,20	0.00410	0.00606		0.00794	1.31	
S1'		0.125	2.48	2.00	15.99	
S2b''		0.611	1.40	8.03	13.13	
S2c'		0.239	0.655	2.34	9.79	
S4''		0.194	0.948	0.579	2.98	
S1		0.146	30.00	2.09	14.31	
S2a		0.151	150.00	63.5	419.9	
S2b		0.106	5.28	2.37	22.37	
S2c		0.222		1.22	5.48	
S3		0.158	13.47	7.71	48.96	
S4		0.132	1.53	0.290	2.20	
S2d		0.143		0.544	3.82	

Table A.2: G.P.C. Results

	$M \times 10^{-6}$					
Fraction	$\bar{M}_n$	$\bar{M}_w$	$\bar{M}_z$	$\bar{M}_v$	$\bar{M}_w/\bar{M}_n$	$\bar{M}_z/\bar{M}_n$
F1b	0.050	0.403	86.9	0.151	8.00	1725
F2b	0.039	0.085	6.99	0.062	2.17	178.9
F3b	0.031	0.050	13.9	0.043	1.63	44.8
F4b	0.015	0.025	0.045	0.023	1.71	3.07
F3	0.022	0.031	0.133	0.029	1.40	5.97
F4	0.015	0.018	0.026	0.018	1.26	1.79
F6	0.009	0.027	0.075	0.022	3.01	8.51
P34	0.040	0.065	0.118	0.059	1.61	2.91
P55	0.025	0.035	0.053	0.032	1.42	2.15
P6	0.022	0.029	0.038	0.028	1.30	1.69
P14	0.011	0.021	0.037	0.018	1.81	3.19
P15	0.011	0.017	0.064	0.015	1.57	6.02
P16	0.010	0.014	0.017	0.013	1.37	1.76
P17	0.008	0.011	0.014	0.011	1.35	1.67
P19,20	0.006	0.008	0.010	0.008	1.31	1.59
S1	0.146	2.09	58.4	0.923	14.3	400
S2a	0.151	63.5	6480	12.7	420	42871
S2b	0.106	2.37	55.0	1.12	22.4	519
S2c	0.222	1.22	220	0.477	5.48	991
S2d	0.143	0.544	18.3	0.318	3.82	128.4
S3	0.158	7.71	731	1.52	49	4640
S4	0.132	0.290	10.9	0.207	2.20	83.1

Table A.2: Continued

	$M \times 10^{-6}$					
Fraction	$\bar{M}_n$	$\bar{M}_w$	$\bar{M}_z$	$\bar{M}_v$	$\bar{M}_w/\bar{M}_n$	$\bar{M}_z/\bar{M}_n$
S1'	0.125	2.00	150	0.520	16.0	1197
S2b"	0.611	8.03	143	3.65	13.1	233
S2c'	0.239	2.34	202	0.755	9.79	844
S4"	0.194	0.579	13.4	0.372	2.98	69.2
B3	0.250	0.577	0.375	0.482	2.31	15.0
B4	0.136	0.209	0.359	0.195	1.53	2.63
B5	0.075	0.125	1.55	0.110	1.67	20.5
X9	0.087	0.145	0.308	0.133	1.66	3.54
X10b	0.048	0.076	0.117	0.071	1.57	2.43
X11	0.047	0.071	0.109	0.067	1.52	2.34
X12	0.037	0.060	0.370	0.055	1.60	9.88
X13	0.028	0.040	0.061	0.038	1.43	2.16

BIBLIOGRAPHY

1. C.T. Greenwood and J. Thomson, J. Chem. Soc. 222 (1962)
2. For a review see:
   (a) W. Banks and C.T. Greenwood, Starke 19, 197 (1967)
   (b) C.T. Greenwood, Periodica Polytechnica (Budapest) 12, 25 (1968)
3. F.L. Bates, D. French and R.E. Rundle, J. Amer. Chem. Soc. 65, 142 (1943)
4. W. Banks and C.T. Greenwood, Arch. Biochem. Biophys. 117, 674 (1966)
5. W. Banks, C.T. Greenwood and J. Thomson, Chem. and Ind. (London) 928 (1959)
6. J.M.G. Cowie, J. Polymer Sci. 49, 455 (1961)
7. J.M.G. Cowie, Polymer 5, 601 (1964)
8. R.S. Patel and R.D. Patel, J. Polymer Sci A 3, 2123 (1965)
9. R.S. Patel and R.D. Patel, Makromol. Chem. 90, 262 (1966)
10. J.F. Foster and R.M. Hixon, J. Amer. Chem. Soc. 66, 557 (1944)
11. A.L. Potter and W.Z. Hassid, J. Amer. Chem. Soc. 73, 593 (1951)
12. J. Szejtli and S. Augustat, Starke 18, 38 (1966)
13. W. Burchard, Solution Properties of Natural Polymers, Chem. Soc. Spec. Publ. No. 23 (1968)
14. W. Banks and C.T. Greenwood, Eur. Polym. J. 5, 649 (1969)
15. W.W. Everett and J.F. Foster, J. Amer. Chem. Soc. 81, 3464 (1959)
16. J.M.G. Cowie, Makromol. Chem. 59, 189 (1963)
17. M. Kurata and W.H. Stockmayer, Fortschr. Hochpolym.-Forsch. 3, 196 (1963)
18. V.P. Shanbhag, Arkiv For Kemi 29, 1 (1968)
19. L. Huppenthal, Roczniki Chemii 41, 1793 (1967)
20. W. Burchard and E. Husemann, Makromol. Chem. 44, 358 (1961)

21. W. Brown and D. Henley, Makromol. Chem. 79, 68 (1964)

22. D. Henley, Arkiv For Kemi 18, 327 (1961)

23. W.G. Harland, Recent Adv. in Chemistry of Cellulose and Starch ed. Honeyman. N.Y. Interscience Pub. Inc. 1959

24. L. Mandelkern and P.J. Flory, J. Amer. Chem. Soc. 74, 2517 (1952)

25. W. Banks, C.T. Greenwood and D.J. Hourston, Trans. Far. Soc. 64, 363 (1968)

26. W. Banks and C.T. Greenwood, Makromol. Chem. 114, 245 (1968)

27. W. Banks, C.T. Greenwood and J. Sloss, Makromol. Chem. 140, 109 (1970)

28. A. Sarko and R.H. Marchessault, Science 154, 1658 (1966)

29. D.A. Bryant and Byung Kwon Min, Macromolecules 2, 1 (1969)

30. R.H. Marchessault and A. Sarko, Adv. Carb. Chem. 22, 421 (1967)

31. J.M.G. Cowie, Makromol. Chem. 42, 230 (1961)

32. H. Staudinger and W. Heuer, Ber. 63, 222 (1930); H. Staudinger and R. Nodzu, ibid. 63, 721 (1930)

33. H. Mark, "Der feste Korper", Leipzig, 103 (1938)

34. R. Houwink, J. Prakt. Chem. 155, 15 (1940)

35. P.J. Flory, "Principles of Polymer Chemistry", (1953)

36. M.R. Cannon, R.E. Manning and J.D. Bell, Anal. Chem. 32, 355 (1960)

37. P. Debye, J. Appl. Phys. 15, 338 (1944); J. Phys and Colloid Chem. 51, 18 (1947)

38. B.H. Zimm, J. Chem. Phys. 16, 1099 (1948)

39. R.S. Higginbotham and G.A. Morrison, Shirley Inst. Mem. 22, 148 (1948)

40. G.C. Berry and E.F. Casassa, J. Polymer Sci. D 4, 1 (1970)

41. M. Kurata, M. Fukatsu, H. Sotobayashi and H. Yamakawa, J. Chem. Phys. 41, 139 (1964)

42. (a) J.G. Kirkwood and J. Riseman, J. Chem. Phys. 16, 565 (1948)
(b) P.L. Auer and C.S. Gardner, J. Chem. Phys. 23, 1545 (1955)

43. S. Newman, W.R. Krigbaum, C. Laugier and P.J. Flory, J. Polymer Sci. 14, 451 (1954)

44. M. Kurata, W.H. Stockmayer and A. Roig, J. Chem. Phys. 33, 151 (1960)

45. V.P. Shanbhag, Arkiv For Kemi 29, 139 (1968)

46. P.J. Flory and T.G. Fox,
(a) J. Amer. Chem. Soc. 73, 1904 (1951)
(b) ibid. 73, 1915 (1951)

47. L. Huppenthal and S. Claesson, Roczniki Chemii 39, 1867 (1965)

48. B.H. Zimm, W.H. Stockmayer and M. Fixman, J. Chem. Phys. ~~24~~ 21, ~~269~~ 10 (1953)

49. M. Fixman, J. Chem. Phys. 23, 1656 (1955)

50. H. Yamakawa and M. Kurata, J. Phys. Soc. Japan 13, 78 (1958)

51. P.J. Flory, J. Chem. Phys. 10, 51 (1949)

52. M. Kurata and H. Yamakawa, J. Chem. Phys. 29, 311 (1958)

53. W. Burchard, Makromol. Chem. 50, 20 (1961)

54. W.H. Stockmayer and M. Fixman, J. Polymer Sci. C 1, 137 (1963)

55. H. Inagaki, H. Suzuki and M. Kurata, J. Polymer Sci. C 15, 409 (1966)

56. O.B. Ptitsyn, Vysokomol. Soedin. 3, 1673 (1961)

57. G.C. Berry, J. Chem. Phys. 46, 1338 (1967)

58. M. Bohdanecky, J. Polymer Sci.B3, 201 (1965)

59. W.R. Krigbaum, J. Polymer Sci. 18, 315 (1955)

60. W.R. Krigbaum, J. Polymer Sci. 28, 213 (1958)

61. J.M.G. Cowie, Polymer 7, 487 (1966)

62. O.B. Ptitsyn and Y.E. Eizner, Soviet Phys-Tech. Phys. (transl.) 4, 1020 (1960)

63. H. Baumann, J. Polymer Sci. B 3, 1069 (1965)

64. W. Banks and C.T. Greenwood, Eur. Poly. J. 4, 457 (1968)

65. J.G. Kirkwood, R.W. Zwanzig and R.J. Plock, J. Chem. Phys. 23, 213 (1955)

66. H. Kuhn and W. Kuhn, J. Colloid Sci. 5, 331 (1950); J. Polymer Sci. 5, 519 (1950); ibid 2, 1 (1952)

67. W. Kuhn, H. Kuhn and A. Silberberg, J. Polymer Sci. 14, 193 (1954)

68. O. Kratky and G. Porod, Rev. Trav. Chim. 68, 1108 (1949)

69. H. Benoit and P. Doty, J. Phys. Chem. 57, 958 (1953)

70. W. Burchard, Makromol. Chem. 42, 151 (1960)

71. H.-G. Elias, Chapter 9, "Light-Scattering from polymer solutions", ed. M.B. Huglin, Academic Press (1972) London

72. H. Morawetz, "Macromolecules in solution", High Polymer Vol. XXI. Interscience (1965)

73. W. Banks and C.T. Greenwood, Eur. Poly. J. 4, 249 (1968)

74. T.A. Orofino and P.J. Flory, J. Chem. Phys. 26, 1067 (1957)

75. J.M.G. Cowie, Biopolymers 3, 69 (1965)

76. J.M.G. Cowie, Ann Maconnachie and Susan Levvy, Paper given at I.U.P.A.C. meeting, Helsinki (1972)

77. J.M.G. Cowie and P.M. Toporowski, J. Macromol. Sci. - Phys. B 3, 81 (1969)

78. P.J. Flory, O.K. Spurr and D.K. Carpenter, J. Polymer Sci. 27, 231 (1958)

79. N. Kuwahara, K. Ogino, M. Konuma, N. Ida and M. Kaneko, J. Polymer Sci. A2 4, 173 (1966)

80. W.R. Krigbaum and L.H. Sperling, J. Phys. Chem. 64, 99 (1960)

81. G.V. Schulz and R. Kirste, Z. Phys. Chem. 30, 171 (1961)

82. P.J. Flory and W.R. Krigbaum, J. Chem. Phys. 18, 1086 (1950)

83. W.H. Stockmayer, Makromol. Chem. 35, 54 (1959)

84. E.F. Casassa and H. Markovitz, J. Chem. Phys. 29, 493 (1958)

85. W.R. Moore, J.A. Epstein, A.M. Brown and B.M. Tidswell, J. Polymer Sci. 23, 23 (1957)

86. D.O. Hummel and F. Scholl, "Infra red analysis of Polymers, Resins and Additives", Wiley-Interscience (1969)

87. B. Casu, M. Reggiani, G.G. Gallo and A. Vigevani, Carb. Res. 12, 157 1970)

88. For reviews see:

(a) "Polymer Fractionation", ed. M.J.R. Cantow, Academic Press (1960)

(b) J.F. Johnson and R.S. Porter, Chapter 4, Progress in Polymer Science Vol.2 ed. A.D. Jenkins.

(c) T. Williams, J. Material Sci. 5, 811 (1970)

(d) H. Coll and D.K. Gilding, J. Polymer Sci. A2 8, 89 (1970)

89. Z. Grubisc, P. Remp and H. Benoit, J. Polymer Sci. B 5, 753 (1967)

90. L.H. Tung, J. Appl. Poly. Sci. 10, 1271 (1966)